

THESIS

THREE-DIMENSIONAL STRAIN AT FORELAND ARCH TRANSITIONS:  
STRUCTURAL MODELING OF THE SOUTHERN BEARTOOTH ARCH  
TRANSITION ZONE, NORTHWEST WYOMING

Submitted by

Thomas Gardner Neely

Department of Geosciences

In partial fulfillment of the requirements

for the Degree of Master of Science

Colorado State University

Fort Collins, Colorado

Fall 2006

COLORADO STATE UNIVERSITY

August 29, 2006

WE HEREBY RECOMMEND THAT THE THESIS PREPARED UNDER OUR SUPERVISION BY THOMAS G. NEELY ENTITLED “THREE-DIMENSIONAL STRAIN AT FORELAND ARCH TRANSITIONS: STRUCTURAL MODELING OF THE SOUTHERN BEARTOOTH ARCH TRANSITION ZONE, NORTHWEST WYOMING” BE ACCEPTED AS FULFILLING IN PART REQUIREMENTS FOR THE DEGREE OF MASTER OF SCIENCE.

Committee on Graduate Work

---

---

---

**Adviser**

---

**Department Head**

## ABSTRACT OF THESIS

### THREE-DIMENSIONAL STRAIN AT FORELAND ARCH TRANSITIONS: STRUCTURAL MODELING OF THE SOUTHERN BEARTOOTH ARCH TRANSITION ZONE, NORTHWEST WYOMING

Basement-involved foreland orogens commonly exhibit anastomosing networks of bifurcating basement arches whose structural culminations are linked by complex transition zones. Transitions between arches of differing orientation and vergence display structural complexity, commonly characterized by suites of diversely-oriented faults and folds. This study addresses the detailed geometry, the controls on along-strike changes in geometry, and the role of secondary structures at foreland arch transitions.

Data from 1,581 slickensided minor faults, more than 1,000 km of 2D seismic data, and 187 wells were used to define a regional kinematic model, 16 balanced cross-sections, and restorable 3D surface models within the southern Beartooth arch transition zone. This transition zone is composed of three primary fault systems, the N-striking Beartooth Fault system, the NW-striking Line Creek Fault system, and the N-striking Oregon Basin Fault, as well as the Rattlesnake Mountain and Pat O'Hara Mountain hanging-wall backthrust structures. Slickensided minor faults from areas away from steeply-dipping fold limbs indicate a regionally-consistent  $065^\circ$  compression and shortening direction. Minor faults from the flanks of the Beartooth arch, Pat O'Hara Mountain, Rattlesnake Mountain, and Canyon Mouth anticlines show ideal  $\sigma_1$  and shortening directions oblique to both local fold trends and the regional  $065^\circ$  signature. This oblique-slip may have resulted from vertical-axis rotation, fold-related stress

refraction, and/or strain partitioning between strike-slip and thrust faulting, perhaps during movement on pre-existing basement weaknesses.

The Oregon Basin Fault and Beartooth Fault system show minimal folding of the basement surface, whereas the Line Creek Fault system shows basement surface folding near fault cut-offs up to approximately 25°. The Beartooth and Line Creek Fault systems are characterized by multiple fault splays and slip transfer between splays, and the Oregon Basin Fault is a single fault whose hanging wall is monoclinally-folded into the footwall of the Line Creek Fault system. Restorable, 2D basement block models of the Line Creek and Rattlesnake Mountain Fault systems suggest that the two are linked at depth and were active synchronously during progressive, rigid-block rotational backthrusting of the Line Creek Fault hanging wall.

Three-dimensional restoration of the basement surface suggests that 1) shortening in the area is greatest on the Beartooth and Oregon Basin Fault systems and that comparatively less shortening occurred on the Line Creek Fault system, and 2) regional, clockwise vertical-axis rotation of several degrees may have occurred within the Beartooth and Line Creek Fault systems. Although both abrupt and gradual structural transitions are present within the area, the primary fault systems bounding the Beartooth arch and northwest margin of the Bighorn Basin are best characterized as defining gradual and continuous structural transitions. Secondary basement-involved structures in the area likely resulted from reactivation of pre-existing basement structures and do not appear to have accommodated large-scale rotations or changes in shortening direction.

Thomas Gardner Neely  
Department of Geosciences  
Colorado State University  
Fort Collins, CO 80523  
Fall 2006

## ACKNOWLEDGMENTS

This research was funded by grants from the Geological Society of America, the American Association of Petroleum Geologists, the Rocky Mountain Association of Geologists, the Wyoming Geological Association, the Colorado Scientific Society, Colorado State University/Edward Warner, and ConocoPhillips. 2DMove and 3DMove software were provided to Colorado State University by Midland Valley. Steve Bridges and Windsor Energy provided helpful discussion and access to several well and 2D and 3D seismic data sets. ConocoPhillips provided useful training in 3DMove software during a 2005 internship and access to an extensive 2D seismic data set that greatly improved the study. Particular thanks goes to Peter Hennings at ConocoPhillips for his scientific guidance and enthusiastic coordination of software training and access to seismic data.

A special thanks goes to my adviser Eric Erslev, who rigorously encouraged me to analyze deeply, broadly, and passionately. Our discussions were a constant source of motivation and pleasure. Thank you, Eric. Thanks goes to my thesis committee members Jerry Magloughlin and Wayne Charlie for their helpful suggestions and discussion. Thanks also goes to friends and faculty at Colorado State University and the University of California, Santa Barbara, whose cheer and engagement made six years in geoscience department hallways jovial and stimulating. Lastly, a warm thank you goes to my family - Mom, Dad, and Jordan, for their open support of unfamiliar endeavors.

## TABLE OF CONTENTS

<b>1. INTRODUCTION.....</b>	<b>1</b>
<b>2. PREVIOUS WORK.....</b>	<b>7</b>
TECTONIC SETTING .....	7
REGIONAL KINEMATICS DEBATE .....	8
STRUCTURAL STYLES AND DEFORMATION MECHANISMS.....	9
REGIONAL GEOLOGY .....	11
<b>3. METHODS .....</b>	<b>15</b>
MINOR FAULT ANALYSIS.....	15
CROSS-SECTION ANALYSIS.....	16
3D SURFACE ANALYSIS AND RESTORATION .....	17
<b>4. KINEMATIC ANALYSIS .....</b>	<b>18</b>
OBSERVATIONS.....	18
ROTATION TO HORIZONTAL .....	25
INTERPRETATIONS.....	28
<b>5. TWO-DIMENSIONAL CROSS-SECTION ANALYSIS .....</b>	<b>34</b>
TWO-DIMENSIONAL MODELING CONSTRAINTS .....	34
OBSERVATIONS.....	37
<i>Regional Observations.....</i>	<i>37</i>
<i>Rattlesnake Mountain and Pat O’Hara Mountain Anticlines.....</i>	<i>38</i>
<i>Horse Center and Oregon Basin Anticlines.....</i>	<i>41</i>
INTERPRETATIONS.....	41
<i>Beartooth/Line Creek/Oregon Basin Fault Systems.....</i>	<i>41</i>
<i>Rattlesnake Mountain/Pat O’Hara Mountain Anticlines .....</i>	<i>53</i>
<i>Line Length Balancing.....</i>	<i>59</i>
<i>Summary of Sequential Kinematic Development.....</i>	<i>69</i>
<b>6. THREE-DIMENSIONAL ANALYSIS.....</b>	<b>71</b>
CONSTRAINTS FROM 3D MODELING .....	71
OBSERVATIONS.....	71
INTERPRETATIONS.....	73
<i>Beartooth/Line Creek Fault System.....</i>	<i>73</i>
<i>Rattlesnake Mountain/Pat O’Hara Mountain Anticline Intersection.....</i>	<i>84</i>
<i>Cedar Mountain Tear Fault.....</i>	<i>85</i>
<i>Northern Oregon Basin Anticline .....</i>	<i>89</i>
THREE-DIMENSIONAL RESTORATION .....	89
<b>7. DISCUSSION AND CONCLUSIONS .....</b>	<b>93</b>
CRUSTAL-SCALE IMPLICATIONS .....	99
FUTURE WORK .....	100
<b>REFERENCES.....</b>	<b>102</b>

## 1. INTRODUCTION

Basement-involved foreland orogens, including the Sierras Pampeanas of western Argentina, the Tien Shan of central Asia, and the Laramide arches of western North America, document subduction and collision-related crustal strain thousands of kilometers from plate boundaries. Their genetic relationships to plate boundary processes remain enigmatic, however. The upper crustal expression of foreland deformation is commonly an anastomosing network of bifurcating basement arches whose structural culminations are linked by complex transition zones. These zones between arches of differing orientation and vergence commonly exhibit 3D structural complexity characterized by suites of secondary structures that include diversely-oriented faults and folds. This study analyzes the kinematic and 3D structural development of a Laramide arch transition in northern Wyoming, USA, in order to address basic questions about crustal and structural processes within foreland regions.

Precambrian basement rocks exposed in fault-bounded Rocky Mountain ranges display up to 10 km of vertical separation relative to basement rocks in adjacent basins (Keefer and Love, 1963; Fig. 1). Although early interpretations of the structural geometry of these ranges often relied on near-vertical faults to explain the basement topography (Stearns, 1971), subsequent geophysical and kinematic studies documented horizontal shortening on range-bounding thrust and reverse faults (Allmendinger et al., 1983; Gries, 1983). The term “arch” describes the genetic and geometrical observation that the foreland basement nonconformity is gently bowed into asymmetric basement highs up to 100 km wide and hundreds of km long (Fig. 1). Along- strike changes

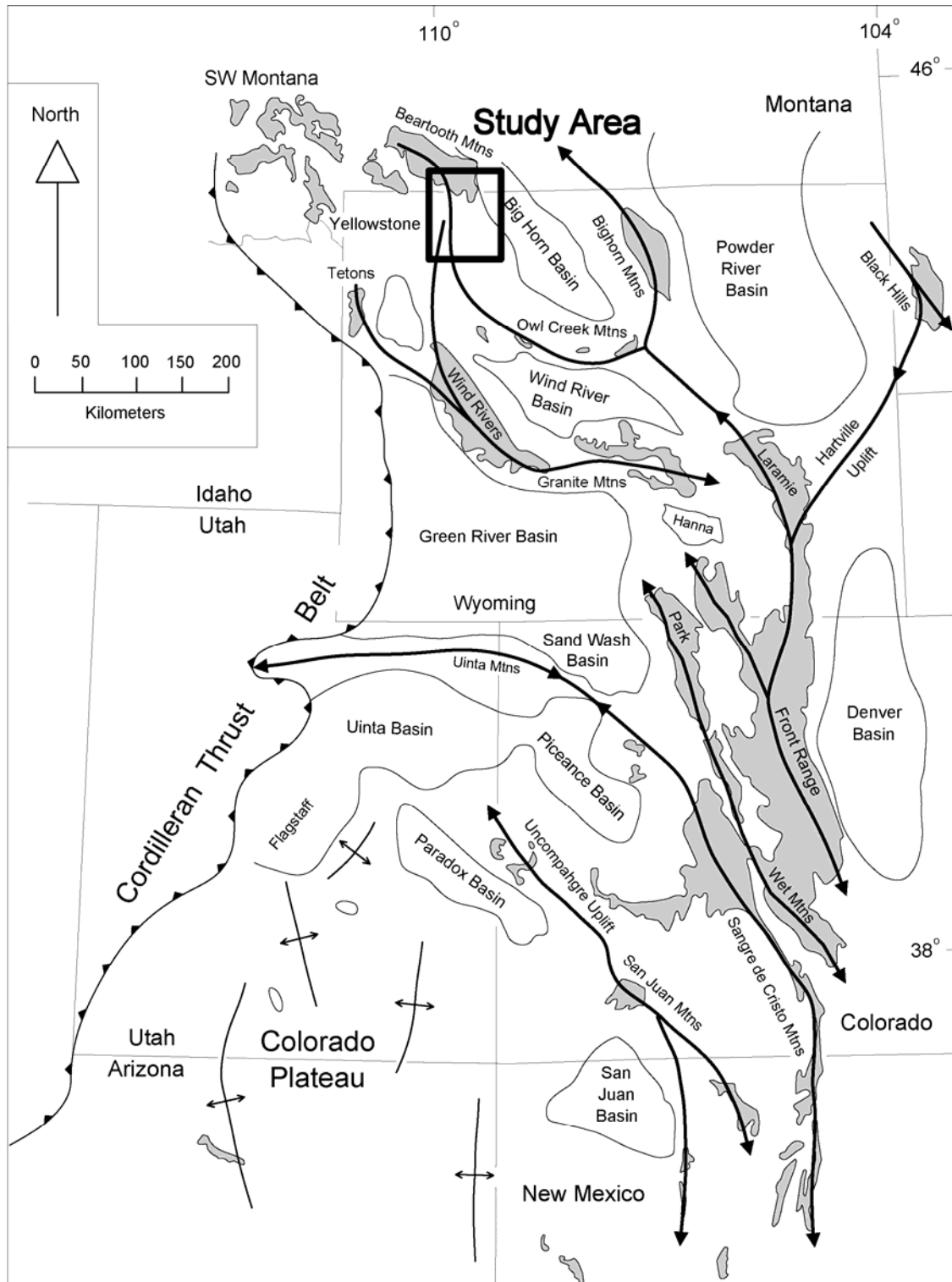


Fig. 1. Map showing exposures of Precambrian basement rocks (gray), Laramide-age basins (black outlines), principal Laramide arch trends (thick lines), and study area location; from Erslev (2005).

in arch geometry may be abrupt, gradual, or transitional between neighboring arches, and are commonly accompanied by secondary fault and fold structures ranging from one to tens of km in length. These secondary structures have produced oil and gas and have been interpreted to have formed from a variety of fault and fold mechanisms, including fault-propagation folding, fault-bend folding, folding and rotation of crystalline basement rocks, and reactivation of pre-existing structures (Erslev and Hennings, 2004).

The objectives of this study are to determine the 3D geometry and kinematic development of a basement-involved foreland arch transition and to use these geometric and kinematic insights to test hypotheses concerning the roles of local versus regional processes at arch transitions. The following questions and hypotheses address fundamental problems concerning foreland orogenesis by focusing on specific processes in foreland arch structural development:

- What is the detailed geometry of a foreland arch transition? Specifically, are abrupt geometric transitions facilitated by transfer faults, tear faults, or abrupt changes in along-strike offset? Are gradual geometric changes facilitated by smooth lateral changes in fault offset, gradually plunging folds, or smoothly distributed internal deformation?
- What controls along-strike changes in arch geometry? Possibilities include a) reactivation of pre-existing basement structures; b) linking of two or more arches; c) changes in the orientation of arch vergence; d) changes in shortening direction; and e) changes in either along-strike or regional shortening amount.

- How do secondary structures accommodate strain? Specifically, what is the role of backthrusts, anomalously-oriented structures, ramps, and other secondary features at arch transitions? Are secondary structures caused by a) large-scale rotations; b) gravitational spreading of arch terminations; c) local or regional changes in vergence orientation or shortening amount; e) movement on basement weaknesses; or f) linkage of independent, laterally propagating basement arches?

This study integrated new and published geologic mapping, new minor fault and fracture data, and existing industry seismic and well data into a 3D kinematic model. The slip and vergence of faults and folds, and the possible presence of obliquely-reactivated basement weaknesses were evaluated by analyzing slip data from slickensided minor faults in Paleozoic and Mesozoic sandstone units. Geometric and genetic relationships between structures were defined through 2D and 3D qualitative analysis of along-strike differences in cross-sectional geometries and the presence and nature of along-strike linking structures. The possibilities of vertical-axis rotations and along-strike variations in the amount of shortening were tested by restoring deformed surfaces using the 2DMove and 3DMove software packages from Midland Valley.

The area chosen for this study is the transition of the southern WNW-trending Beartooth arch into the northern NW-trending structural margin of the western Bighorn Basin in NW Wyoming, located within the Laramide (approximately 70-55 Ma) basement-involved foreland of the Rocky Mountains of the conterminous USA (Figs. 1, 2). The area is well suited for testing the study's hypotheses because it contains:

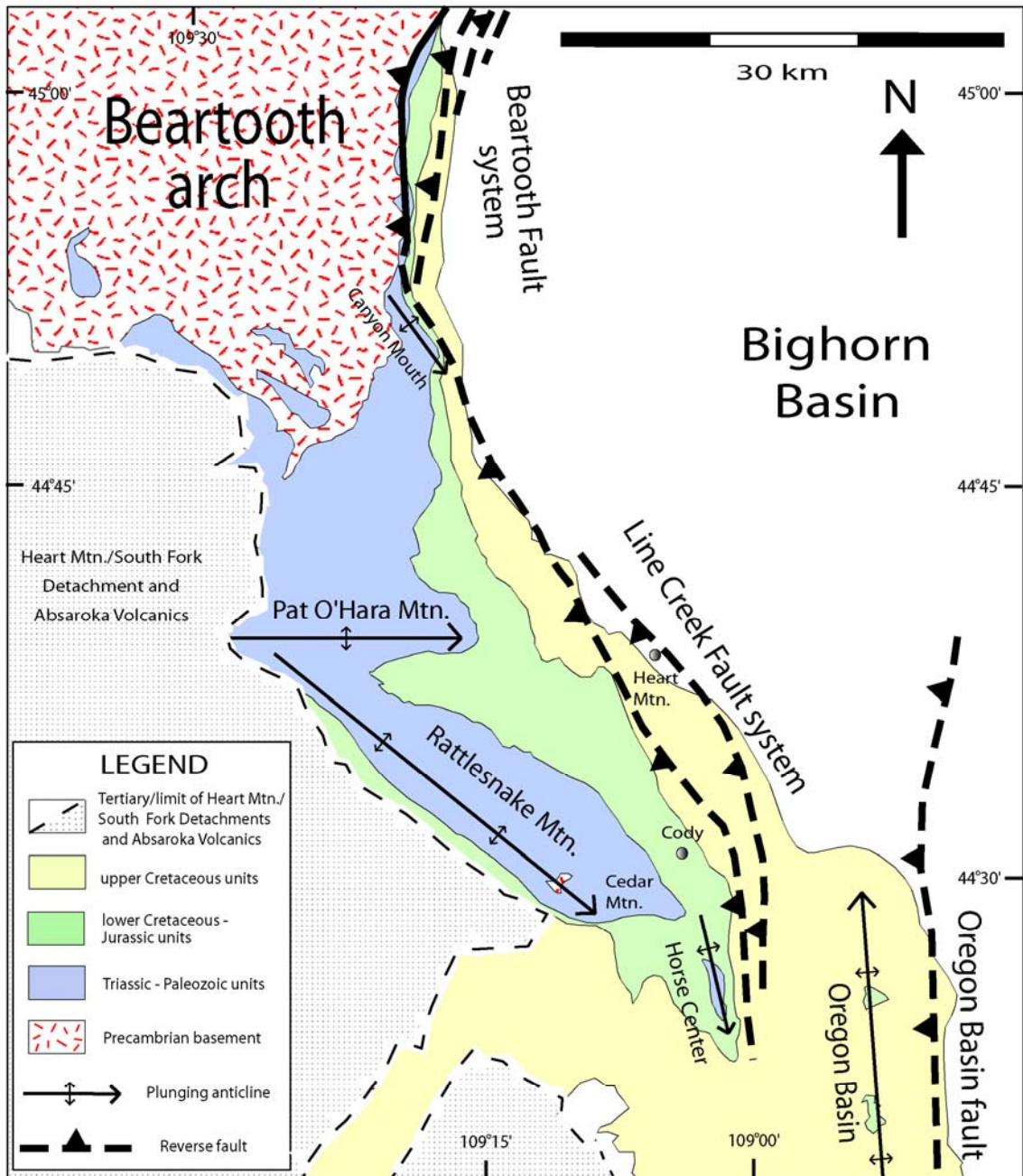


Fig. 2. Simplified geologic map of study area including primary fault systems, primary and secondary folds, and exposures of Precambrian basement rocks; after Love and Christiansen (1985).

- 1) basement-involved structures of tens to 100's of km in scale – the Beartooth, Line Creek, and Oregon Basin Fault systems;
- 2) first-order changes in arch trends – from WNW to N-S to NW;
- 3) diverse fault and fold orientations – from NW-trending (Rattlesnake Mountain anticline) to E-W trending (Pat O'Hara Mountain anticline) to N-S-trending (east flank of Beartooth arch, Horse Center anticline, Oregon Basin anticline) structures;
- 4) abundant industry well and seismic data; and
- 5) excellent surface exposure.

Because secondary structures near foreland arch transitions can produce oil and gas traps, an improved understanding of the origin and kinematic development of arch transition zones and associated secondary structures may improve hydrocarbon exploration and production by predicting the presence and location of structural terminations, 3D structural closures, and fracture distributions. In tectonically active foreland regions such as the Tien Shan in central Asia and the Sierras Pampeanas in Argentina, an improved understanding of surface deformation above major foreland fault systems may improve earthquake hazard assessment.

## 2. PREVIOUS WORK

### Tectonic Setting

The modern understanding of basement-involved foreland orogenesis was revolutionized by early studies that linked plate subduction processes to mountain building processes within continental interiors. The recognition by Coney and Reynolds (1977) and Dickinson and Snyder (1978) that gaps in volcanic activity within subduction-related magmatic arcs and associated cratonward shifts in foreland orogenic fronts may result from abnormally shallow subduction, placed the Rocky Mountain basement-involved arches within a global tectonic context. These and other early studies were refined by detailed comparisons between the Laramide Rocky Mountains and modern analogues of shallow subduction in the northern and central Andes (Jordan et al., 1983, Jordan and Allmendinger, 1986). Jordan and Allmendinger (1986) showed that the distribution and 2D geometry of active basement-involved structures of the Sierras Pampeanas in western Argentina resembled those of the Rocky Mountain foreland, suggesting similar tectonic origins. Further geophysical and field studies on subduction-related processes in the Andes identified the oceanic slab beneath the magmatically quiescent shallow subduction zone west of the Sierras Pampeanas and linked the timing of individual basement-involved foreland structures to progressive subduction of the Juan Fernandez Ridge beneath the South America Plate (Cahill and Isacks, 1985; Smalley and Isacks, 1987; Mpodozis and Ramos, 1989; Allmendinger et al., 1990).

Although these and other studies offered spatial and temporal evidence for the relationship between shallow subduction/ridge subduction and a cratonward shift in foreland orogenic processes, the mechanism by which plate boundary stresses could be

transmitted and/or focused up to 1,000 km inland of plate boundaries remains elusive. Several hypotheses have been proposed, including 1) subcrustal shear resulting from basal tractions exerted by subducted oceanic lithosphere (Bird, 1988); 2) pure-shear lithospheric thickening resulting from continental end-loading (Egan and Urquart, 1994) and/or subduction hydration (Humphreys et al., 2003); 3) crustal thickening and uplift resulting from lateral injection of ductile lower crust (McQuarrie and Chase, 2000); 4) wholesale buckling of the North American continental lithosphere (Tikoff and Maxson, 2001); and 5) detachment and buckling of the crust (Lowell, 1983; Oldow et al., 1989; Erslev, 1993).

#### Regional Kinematics Debate

An important, yet unresolved question regarding the tectonic development of the Rocky Mountains is why Laramide arches display a wide range of structural trends. Arch trends vary between E-W (Uinta, Owl Creek, Sweetwater arches), NW-SE (Wind River, Beartooth, Bighorn arches), and N-S (Front Range, Sangre de Cristo arches) and have been explained by a variety of hypotheses that have related the observed diversity of trends to plate kinematics. The regional kinematics debate has bearing on this study because it addresses questions surrounding the influence of local versus regional horizontal shortening and transport directions during arch formation. Chapin and Cather (1981) and Gries (1983, 1990) suggested that counter-clockwise changes in North American plate convergence direction during the Laramide orogeny resulted in multi-stage, multi-directional shortening and the observed variety of arch orientations. Bird (1998) suggested that a clockwise rotation in foreland shortening direction from 040° to 055° could be related to changes in plate convergence direction associated with

sequential subduction of the Kula and Farallon plates. Saleeby (2003) suggested that subduction of a large igneous province on the Farallon plate, correlative to the Pacific plate's Hess-Shatsky ridge, created a "corridor" of cratonal deformation within which Laramide arches formed during an approximately 30° clockwise plate vector rotation, similar to that of Bird (1998). In contrast, Molzer and Erslev (1995) documented NE-SW oriented oblique-slip using minor fault slip data on the E-W trending Owl Creek arch and suggested that shortening on diversely-oriented arches was unidirectional throughout Laramide time (approximately NE directed). Complexities in interpreting regional vergence patterns were illustrated by Varga (1993), who showed that local stress re-orientation or strain partitioning can complicate interpretations of inferred shortening directions found in the Rocky Mountain foreland.

#### Structural Styles and Deformation Mechanisms

A vast body of literature on structural styles, deformation mechanisms, and balanced 2D models of basement-involved structures, particularly those in the Laramide Rocky Mountains, has been compiled over the last several decades. Early attempts to characterize the nature of basement-involved folding relied on vertical tectonic models to explain basement faulting patterns based on exposures of steeply-dipping faults within anticlinal hinges, such as the nearly vertical normal fault bounding basement exposed in Shoshone Canyon at Rattlesnake Mountain (Stearns, 1971, 1975, 1978). Subsequent studies by Brown (1984), Stone (1984), Erslev (1986), and Cook (1988) demonstrated that such vertical uplift, or "drape fold" models are untenable because restoration constraints of surface fold geometries require reverse fault interpretations at the basement level. Brown (1984) and Stone (1984) used line-length balancing to show that asymmetric,

basement-involved Laramide folds require reverse faults at the basement level, and that steeply-dipping fault geometries underlying these folds are untenable. Similarly, Erslev (1986) used area-balancing to validate reverse fault geometries below asymmetric, basement-involved Laramide folds and to infer the presence of intermediate, rotational fault blocks within basement fault zones. In a review of Rocky Mountain structural styles based on surface, seismic, and clay modeling data, Stone (1993) showed that shallowly dipping basement faults ( $20^{\circ}$ - $35^{\circ}$ ), thinning of the forelimb sedimentary section, simple shear-like folding of footwall strata, strain within the basement hanging wall tip, and fault-propagation folding, or “thrust folding”, commonly characterize deformation patterns within primary and secondary basement-involved structures.

Erslev (1986), Stanton (2002), and Stanton and Erslev (2004) proposed the rotational fault-bend fold model to simulate rigid-block motion, particularly rigid-block rotation, that appeared to characterize basement behavior in the Laramide foreland. These studies explained the common field observation that asymmetric Laramide folds exhibit shallowly-dipping backlimbs and steeply-dipping forelimbs by suggesting that translation of approximately rigid basement blocks occurred on curved master faults. Furthermore, these studies provided a mechanistic explanation for how fault-related folding within strata overlying basement could be produced by approximately rigid basement-block motion. Erslev (1991) suggested that previously invoked simple shear and kink-band geometries of fault-bend and fault-propagation folding (Suppe and Medwedeff, 1984, 1990) models do not adequately model the curved surfaces and complex strain patterns commonly observed in folds. Instead, he proposed the trishear kinematic model of fault-propagation folding offered a mechanism by which folding of

sedimentary rocks above rigid basement blocks occurs within an upward-widening triangular zone of shear with downward-tightening fold hinges. Theoretical modeling of trishear and other fault-propagation fold mechanisms has used numerical, finite-element, and computer models to describe and predict deformation geometries (e.g. Erslev and Rodgers, 1993; Hardy and Ford, 1997; Allmendinger, 1998; Zendher and Allmendinger, 2000; Johnson and Johnson, 2002). These studies demonstrated that in compressional settings, the diversity of fold geometries observed in the subsurface and in outcrop suggests multiple modes of folding. Erslev and Hennings (2004) integrated the rotational fault-bend fold model of Erslev (1986), Stanton (2002), and Stanton and Erslev (2004) with trishear fault-propagation folding to analyze basement-involved deformation, thus providing a modern approach by integrating multiple deformation mechanisms.

### Regional Geology

Cambrian to Tertiary sedimentary rock units within the region surrounding the southern Beartooth arch form an approximately 7 km-thick succession that nonconformably overlies Precambrian crystalline basement (Johnson, 1934; Pierce, 1966; Pierce and Nelson, 1968; Fig. 3). The heterogeneity of the Phanerozoic sedimentary section, characterized by strongly resistant Paleozoic limestones and weakly resistant Cretaceous shales, has produced spectacular exposures of fault-related folds. Laramide-age deformation of the Phanerozoic sedimentary section is principally displayed in Cambrian through Cretaceous age rocks, but seismic data and limited surface exposures of folding within Paleocene synorogenic units document Paleogene faulting on the NW margin of the Bighorn Basin (Pierce, 1966; Pierce and Nelson, 1968; DeCelles et al., 1991).

Tertiary	Willwood	Twi
	Fort Union	Tfu
Cretaceous	Lance (335m)	Kl
	Meeteetse (335m)	Km
	Mesaverde (365m)	Kmv
	Cody (640-765m)	Kc
	Frontier (150-170m)	Kf
	Mowry (120m)	Kmr
	Thermopolis (185m)	Kt
	Cloverly & Morrison (185m)	KJcm
Jurassic	Sundance (120m) Gypsum Spring (30m)	Jsg
Triassic	Chugwater (230-290m)	Tc
Permian	Phosphoria (25-50m)	Pp
Pennsylvanian	Tensleep (50-65m)	IPt
	Amsden (70-90m)	MIPa
Mississippian	Madison (215-245m)	Mm
Devonian	Three Forks (60m)	Dt
Ordovician	Bighorn (120m)	Ob
Cambrian	Gallatin (130m) Gros Ventre (225m) Flathead (35-45m)	C
Precambrian	Granite & Gneiss	pC

Fig. 3. Generalized stratigraphic column of the Precambrian through early Tertiary rocks of the Bighorn Basin, from Durdella (2001).

Published geologic mapping of the study area includes regional mapping at 1:62,500 by Pierce (1965a, 1965b, 1966, 1970) and Pierce and Nelson (1968, 1969), 1:24,000 mapping along the east flank of the Beartooth arch (O'Connell, 1996), and 1:24,000 mapping of the Horse Center anticline by Durdella (2001). Foose et al. (1961) and Wise (1983, 2000) described the structural geology of the northeastern and eastern Beartooth Mountains and documented a variety of complex range-front structures along the arch margins, including thrust, vertical, and tear faults associated with WSW-dipping master faults with nearly 8 km of structural relief. The Amoco 1 well, located on the NE corner of the Beartooth arch near Red Lodge, Montana, drilled through 2.5 km of Precambrian basement in the Beartooth hanging wall before passing through the Beartooth thrust and into Mesozoic units, demonstrating low-angle (10-15°) basement faulting in this area (Wise, 2000). In a series of cross-sections through the east flank of the Beartooth arch, O'Connell (1996) used this and other well data to suggest large-scale folding of the basement surface. This interpretation suggested that much of the strain along this segment of the arch margin occurred via parallel-folding of the basement surface.

Blackstone (1986a, 1986b) used abundant industry well data to map the regional subsurface structure along the western margin of the Bighorn Basin. These studies showed that deformation of the basement surface along this western margin occurred on diversely-oriented primary and secondary structures and that west-directed backthrusting within the basement hanging wall was common. Perhaps the best exposed of these secondary backthrust structures is Rattlesnake Mountain anticline. At Shoshone Canyon west of Cody, Wyoming, basement rocks are exposed in fault contact with tilted

Cambrian and Ordovician rocks of the anticlinal forelimb. The exposure of this steeply dipping ( $86^{\circ}$  SW) basement fault made this a classic locality for the school of vertical tectonics (Stearns, 1971, 1975, 1978). Subsequent studies using balancing constraints showed that a basement reverse fault was required at depth (Brown, 1984; Stone, 1984; Erslev, 1986; see discussion above). Complexity was added to the interpretation of this and other structures along the NW margin of the Bighorn Basin by Cenozoic detachment faulting on the Heart Mountain detachment and South Fork detachment structures (Pierce, 1987). Hennings and Hager (1996) documented both basement-involved and basement-detached hanging wall backthrusts along the western margin of the Bighorn Basin south of Oregon Basin anticline. Seismic data and interpreted cross-sections in this study showed that 1) offset on the southern segment of the Oregon Basin fault in this area was considerably less relative than offset to the north at Oregon Basin anticline; 2) basement backthrusting and/or large-scale folding of the basement surface may have accommodated much of the shortening in this area; and 3) a pre-existing basement weakness, the Tensleep Fault, appeared to influence the geometry of basement-involved backthrusts. The Tensleep Fault was also shown by Allison (1983) to influence the geometry of faults and folds exposed in sedimentary cover rocks on the east side of the Bighorn Basin.

### 3. METHODS

#### Minor Fault Analysis

Slip data from minor faults were collected from approximately 1,500 faults from diversely-oriented structures throughout the study area to test hypotheses concerning the influence of local versus regional inferred shortening directions. The kinematic, or movement, history of these structures was constrained by orientation and slip sense data from slickensided minor faults within sandstone-dominated units. Fault slip sense was determined in the field using the fracture criteria of Petit (1987), and orientation and slip sense data were analyzed using the stress inversion techniques of Compton (1966) and Erslev (2001). Fault plane attitudes, slickenside trends, plunges, and slip sense measurements were collected from 24 locations both within and away from anticlinal hinges/forelimbs. This analysis assumes that minor faults represent internal rock strain in response to an applied stress, and that the orientation of minor faults can be used to infer principal stress directions active during deformation. These data were compiled and sorted using Microsoft Access software, then analyzed in stereographic projection using the Orient software program (Vollmer, 1989), which calculates eigen data on groups of planes and lines. Ideal  $\sigma_1$  (principal stress) orientations for each fault in the data set were calculated based on an  $\alpha$  angle (half of the acute bisector of conjugate fault pairs) assigned by the investigator using the Select software program (Erslev, 1998). A  $\alpha$  value of  $20^\circ$  was used in this study based on the observation that this value most closely fits the conjugate faulting patterns of rock units within the study area, as well as its successful application in other areas of the Rocky Mountain foreland with similar stratigraphy and

basement faulting patterns (Erslev and Larson, 2006). The average ideal  $\sigma_1$  orientation for each data set was calculated using eigenvector analysis and eigenvalues were used to judge the consistency and/or scattering of the data. Eigenvalues can range from 0 to 1, and a highly clustered data set will have an eigenvalue close to 1 for its  $E_1$  eigenvector (ideal  $\sigma_1$ , or principal stress direction) and low eigenvalues for its  $E_2$  and  $E_3$  eigenvectors. Finally, overall kinematic patterns were analyzed by plotting the trends of ideal  $\sigma_1$  values as rose diagrams with smoothed,  $10^\circ$  increments for each data set in map view.

### Cross-Section Analysis

Two dimensional analysis was performed by constructing 16 restorable cross-sections aligned in orientations that approximate slip directions (see discussion, chapter 4) using 2DMove software. Surfaces used in the cross-sections include the Precambrian basement nonconformity, and the tops of the Cambrian Snowy Range Formation, Mississippian Madison Limestone, Triassic Chugwater Formation, Cretaceous Frontier Formation, and Cretaceous Meeteetsee Formation. Sections were constrained using new 1:12,000 scale field mapping within the hinges and forelimbs of the Rattlesnake Mountain and Pat O'Hara Mountain anticlines (mapping conducted summer, 2004), previously published 1:62,500 geologic mapping (Pierce, 1965a, 1965b, 1966, 1970; Pierce and Nelson, 1968a, 1969), publicly available industry well data (WYOGCC) from 173 wells, over 1,000 km of proprietary industry 2D seismic data (viewed during employment with ConocoPhillips, summer 2005), and several well, 2D, and 3D seismic data sets provided by Windsor Energy Company. Cross-section geometries were further constrained using restoration algorithms in the 2DMove software package including line

length unfolding, fault-parallel flow combined with inclined shear, and trishear fault-propagation folding. Line length and area balance were maintained where appropriate.

### 3D Surface Analysis and Restoration

3D surface and kinematic analyses were performed by creating and restoring surfaces of the six stratigraphic levels using surface creation algorithms to extrapolate between the 16 cross-sections in 3D Move software. For each surface, a 3D model was created that honored the 2D cross-section data as well as surface exposures of folds, fault offsets, and individual and branching fault blocks. A 3D restoration of each surface was conducted using the software's flexural slip flattening and jigsaw restoration algorithms. Surfaces were flattened and restored in kinematically appropriate directions (see discussion, chapter 4) using pin walls aligned approximately perpendicular to structural trends in areas of minimal distortion. Overlaps and gaps within restored surfaces were used to evaluate the geometric validity of the interpreted surfaces and hypotheses concerning the general kinematic framework.

## 4. KINEMATIC ANALYSIS

### Observations

Slickensided minor faults are common in tilted sandstone units throughout the area and are particularly abundant in the Pennsylvanian Tensleep Formation at sites where bedding dips steeply within anticlinal limbs. The fault surfaces are 1-10 mm thick, highly striated, quartz-rich zones that lack clay gouge and crop out as either erosionally resistant quartz shear bands or outcrop fracture faces. Where outcrop exposure is favorable, the faults occur as densely distributed sets of either thrust or strike-slip conjugate pairs, with spacings ranging from several meters to several millimeters. The minor fault plane and lineation data for all 24 collection locations are shown in Figures 4a, c, and d, presented collectively (Fig. 4a) and individually (Fig. 4c, d). Sets of both thrust and strike-slip conjugate pairs (relative to bedding orientation) are commonly present where minor faults are exposed in outcrop (e.g. location EF1, Fig. 4), however, one conjugate set can appear more prevalent due to the morphology and erosion patterns of a particular outcrop. At one location, BP1, slickensided quartz shear bands are abundant in outcrop, however, steep north and south facing canyon walls prevent exposure of the fault surfaces, resulting in a data set of 92 shear bands and 2 slickensided faults from this family of orientations (Fig. 4c, d). With several important exceptions, slickenside lineations at the majority of locations are approximately parallel to bedding dip and perpendicular to the line of intersection between the bedding and fault planes, suggesting that they were neo-formed during Laramide time. At several locations, however, minor faults are parallel to, or located on the plane of bedding, suggesting that

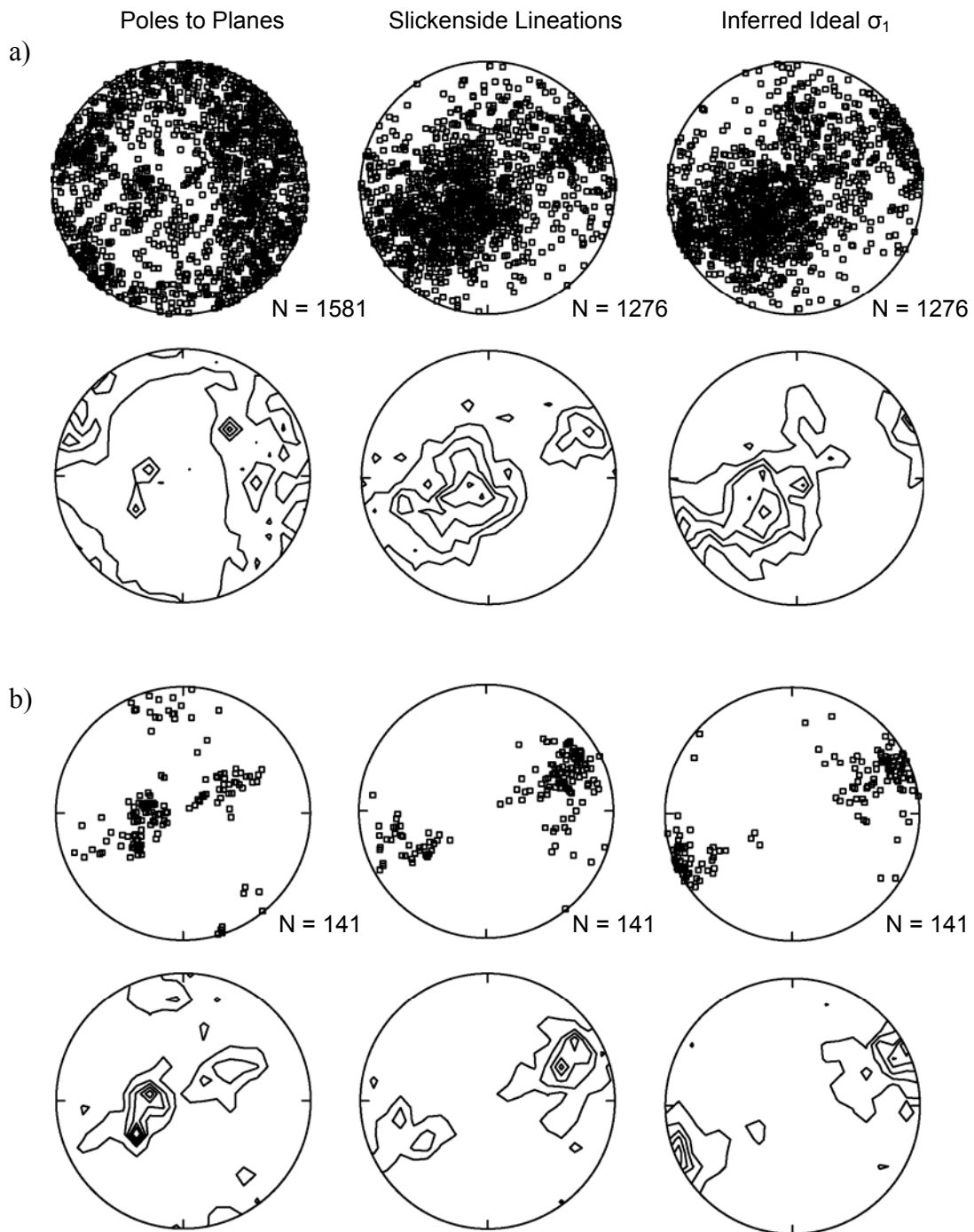
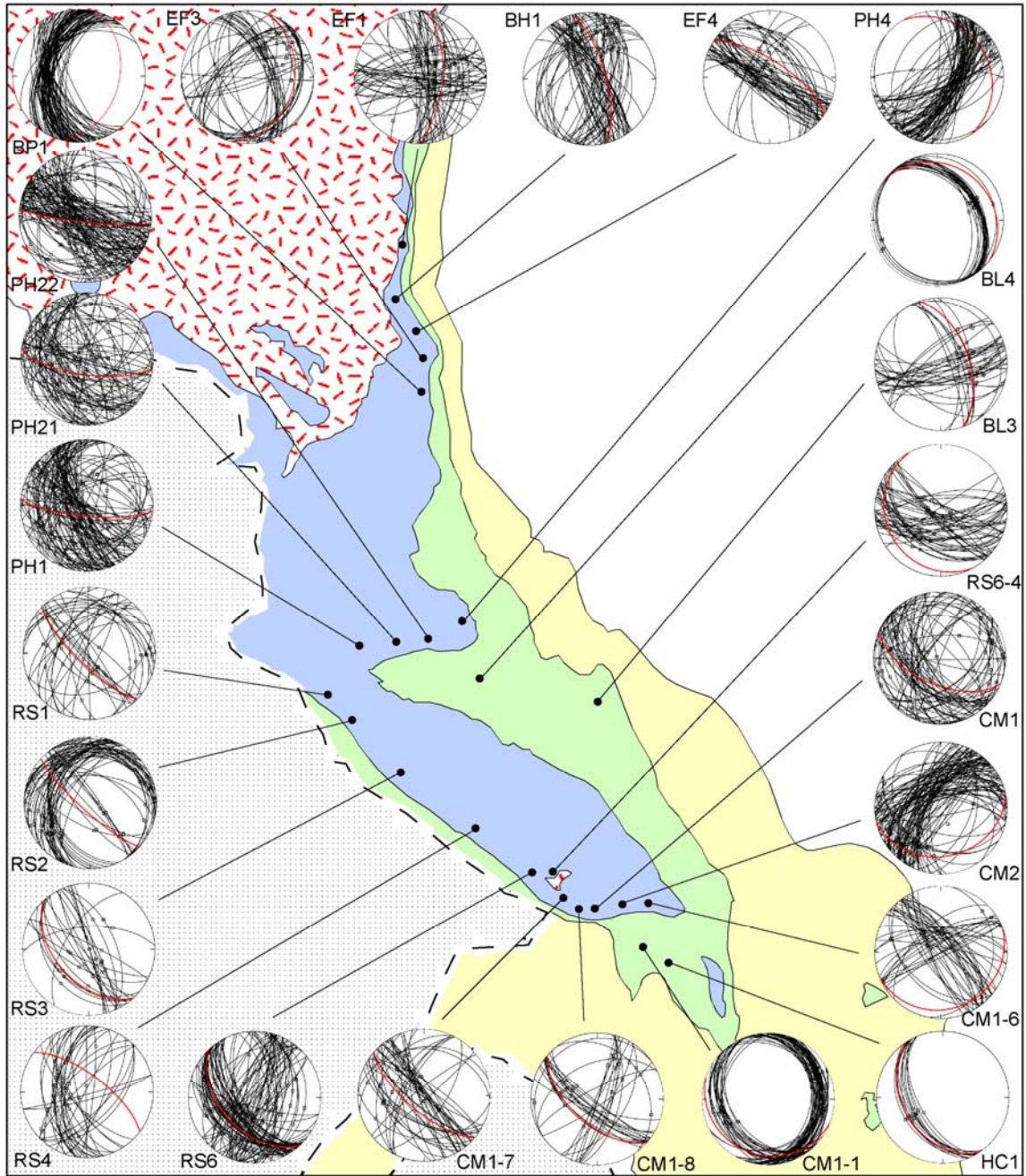
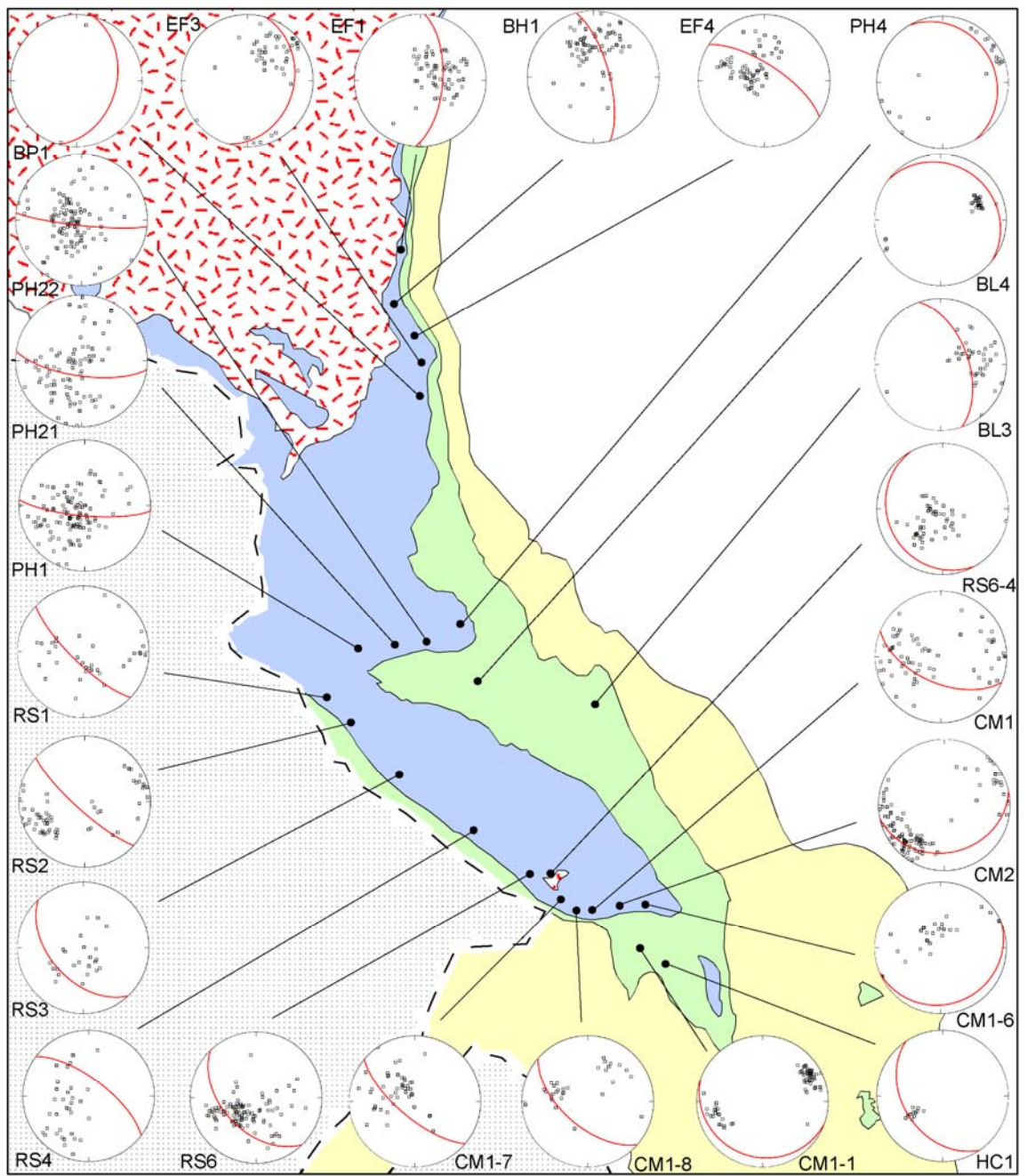


Fig. 4. (a,b) Stereonet plots showing poles to planes, slickenside lineations, inferred ideal  $\sigma_1$  orientations, and their respective contour plots for (a) all minor faults, and for (b) the off-axis subset of minor faults (see text for details). Contour plots are at 4% contour interval (a) and 0.8% contour interval (b). (c, d, following pages) Maps showing locations of 24 minor fault collection locations and stereographic projection of (c) fault plane orientations, slickenside lineations, and local bedding orientations and (d) slickenside lineations only. Geologic map units and scale are the same as those used in Fig. 2.

c)



d)



pre-existing heterogeneities in the rock may have affected minor faulting patterns. The correlation between bedding orientation and minor fault plane orientations is not strong, but can be seen at some locations in the stereonet plots in Fig. 4b. The quartz-rich fault surfaces exhibit well-preserved R, and locally R' fractures (Petit, 1987) perpendicular to slickenline trend, allowing their shear sense to be easily determined in the field.

The consistency of minor fault plane and lineation orientations at individual locations ranges from strongly consistent (values ranging within only 15°) to highly variable (values ranging within 180°). However, most sites show patterns that express themselves as sets of either thrust or strike-slip conjugate pairs (relative to bedding) when viewed in stereographic projection. The tendency for certain minor fault orientations to be favored in the data over others was observed in the field at some locations, particularly where steep canyon walls or other erosion-related outcrop features influence the exposure of fault orientations.

Faulting patterns were analyzed in their current orientations as well as their orientations after bedding dip was rotated to horizontal. Areas with steeply dipping bedding, such as the nearly vertical forelimbs of Pat O'Hara and Rattlesnake Mountain anticlines, show the greatest diversity of fault plane and slip orientations (e.g. locations PH2-1, RS1). Conversely, data collection locations situated away from steeply dipping anticlinal limbs show the strongest internal consistency of minor fault plane and slip orientation (Fig. 4b). Data from these four sites were collected from Jurassic and lower Cretaceous sandstone units, whereas the majority of all other data were collected from the Pennsylvanian Tensleep Formation.

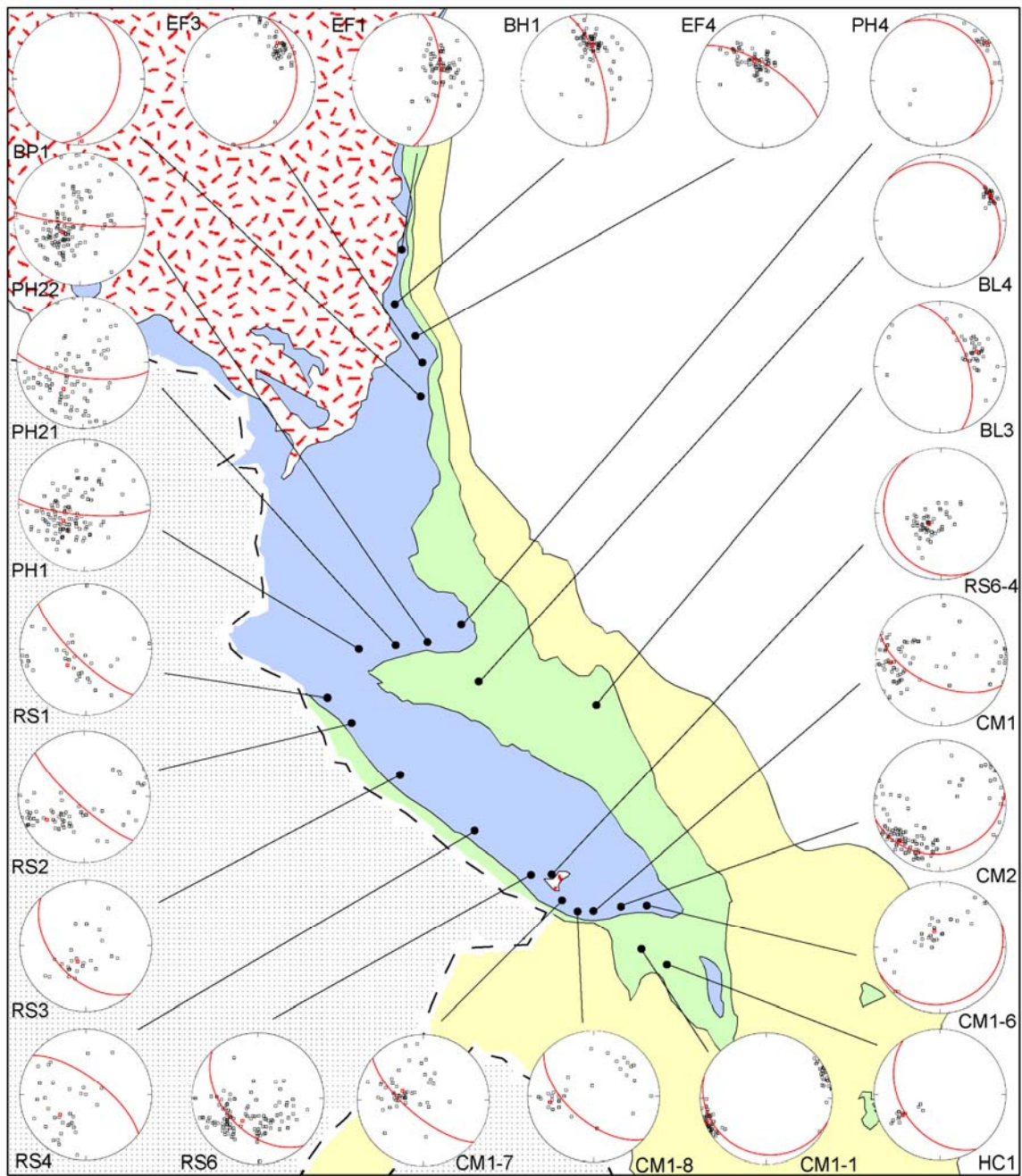


Fig. 5. Map showing 24 minor fault collection location and stereographic projection of inferred ideal  $\sigma_1$  orientations for each fault (black squares), average inferred ideal  $\sigma_1$  orientation for each data set (red squares), and local bedding orientation. Geologic map units and scale are the same as those used in Fig. 2.

Station	UTM (X)	UTM (Y)	Number (#)	Bedding	Average $\sigma_1$	Eigenvalue	Rotated $\sigma_1$
BH1	634209	4968767	70	345/70	010/44	0.8463	215/03
BP1	634801	4962668	2	015/39	177/07	0.961	356/06
CM1	645733	4927221	67	113/57	267/24	0.7069	079/06
CM2	647556	4927345	102	078/28	228/20	0.7359	223/05
CM1-6	649383	4927454	28	068/15	341/69	0.6467	350/84
PH1	630827	4945152	106	095/77	232/57	0.7187	103/41
PH2-1	632719	4945119	81	098/71	216/49	0.6049	027/17
PH2-2	632374	4945181	111	096/83	234/63	0.6617	026/11
PH4	637797	4946276	20	330/21	053/06	0.8581	233/15
CM1-7	645054	4927622	46	130/70	294/62	0.7544	247/11
CM1-8	644632	4927902	31	131/59	262/34	0.5606	075/15
RS1	627918	4942126	34	134/76	229/60	0.5704	047/16
RS2	630003	4942126	60	132/79	238/34	0.6512	060/43
RS3	634116	4935791	24	137/49	207/68	0.7403	219/20
RS6	642899	4929217	101	136/48	214/56	0.6711	219/08
RS4	638808	4932297	33	307/69*	232/49	0.6419	056/60
BL3	649602	4938589	38	341/55	067/40	0.8107	248/15
BL4	640358	4941968	29	308/17	064/16	0.9785	063/01
CM1-1	649818	4925013	62	110/16	248/03	0.9481	068/08
HC1	651767	4925934	12	146/40	241/36	0.9277	060/04
RS6-4	644068	4929296	49	151/17	228/70	0.8634	234/53
EF1	633674	4972731	65	004/62	064/57	0.8448	258/01
EF3	635167	4965069	50	016/30	036/28	0.8402	047/14
EF4	635541	4966247	61	303/70	339/63	0.8765	011/03

Note: Raw data is available through Eric Erslev, Colorado State University.

Table 1. Station names, UTM coordinates, average ideal  $\sigma_1$  orientations (modern and rotated), and eigenvalues for average ideal  $\sigma_1$  orientations for each minor fault collection location. Asterisk (\*) indicates overturned bedding.

The distribution of inferred ideal  $\sigma_1$  orientations for individual faults shows a stronger clustering of orientations at most data locations than do the fault plane and lineation data (Fig. 5). This tendency for faulting patterns to become apparent in inferred ideal  $\sigma_1$  orientation plots appears to result when multiple conjugate fault set orientations occur in steeply dipping strata. Inferred ideal  $\sigma_1$  orientations are most strongly clustered ( $E_1 > 0.8191$ ) at the four locations situated away from anticlinal limbs (BL4, HC1, CM1-1, BL3; Figs. 4b, 5) and the four northernmost locations on the east flank of the Beartooth arch (EF1, EF2, EF4, BH1, Fig. 5). Eigenvalues for these eight data sets range from 0.9785 to 0.8191, higher than at any other locations (Table 1).

#### Rotation to Horizontal

The clustering of inferred ideal  $\sigma_1$  orientations shows a strong correlation with bedding attitude, and the average  $\sigma_1$  orientation for most locations (shown in red, Fig. 5) lies approximately on that station's bedding plane. Because the bedding at most data collection locations dips moderately to steeply, these average inferred ideal  $\sigma_1$  orientations range widely in trend ( $032^\circ$ - $341^\circ$ ), and more tellingly, in plunge ( $3^\circ$ - $70^\circ$ ), (Table 1). Therefore, if the fault and  $\sigma_1$  data are rotated about the bedding strike in the amount of bedding dip, effectively unfolding bedding, most locations show ideal  $\sigma_1$  orientations indicative of approximately horizontal shortening (Figs. 6, 7). Many of the fault plane and lineation patterns become more visually evident through this exercise. For example, the rotation of plane and lineation data from locations RS6 and BH1 each reveal high-angle strike-slip and a low-angle thrust fault conjugate pairs that are difficult to recognize in their modern, tilted orientations (compare Figs. 6 and 4).

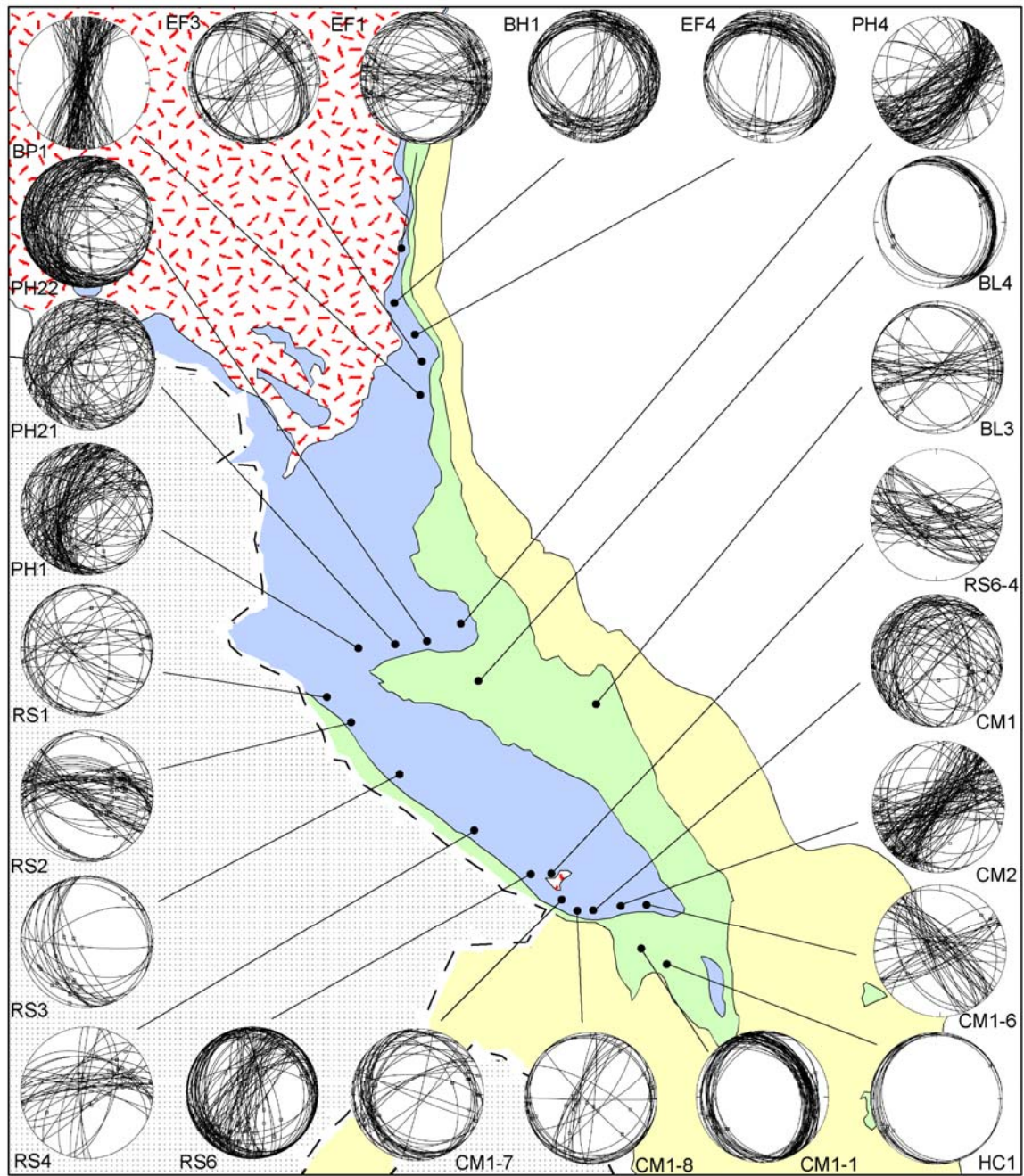


Fig. 6. Map showing locations of 24 minor fault collection location and stereographic projection of rotated fault plane orientation and slickenside lineations (see text for details). Geologic map units and scale are the same as those used in Fig. 2.

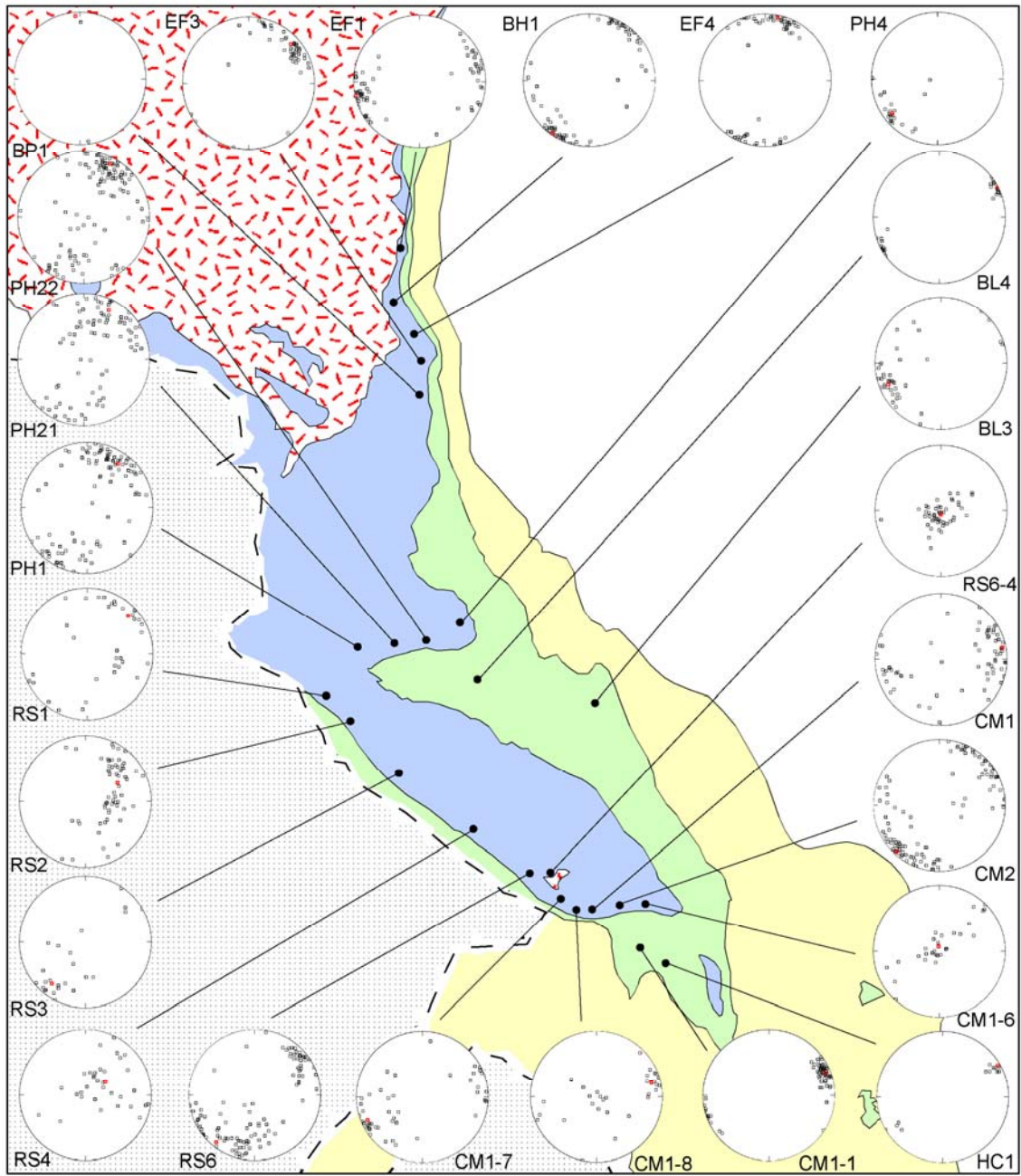


Fig. 7. Map showing locations of 24 minor fault collection location and stereographic projection of rotated inferred ideal  $\sigma_1$  orientations for each fault (black squares) and rotated average inferred ideal  $\sigma_1$  orientation for each data set (red squares). Geologic map units and scale are the same as those used in Fig. 2.

This “rotating out” of bedding, however, makes several fundamental assumptions about the deformation processes active during minor fault formation: 1) the bedding strike used to unfold bedding remained the same during folding and was the only rotation axis operative at that location; 2) vertical axis rotations did not play an important role during anticlinal folding; and 3) either minor faulting occurred in the rocks when bedding was originally sub-horizontal or shallowly dipping, or stresses during deformation were aligned approximately parallel to bedding. Assumptions (1) and (2) can be tested by analyzing the clustering patterns of ideal  $\sigma_1$  orientations because vertical axis rotations should cause weak clustering. Generally, ideal  $\sigma_1$  orientations are clustered, however, in at least one area (Pat O’Hara Mountain forelimb) and possibly another (Rattlesnake Mountain forelimb), minor fault patterns show low eigenvalues and thus can be interpreted as having experienced local vertical-axis rotation, and correspondingly, these two areas also show the weakest ideal  $\sigma_1$  clustering (Fig. 5). Assumption (3) is supported by the remarkable proximity of ideal  $\sigma_1$  orientations to the plane of bedding at most locations and the observation that minor faults are present in the study area within shallowly dipping strata (15°-30°). However, the possibility of local fold-related refraction of the stress field cannot be ruled out, and may have occurred at Rattlesnake Mountain and Canyon Mouth anticlines.

### Interpretations

The orientations of inferred ideal  $\sigma_1$  can be more easily visualized by plotting the spread of shallowly-dipping (<45°), rotated ideal  $\sigma_1$  orientations at each location as a single, smoothed rose diagram, and then geographically plotting each rose diagram on a map (Fig. 8). The shallowly dipping values (<45°) from within the rotated data sets

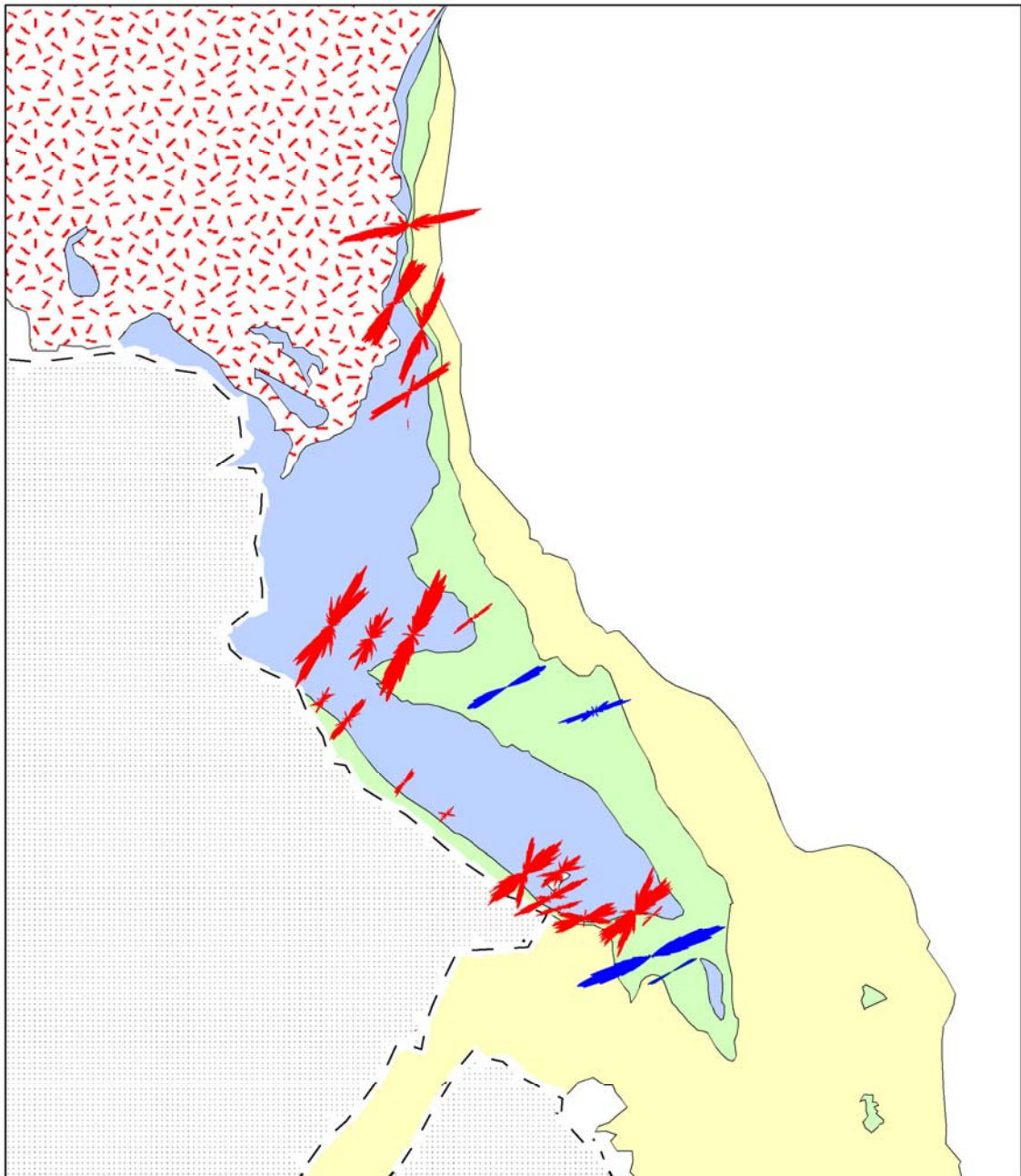


Fig. 8. Map showing rose diagram distributions of inferred ideal  $\sigma_1$  orientations for each of the 24 minor fault collection locations. Red rose diagrams are from sites located within steeply-dipping fold limbs and blue rose diagrams are from sites located away from steeply-dipping fold limbs. Geologic map units and scale are the same as those used in Fig. 2.

comprise the majority of data points at each location and are interpreted to represent horizontal shortening. In Fig. 8, red rose diagrams show the trends of interpreted shortening directions of sites situated within steeply-dipping anticlinal limbs, whereas blue rose diagrams are from the sites located away from the axes of major folds. Four principal observations can be made from this map distribution of interpreted shortening directions:

- 1) The four sites located away from steeply dipping anticlinal limbs (blue rose diagrams) comprise the most internally consistent group of orientation data (highest eigenvalues, least variation in orientation – see Table 1). The average ideal  $\sigma_1$  orientations for each of these sites agree within  $7^\circ$ , with an average orientation of  $065^\circ$ .
- 2) The three sites located within the steeply south-dipping forelimb of Pat O’Hara Mountain anticline show rotated ideal  $\sigma_1$  orientations that are intermediate ( $020^\circ$ - $025^\circ$ ) between the structure’s N-S dip directions and the four aforementioned off-axis orientations (approximately  $065^\circ$ ). Although fault data from these three locations show the greatest diversity of fault plane and slickenside lineation orientations (Fig. 4), their ideal  $\sigma_1$  orientations are surprisingly well clustered and show intermediate eigenvalues (0.7187, 0.6617, and 0.6049; Table 1). This indicates that Pat O’Hara Mountain anticline developed during horizontal shortening oblique to both the structure’s E-W trend and to the off-axis  $065^\circ$  signature.
- 3) The two sites (EF1 and EF3) located within approximately N-S striking strata on the N-S-trending segment of the southern Beartooth arch exhibit inferred

shortening directions oblique to local fault strike. The acute bisector of strike-slip and thrust fault conjugate pairs at EF3 are oblique to bedding dip, resulting in an average ideal  $\sigma_1$  orientation similar to the off-axis  $065^\circ$  signature (Figs. 6, 7).

- 4) Rattlesnake Mountain anticline shows overall inferred shortening directions approximately perpendicular to fold trend ( $219^\circ$ ), which is  $26^\circ$  oblique to the off-axis  $065^\circ$  signature. Locally, Rattlesnake Mountain anticline shows bimodal distributions of shortening directions that range between the overall Rattlesnake Mountain signature and the off-axis  $065^\circ$  signature.

These observations on the interpreted shortening direction data falsify several hypotheses concerning the region's kinematic development. First, the Pat O'Hara Mountain data show that slip on all structures in the area is not perpendicular to fold trends, and that Pat O'Hara Mountain anticline did not form at an ideal orientation to regional or local shortening directions. Instead, the data suggest that oblique-slip occurred on this, and possibly other structures. Second, data distant from anticlinal axes indicate one shortening direction and are incompatible with multi-stage, multi-directional shortening hypotheses.

The off-axis sites appear to represent an approximately uniform regional shortening direction interpreted to have affected the entire study area. Shortening direction data proximal to the Beartooth Fault, except locally on the secondary Canyon Mouth anticline, are clearly oblique to local strike, and show a strong similarity to this regional signature identified by off-axis locations. In this case, sites proximal to a primary fault system appear to document the regional shortening direction. This data suggests that the N-S trending east flank of the southern Beartooth arch is an oblique-slip

segment, as suggested by the oblique-slip EF1 and EF2 data sets. Because all three of the secondary structures in the area (Canyon Mouth, Pat O'Hara, and Rattlesnake Mountain anticlines) show shortening directions oblique to the interpreted regional shortening direction, data proximal to primary faults and away from secondary structures may provide the only opportunities to identify regional shortening directions.

Minor faults from the southernmost location on the east flank Beartooth arch (BP1) are tightly-clustered, high-angle strike-slip faults and shear bands that suggest a N-S shortening direction (Figs. 4, 6). These anomalous data may document the strike-slip component of an overall oblique-slip system that has been partitioned into N-S oriented strike-slip and E-W oriented shortening components. Similar processes have been documented at oblique convergent margins, particularly in Sumatra (Yu, 1993), and was suggested by Varga (1993) as an explanation for divergent shortening directions in other Laramide structures. If slip was partitioned along the Beartooth arch's east flank between E-W thrusting and N-S strike-slip faulting, the more northerly shortening directions observed at Canyon Mouth anticline ( $011^\circ$ ,  $215^\circ$ ) may suggest that this structure formed in response to complex strain partitioning, perhaps guided by basement weaknesses or other processes.

The locally oblique shortening directions documented at the area's three secondary structures may be explained by either 1) local, folding-related stress refraction; or 2) local vertical axis rotation associated with material rotation. At Pat O'Hara Mountain, the widely-scattered ( $000^\circ$  to  $070^\circ$ ), but dominant  $023^\circ$  shortening signature can be interpreted as either fold-related stress refraction, or the product of local material rotation within a zone of oblique-slip. In the latter hypothesis, the early shortening

direction recorded in the rocks ( $065^{\circ}$ ) was progressively rotated in a counter-clockwise sense about a vertical axis to its present average orientation of  $023^{\circ}$ . This hypothesis suggests that Pat O'Hara Mountain anticline formed from an older, inherited, and obliquely-reactivated basement structure. At Rattlesnake Mountain and Canyon Mouth anticlines, however, the shortening directions are approximately perpendicular to the fold trend, suggesting that folding-related stress reorientation was responsible for the observed shortening directions.

There does not appear to be a strong correlation between local dip direction and inferred shortening direction. Because several different processes appear to have contributed to the diversity of local shortening directions with respect to local structural trend, dip direction at individual locations is not strongly correlated with particular directions of inferred shortening. For example, minor fault data from south dipping strata at the SE plunge of Rattlesnake Mountain anticline show average inferred shortening directions ranging between  $065^{\circ}$  and approximately  $045^{\circ}$ , whereas south-dipping strata in the forelimb of Pat O'Hara Mountain anticline show shortening directions closer to  $025^{\circ}$ . This observation suggests that a complex combination of regional and local rotation, refraction and/or strain partitioning processes is necessary to explain the observed minor fault patterns.

## 5. TWO-DIMENSIONAL CROSS-SECTION ANALYSIS

### Two-Dimensional Modeling Constraints

The interpretation that the study area experienced an approximately uniform, regionally-consistent shortening direction during deformation indicates that 2D or 3D restorations are best conducted within a 065° vertical-striking slip plane. Figure 10 shows the locations of the 16 065°-striking cross-sections constructed for 2D analyses. The locations and distributions of cross-sections were based on 1) favorable surface exposures of fault and fold geometries within the newly mapped forelimbs and crests of the Rattlesnake Mountain and Pat O'Hara Mountain anticlines; 2) the location of available well and seismic data; and 3) an attempt to maintain an approximately even spacing between cross-sections for consistent surface extrapolation during 3D model construction.

Surface contact, surface dip, seismic, and well dip and formation top data were used to constrain 2D geometries (Fig. 11). As a general rule, dip data were projected parallel to local strike; wells and surface dip data were projected from exact X, Y, Z locations by first importing their X, Y, and Z coordinates into the 2D Move map database from a GIS database that integrated field mapping with digital elevation models (DEMs). This approach allowed attitude data from field mapping within well-exposed canyons in the Rattlesnake Mountain and Pat O'Hara Mountain anticlinal crests and forelimbs to be accurately projected onto cross-sections.

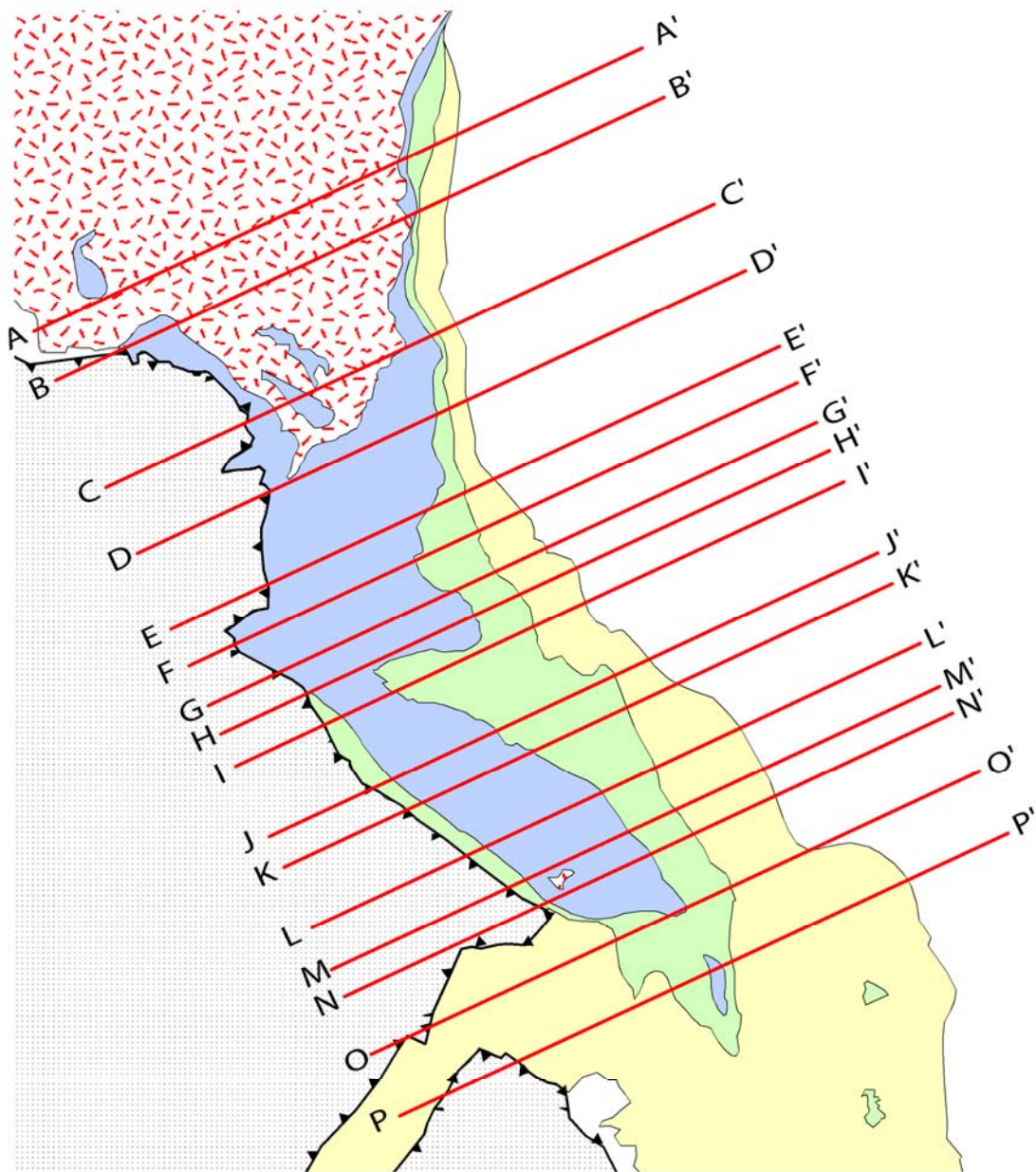


Fig. 10. Map showing locations of cross sections constructed in this study. Geologic map units and scale are the same as those used in Fig. 2.

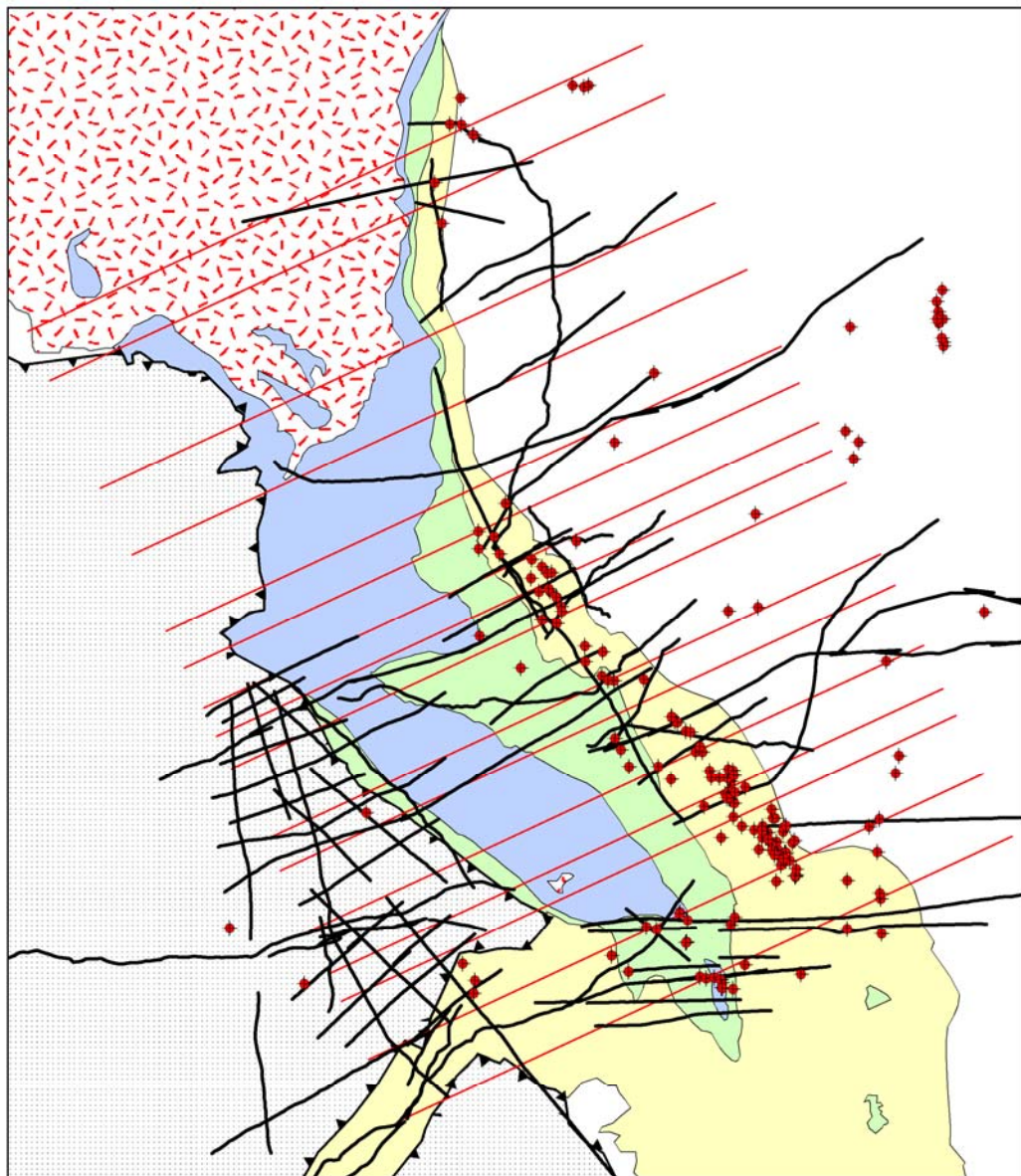


Fig. 11. Map showing locations of cross sections constructed in this study (red lines), proprietary industry seismic data (black lines), and publically available well data (red circles with black crosses) used in this study. Geologic map units and scale are the same as those used in Fig. 2.

## Observations

### *Regional Observations*

The northwest margin of the Bighorn Basin juxtaposes structurally high Precambrian crystalline basement rocks to the west against the Paleozoic through Tertiary sedimentary sequence that overlies basement to the east. On the western side of this margin, basement rocks crop out in the Beartooth Mountains and at Rattlesnake Mountain; within the Bighorn Basin to the east, industry seismic and well data indicate that the basement nonconformity lies approximately 9 km below sea level and dips shallowly to the west. Seismic data across this structural margin ubiquitously show west-dipping null zones, interpreted as faults, that offset the basement nonconformity. This margin is the principal structural feature of the northwest Bighorn Basin and is exposed at the surface only along the east flank of the Beartooth arch, where it crops out as west-dipping splays of the Beartooth Fault. To the south, the fault system is blind at the surface, however, seismic data show that the rocks are faulted and tightly folded at lower structural levels, and open to gently folded at higher structural levels. Previous authors identified this blind feature as the Line Creek and Oregon Basin Faults (e.g. Blackstone, 1986a).

Along the NW Bighorn Basin margin, Cambrian through early Tertiary sedimentary rocks on the west side of the margin dip east except locally within secondary folds. This regional east dip within surface exposures is steep (up to vertical) along the east flank of the Beartooth arch and shallows to the south to approximately 20° at Dead Indian Hill and to 13° farther south, east of Rattlesnake Mountain. Directly above the blind Line Creek Fault, Cretaceous units exposed at the surface steepen abruptly to 40°-

60° where they are unconformably overlain by Tertiary basin fill. Several tight to open secondary folds with strike lengths ranging from approximately 2 to 5 km are present within the shale-rich Cretaceous units above the blind fault segment, including the Shoshone, Fish Hatchery, Cottonwood, and Heart Mountain anticlines.

#### *Rattlesnake Mountain and Pat O'Hara Mountain Anticlines*

The largest, best exposed, and most well-known secondary basement-involved structure in the area is the NW trending, approximately 27 km long Rattlesnake Mountain anticline. The structure is asymmetric with a 12°-15° NE dipping backlimb and an overturned to 45° SW dipping forelimb. Much of the forelimb exposed along the NW half of the structure is uniformly vertical, with an arcuate anticlinal fold exposed at the level of the Mississippian Madison Limestone. Dramatic exposures of the fold crest and vertically-dipping forelimb are present in steep canyons along this segment (Fig. 12a). The forelimb of the SE half of the anticline is vertical to overturned except at two isolated, approximately 1.5 km long stretches, where the forelimb dips 46°-60° (Canyon Creek and Shoshone Canyon, Fig. 12b). Exposures of a planar nonconformity within basement rocks at Shoshone Canyon indicate that little if any folding of the basement rocks occurred during formation of this section of Rattlesnake Mountain anticline. The anticline terminates to the SE at Cedar Mountain in an abruptly plunging anticlinal nose. The NW termination the structure's axis is exposed at the level of the Mississippian Madison Limestone, where the backlimb and crest are gently folded in a smooth transition into the crest of the E-W-trending Pat O'Hara Mountain anticline. The Rattlesnake Mountain backlimb is faulted where it meets Pat O'Hara Mountain, with

a)



b)



Fig. 12. (a) View looking north near cross-section I-I' at the Rattlesnake Mountain anticline, and (b) view looking NW near cross-section J-J' at the Rattlesnake Mountain anticline. In (a), forelimb strata are approximately vertical and in (b), forelimb strata dip between  $45^\circ$  and  $50^\circ$  SW. In both views, the backlimb dips approximately  $13^\circ$  NE.

Triassic through Pennsylvanian rocks abruptly folded into the Pat O'Hara Mountain anticline's forelimb and faulted through at the level of the Pennsylvanian/Mississippian Amsden Formations. Although the confluence of the Rattlesnake Mountain and Pat O'Hara Mountain anticlines is partially covered by rocks of the Heart Mountain Detachment and Tertiary Absaroka volcanics, a south-dipping exposure of Paleozoic rocks directly west of the structural confluence suggests that the Pat O'Hara Mountain anticline extends west beneath the Heart Mountain Detachment and that Rattlesnake Mountain anticline terminates by abutting into Pat O'Hara Mountain anticline.

Seismic data through the northwestern half of Rattlesnake Mountain clearly show the presence of an approximately 15°-20° SW dipping, fault-bounded basement block lying between the Rattlesnake Mountain footwall and backlimb hanging wall. The presence of a similar intermediate fault block in the southeastern half of the anticline was hypothesized in previous studies by Erslev (1986, 1993). In seismic data from NW Rattlesnake Mountain, the basement nonconformity and overlying rocks of this intermediate block are not folded and are bounded by NE-dipping swaths of low resolution data. This block is more clearly imaged in data from the northwestern half of the anticline. The seismic data used in this study were not available to Erslev (1986, 1993), and the intermediate basement block interpretation in that study was based on area balancing of the footwall and hanging wall blocks and analogous, but deeper structural exposures in the northern Teton Range, Wyoming.

Basement rocks are not exposed at Pat O'Hara Mountain, although the structure shows a vertically-dipping forelimb similar to the Rattlesnake Mountain forelimb, which in this case is faulted through, placing Mississippian Madison Limestone in contact with

the Pennsylvanian/Mississippian Amsden Formations. The fold is approximately 17 km long, 4 km wide, and plunges east near the blind margin of the Bighorn Basin.

#### *Horse Center and Oregon Basin Anticlines*

Southeast of Rattlesnake Mountain, the NNW-trending, 10 km long Horse Center anticline originates at the southeastern plunge of Rattlesnake Mountain anticline. The structural culmination at Horse Center anticline is lower than at Rattlesnake Mountain, and the lowest stratigraphic level exposed is the Triassic Chugwater Formation. The fold geometry ranges from open in the north to close in the south, with a more pronounced asymmetry to the west in its southern half (up to 83° WSW dipping forelimb). The backlimb on the structure's east side is non-planar and is folded, with dips ranging from 12° to overturned.

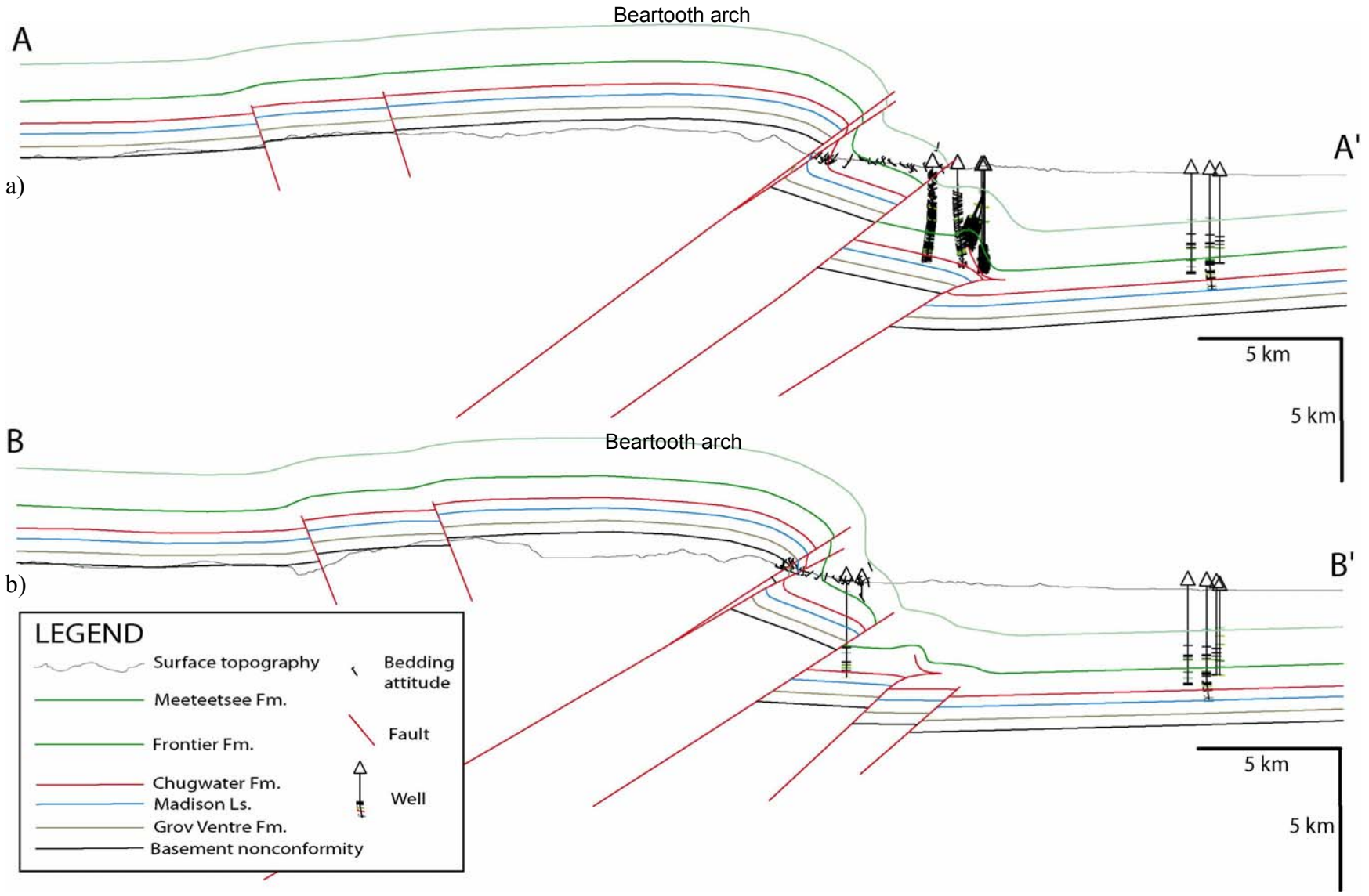
East of Horse Center anticline, a synclinal axis exposed within Cretaceous rocks forms the western boundary of the N-S-trending, northern segment of the Oregon Basin anticline. The Oregon Basin anticline is the western margin of the Bighorn Basin at this latitude, which defines an eastward step in the basin margin from the Line Creek Fault to the north. Seismic data through this structure shows a west-dipping fault zone that offsets the basement nonconformity with approximately 6 km of vertical separation (Stone, 1984). Cretaceous rocks exposed at the surface are gently to openly folded in a symmetric fold that gently plunges north at the latitude of Cedar Mountain.

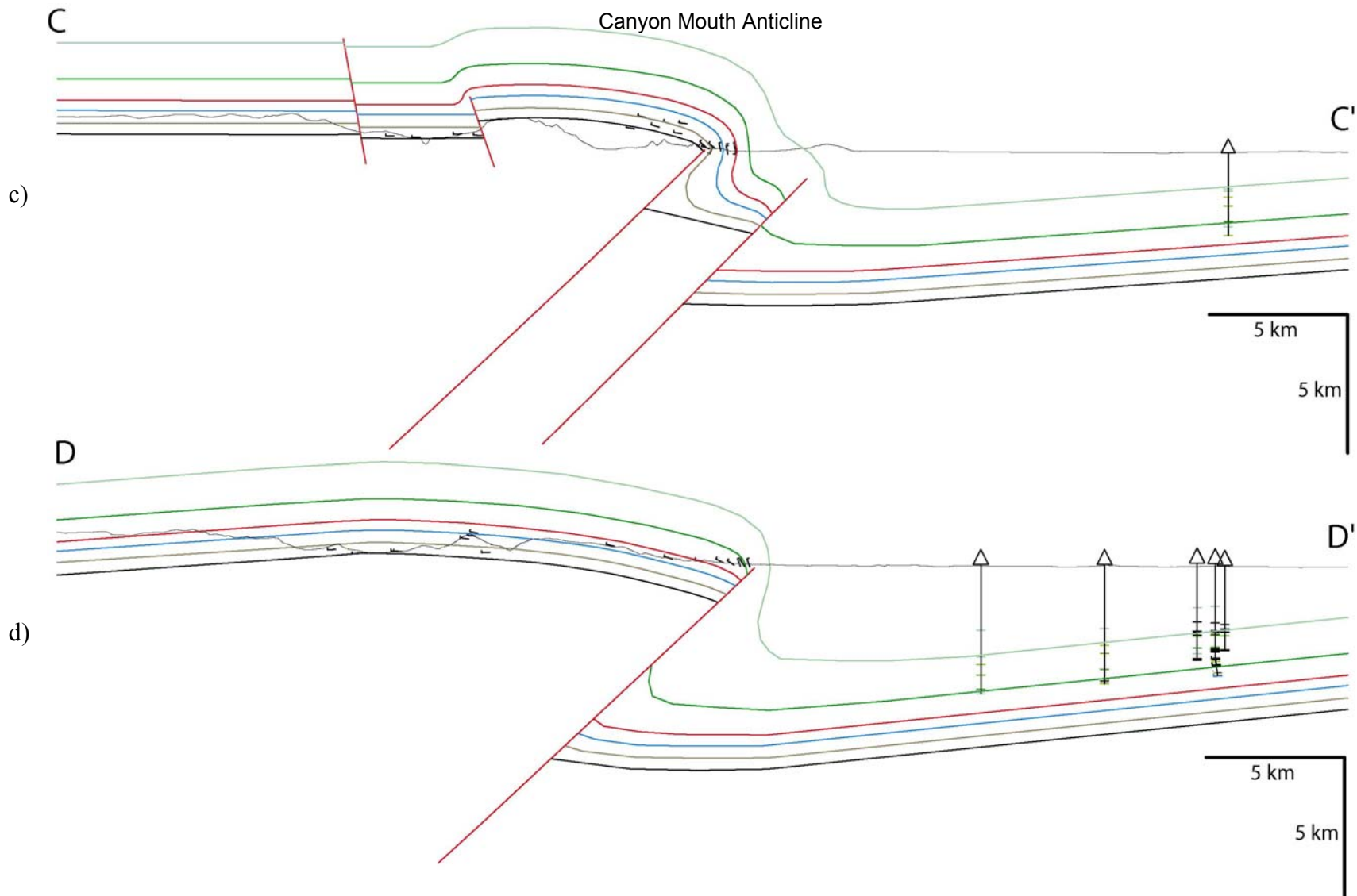
#### Interpretations

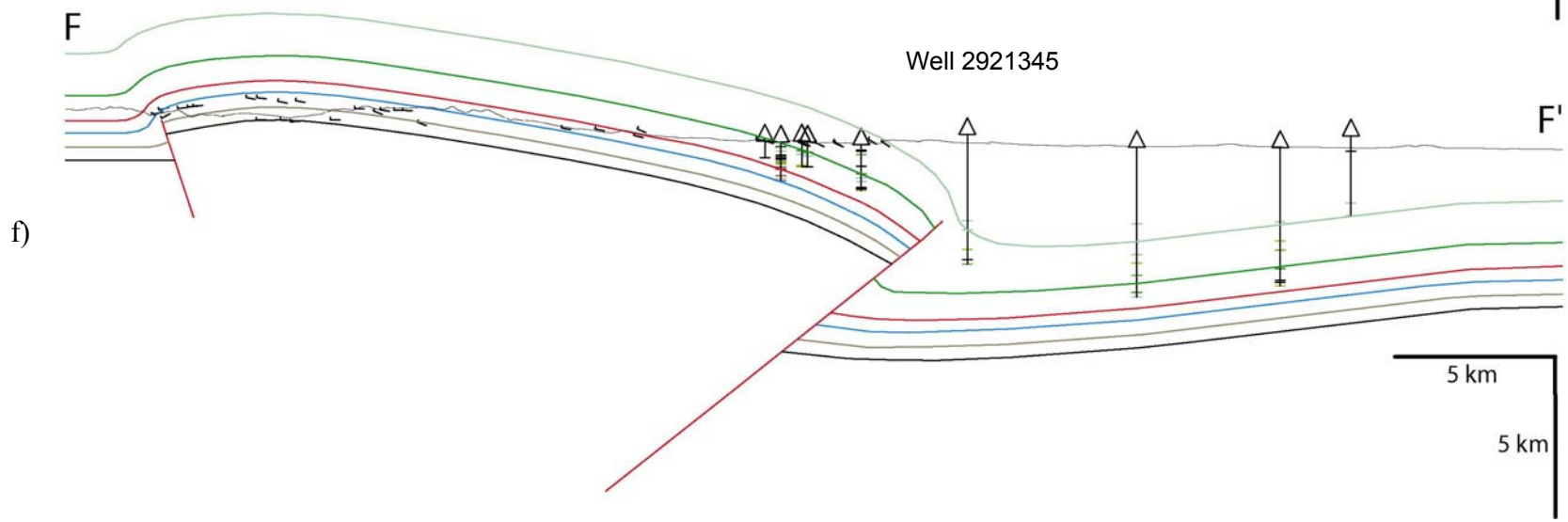
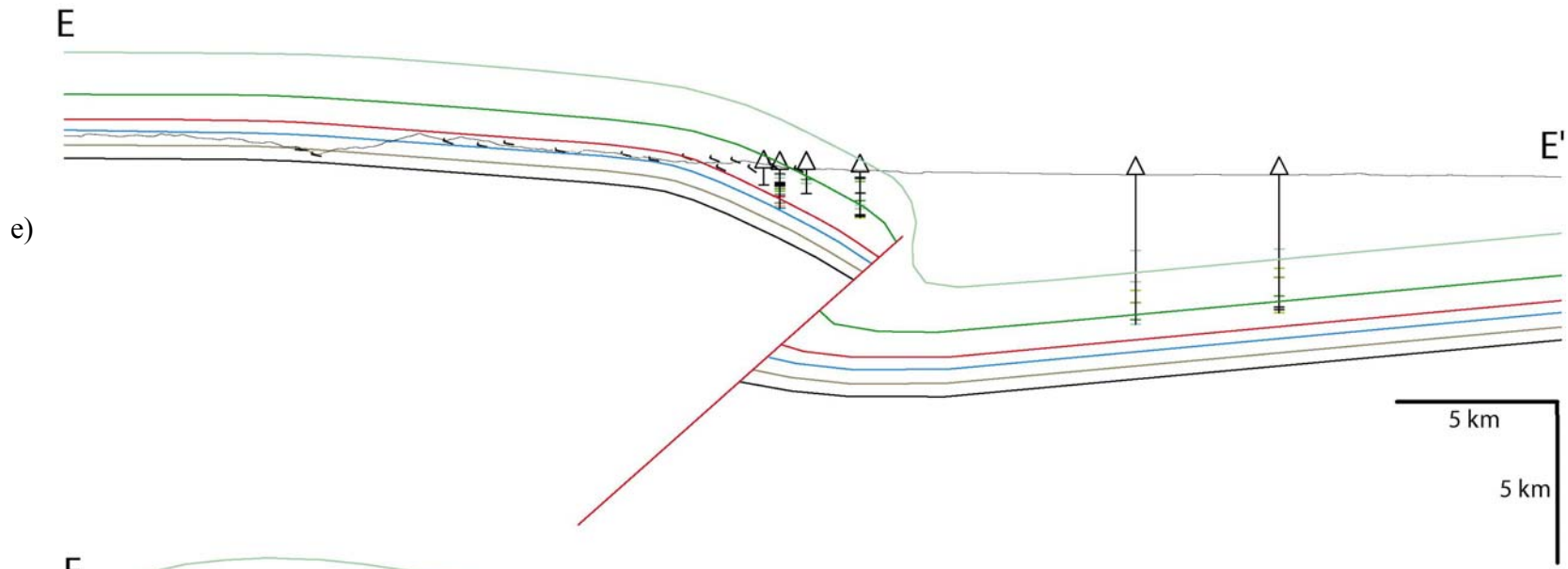
##### *Beartooth/Line Creek/Oregon Basin Fault Systems*

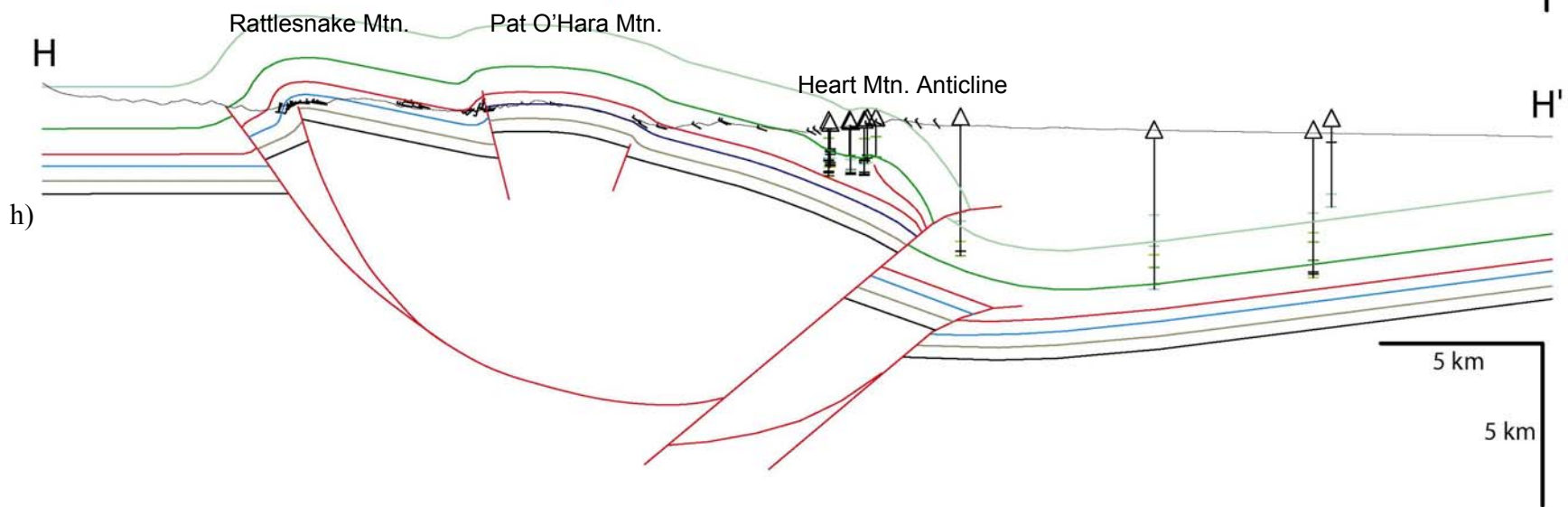
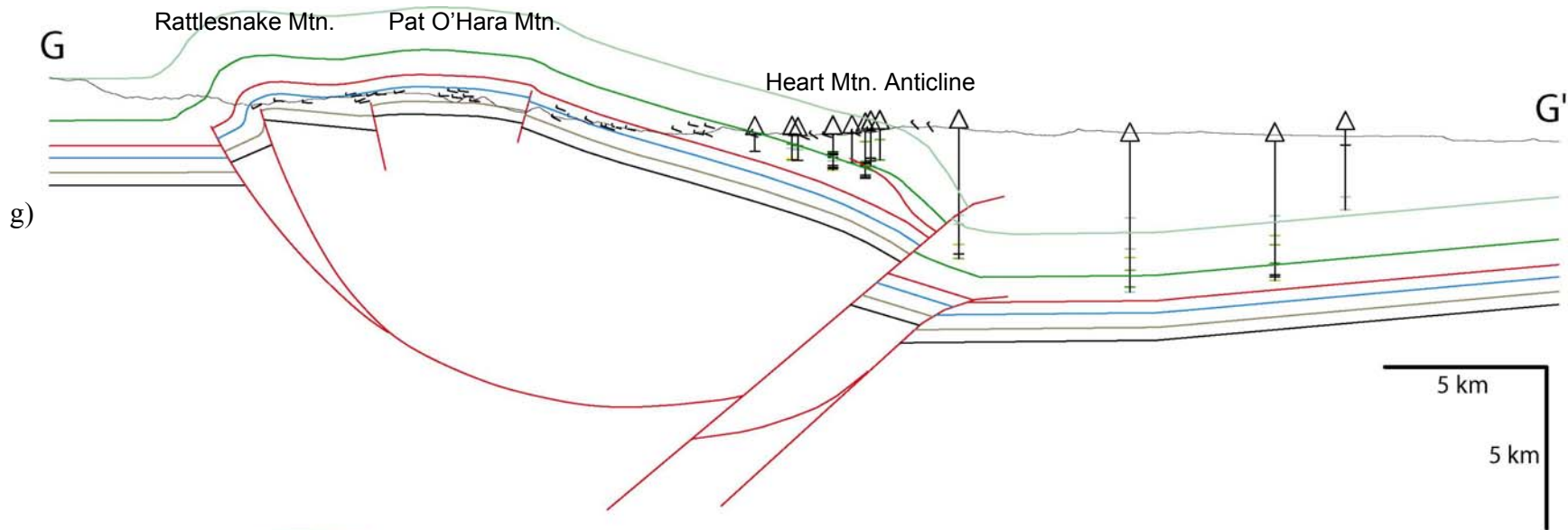
The 2D geometry of the fault systems bounding the NW margin of the Bighorn Basin vary along strike in number of faults, fault proximity, fault offset, and associated

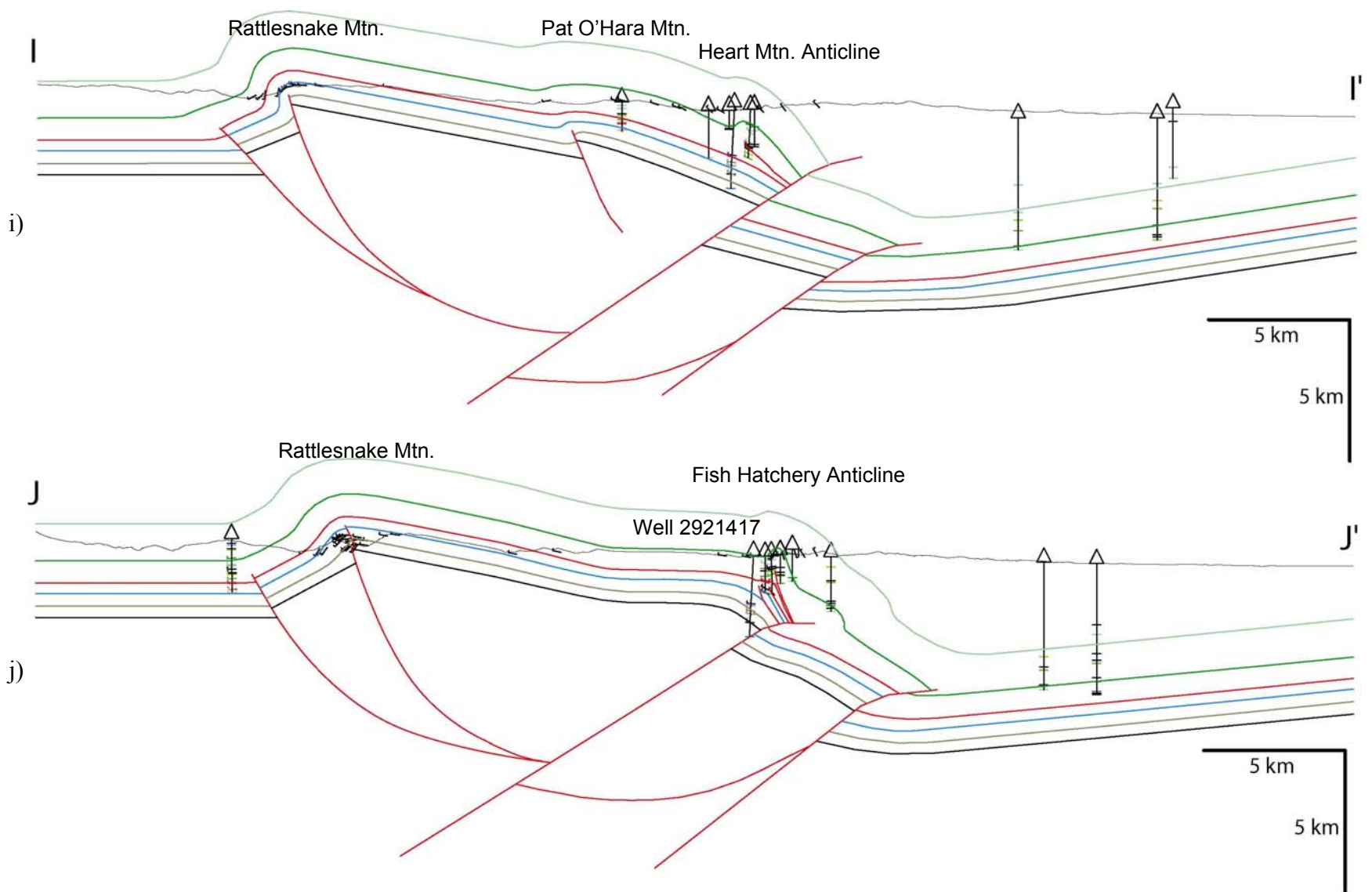
Fig. 13. Cross sections A-A' through P-P' (a-p) showing interpreted 2D geometries based on surface, well, and seismic data, as discussed in chapter 5. An explanation of fault geometries is also provided in chapter 5. Cross section locations and the locations of available well and seismic data are shown in Figs. 10 and 11. The Heart Mountain Detachment is not shown.

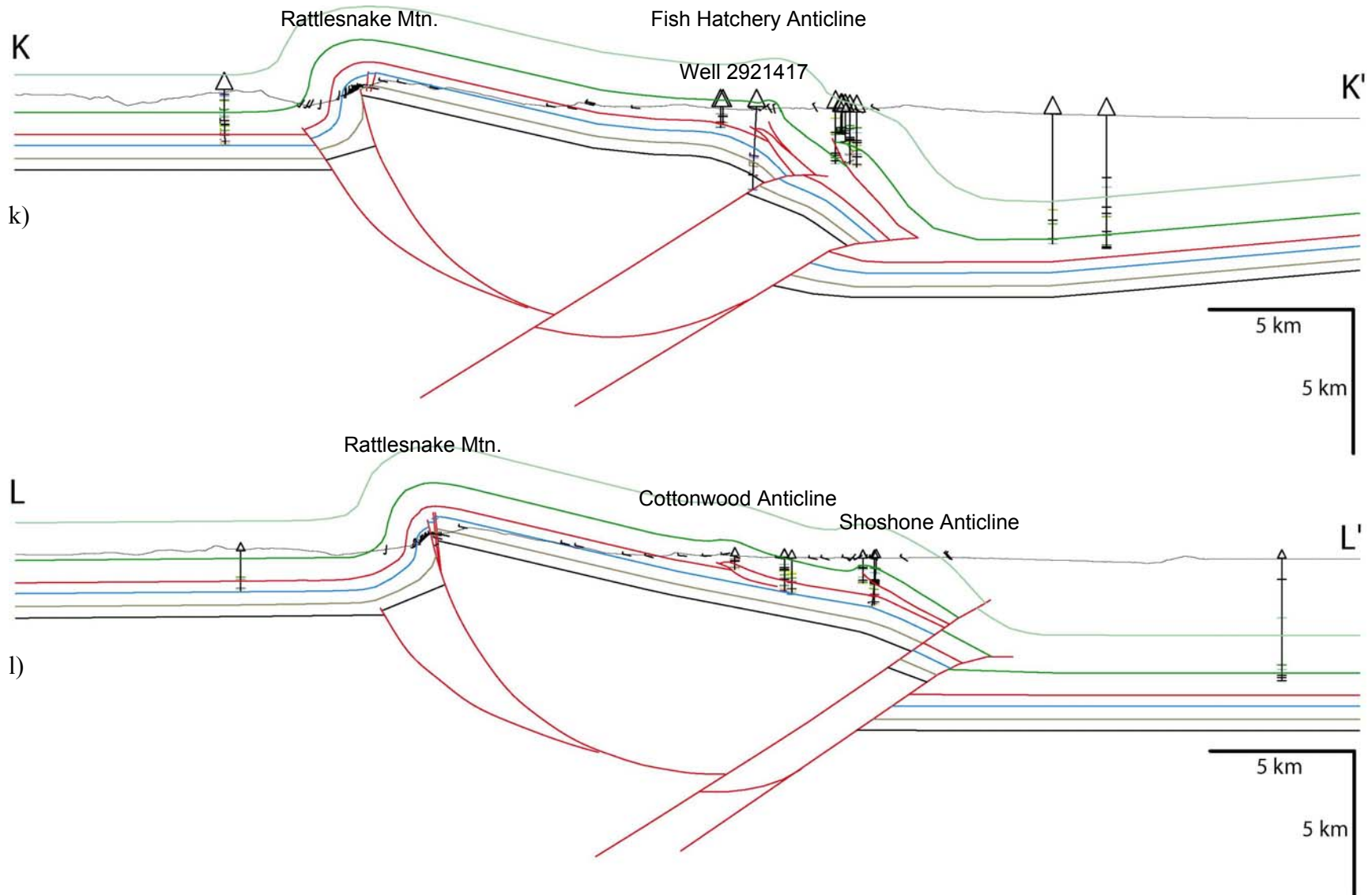


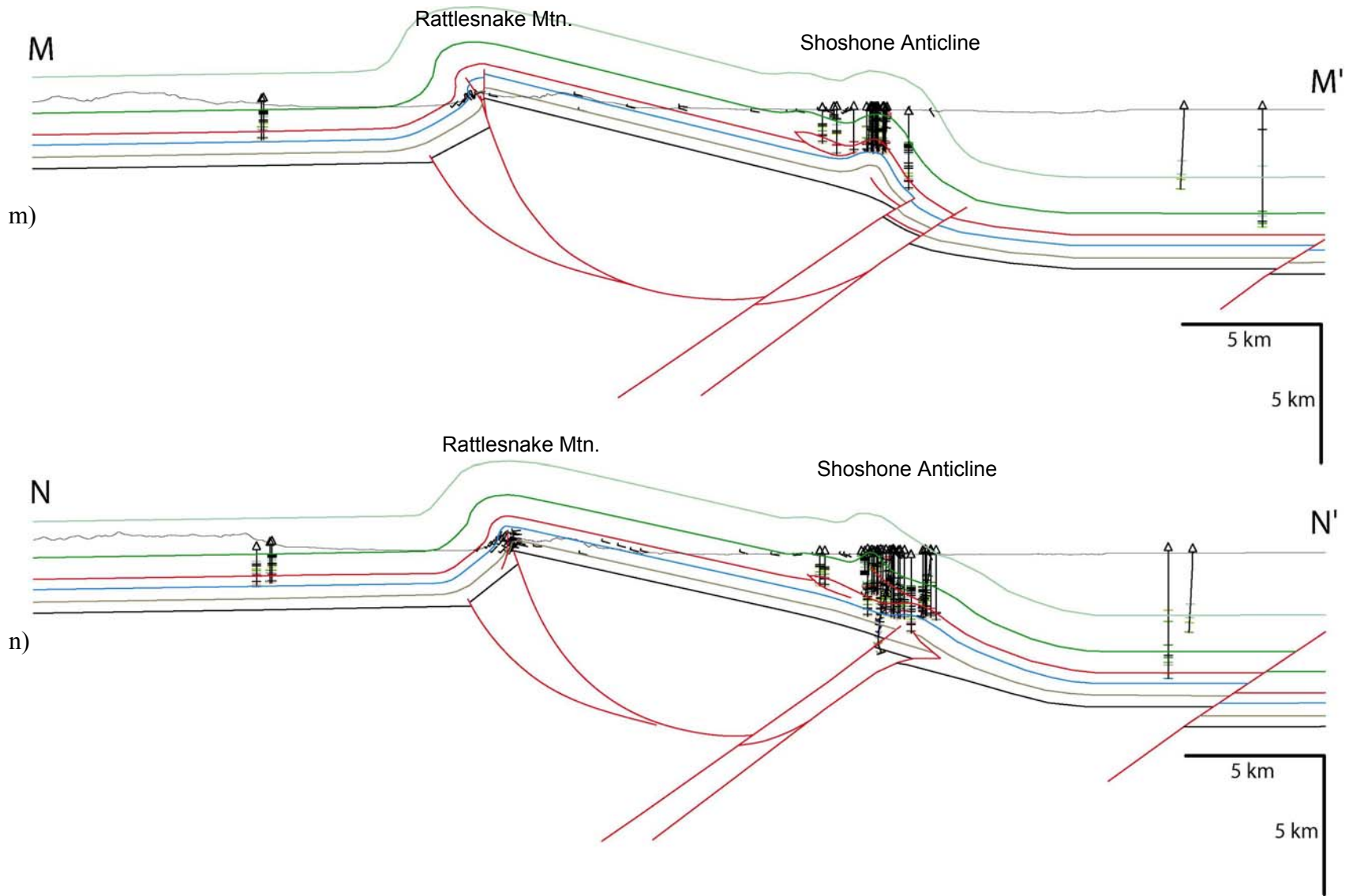


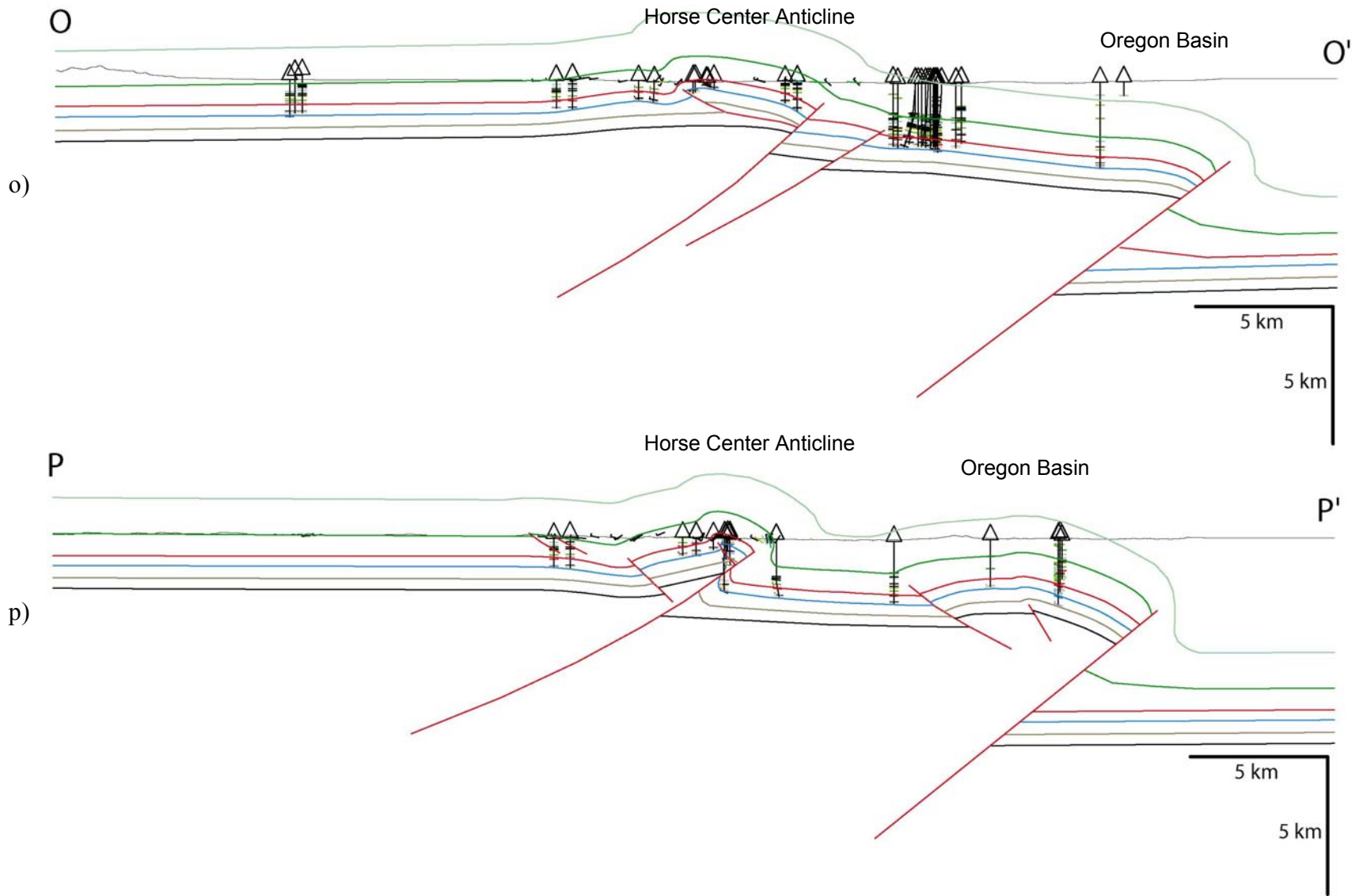












folding of the basement surface (Figs. 13a-p). For the Beartooth, Line Creek, and Oregon Basin Fault systems, interpretations of the location of the Bighorn Basin footwall using seismic data suggest that the dip angle of these faults, however, is similar, approximately 40°-50° to the west. Velocity pull-up, sideswipe, and steeply dipping strata all likely contribute to complications in interpreting sub-thrust geometries of the time-migrated seismic data available to this study, however, several 2D seismic lines image both the footwall and hanging wall cutoffs of these fault systems. Cross-sections A-A' and B-B' show two and three blind fault blocks, respectively, associated with the Beartooth Fault system basinward of the fault exposed at the surface. Seismic and well data from this area suggest that strata in these intermediate fault blocks dip east approximately 0°-20°. South of sections A-A' and B-B', seismic data indicates that slip was transferred from these splays to a single, approximately 50° SW dipping fault (Figs. 13d, e, f). Farther south, seismic imagery of an approximately 25°-30° NE dipping intermediate fault block suggest that slip on the Line Creek Fault system is again distributed between multiple faults, in this case two (G-G' – O-O'). For this segment of the Line Creek Fault system, the multiple fault interpretation is also supported by formation top data from well 2921417, which penetrated the basement surface at -7,860' and re-entered Paleozoic limestone at -9,530' (Figs. 13j, k). The structural elevation of the Paleozoic section beneath the basement overhang is too structurally high to be the basin floor footwall, because wells approximately 8 km east penetrated equivalent strata nearly 2 km deeper, supporting the interpretation of an intermediate fault block. Although an interpretation invoking large scale folding of the basement surface could also explain the anomalously

high sub-thrust Paleozoic section penetrated in well 2921417, seismic evidence of a faulted basement surface favors the two fault interpretation.

Although seismic and well data do not support a basin margin interpretation of a single, continuously folded basement surface from basin floor to the Beartooth arch/Rattlesnake Mountain backlimb, some folding of the basement surface proximal to the Line Creek Fault system is evident. In cross-sections J-J' and K-K', surface dip data immediately above the Line Creek hanging wall indicate a subhorizontal stretch of the basement surface approximately 200 m above sea level (Fig. 13). Well 2921417, located immediately east of this stretch of subhorizontal basement, documents an abrupt fold in the basement surface in that it penetrated the basement surface approximately 600 m below sea level (Figs. 13J, k). The interpreted basement fold shape follows the abrupt dip change in surface bedding attitudes within the superjacent Cretaceous units. A more gentle fold is similarly documented by a kink-like increase in the eastward dip of surface bedding, as well as in the five nearby wells, above the Line Creek hanging wall in section E-E'.

The presence of a triangle zone above the Line Creek Fault system (Figs. 13j, k, l, n) was interpreted based on the following observations: 1) an interpreted kink-like synclinal axis within Cretaceous units above the Line Creek Fault system projects approximately into the plane of the Line Creek Fault system; and 2) southwest-vergent detachment folds (e.g. Shoshone, Fish Hatchery anticlines) project basinward into this synclinal axis. This interpretation requires that the Line Creek Fault system shallows upward as it enters Cretaceous units (e.g. Figs. 13j, k). The Fish Hatchery anticline (Fig. 13j), which is geometrically constrained by abundant surface and subsurface dip data,

exhibits a decrease in amplitude with depth from the level of the Frontier Formation to the Chugwater Formation. This downward decrease in fold amplitude is best modeled without the presence of a single, controlling detachment fault. Instead, the fold geometry requires detachment faulting at multiple levels between the Frontier Formation and Madison Limestone. This suggests that distributed out-of-the-basin shear occurred along the basin margin during deformation, which may have played a role in causing the Line Creek Faults to shallow upward into the Cretaceous section. Variations in the stratigraphic level of detachment faulting/folding are observed throughout this area and they appear to occur as deep as within Cambrian shales (Fig. 13n). In this case, however, the anomalously low level of detachment may be related to a primary fold in the basement surface near this location, as discussed in chapter 6.

#### *Rattlesnake Mountain/Pat O'Hara Mountain Anticlines*

The largest basement-involved structure secondary to the basin bounding Beartooth/Line Creek/Oregon Basin Fault systems is Rattlesnake Mountain anticline, a west-vergent backthrust within the Line Creek hanging wall block. Structural balance of the fold's forelimb lengths requires a NE-dipping basement reverse fault below the surface exposure of the fold (Erslev, 1986; Brown, 1984). Therefore, the SW-dipping Line Creek Fault system and the NE-dipping Rattlesnake Mountain fault must either cross-cut or link at depth. Several lines of evidence suggest that the timing of slip on the two fault systems was synchronous and geometrically related. First, the Line Creek hanging wall basement cutoff is at a lower elevation than the basement surface of the Rattlesnake Mountain footwall block (particularly cross-sections G-G', H-H'). Such geometry requires that either fault inversion (i.e. normal faulting) or down-to-the-NE

rotation of the Line Creek hanging wall occurred. In any area balanced model of this geometry, a down-to-the-NE rotation would require a complementary up-to-the-SW rotational component, and the most likely candidate for this complement would be the Rattlesnake Mountain structure. Second, the Rattlesnake Mountain backlimb is uniformly tilted from anticlinal crest to its cutoff by the Line Creek Fault. This suggests that rotational block movement of the Rattlesnake Mountain hanging wall occurred on a curved, concave-up fault. Third, in clay model studies of the Line Creek/Rattlesnake Mountain fault system (Erslev, 1993), backthrusting within the Line Creek hanging wall could only be simulated by introducing resistance to slip on the Line Creek Fault system. This observation, combined with the observation of basement folding near the Line Creek Fault zone, suggests that the kinematic sequence of faulting within the Line Creek and Rattlesnake Mountain fault systems may have been 1) basement folding above the incipient Line Creek Fault, 2) Rattlesnake Mountain backthrusting in response to resistance (basement folding instead of faulting) on the incipient Line Creek Fault, and 3) synchronous up-to-the-SW rotation of the Rattlesnake Mountain hanging wall and down-to-the-NE rotation of the Line Creek hanging wall.

Erslev (1986) proposed a rotational basement backthrust model for the Rattlesnake Mountain anticline in the area near sections M-M' and N-N'. However, variations in along-strike geometry of the Line Creek and Rattlesnake Mountain hanging walls require more diverse geometric configurations NW of sections M-M' and N-N' for structural balance to be maintained. A balanced rotational fault block model in which the Rattlesnake Mountain fault curves concave-upward into the eastern of the two Line Creek Faults restores the basement surface reasonably well to its hypothesized pre-faulting

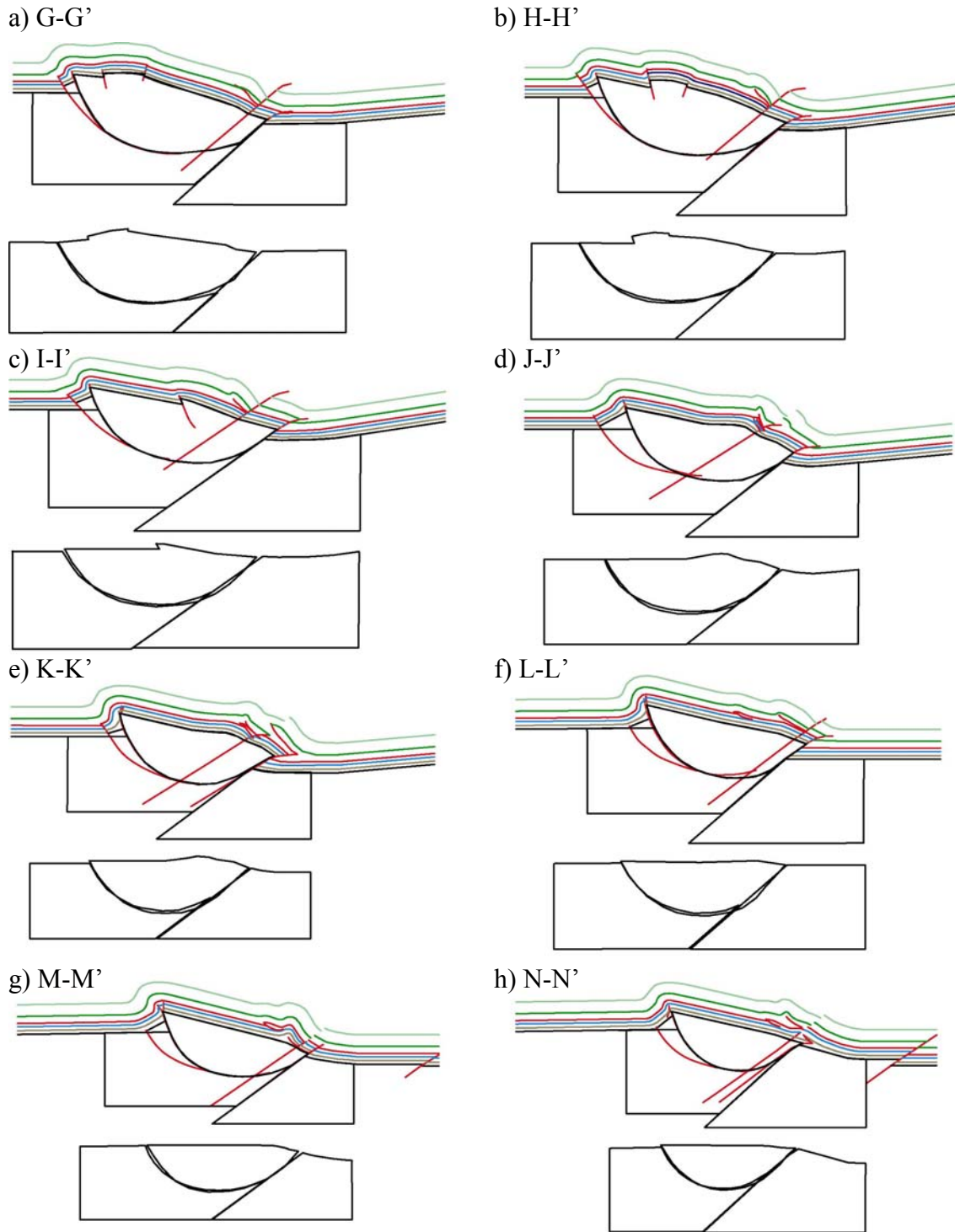


Fig. 14. Restorable basement block models of cross sections G-G' through N-N' using rotational backthrusting on the Rattlesnake Mountain structure. Slip was restored on the western Line Creek Fault and Rattlesnake Mountain "wedge" before block restoration.

geometry (Fig. 14). In these models, restoration of the Rattlesnake Mountain's intermediate fault block, or "wedge" (see discussion below), and restored slip on the western splay of the Line Creek Fault system were performed before basement block balancing, in accord with the interpreted kinematic sequence of events proposed in this chapter. The geometry of the wedge's southwestern fault, as interpreted from seismic data, was a first-order constraint for the fault dip angles of the Rattlesnake Mountain fault system. Applying this constraint, area balance of the rotational block could not be modeled using the western of the two Line Creek faults, however, was successfully modeled using the eastern of the two Line Creek Faults (Fig. 14).

The length of the Line Creek hanging wall block from the crest of the Rattlesnake Mountain anticline to the Line Creek Fault zone increases while maintaining an approximately constant backlimb dip from SE to NW (N-N' to G-G', Fig. 13). This fault block can only be modeled as a rigidly rotating block if the Rattlesnake Mountain master fault steepens along strike to become a deeper and wider cylindrical block. Slip on the eastern splay of the Line Creek Fault system first appears from NW to SE at a location approximately perpendicular to the initiation of hanging wall backthrusting. This may suggest that this eastern Line Creek Fault formed in response to the need to accommodate the between-fault width of a rotating backthrust chip (Figs. 13g-n).

Rattlesnake Mountain's tilted backlimb transitions from tilted to horizontal in sections J-J' and K-K', casting some doubt over the simplicity of the rotating backthrust chip model (Fig. 14). This geometry may be explained by either:

- 1) changes in the geometry of the Rattlesnake Mountain basement master fault at depth (e.g. flattening or terminating).

- 2) Flattening of the backlimb at this location may be the easternmost expression of the Pat O'Hara Mountain structure. This horizontal backlimb segment of lies approximately along trend with the Pat O'Hara Mountain anticline.
- 3) A northeastward widening of the rotating backthrust chip, caused by the divergence of the Line Creek and Rattlesnake Mountain fault systems, which may have precluded the need for a uniformly tilted backlimb.

2D seismic data near section I-I' indicates that the tilted basement wedge between Rattlesnake Mountain's footwall and hanging wall is bounded to the SW by an approximately planar, 50°-70° NE dipping fault. The sub-planar appearance of this fault imaged within the sedimentary section above basement favors a kinematic interpretation of wedge development in which tilting of the basement wedge occurred via internal strain, rather than by block rotation on a concave-down fault, as suggested by Erslev (1986). This hypothesized kinematic development was modeled using a combination of the fault-parallel flow and inclined shear algorithms in 2DMove to simulate internal strain during faulting (Fig. 15). Using the fault-parallel flow and inclined shear algorithms, an at-depth wedge fault geometry that is close to parallel with the main Rattlesnake Mountain basement fault produces the least space problems with the Rattlesnake Mountain hanging wall block NE of the wedge. The anomalous width of the basement wedge in section J-J' requires that the Rattlesnake Mountain master fault steepen at this location in order to successfully restore the wedge using 2DMove's fault-parallel flow/inclined shear restoration algorithm. If the basement wedge's SW bounding fault were to connect to the

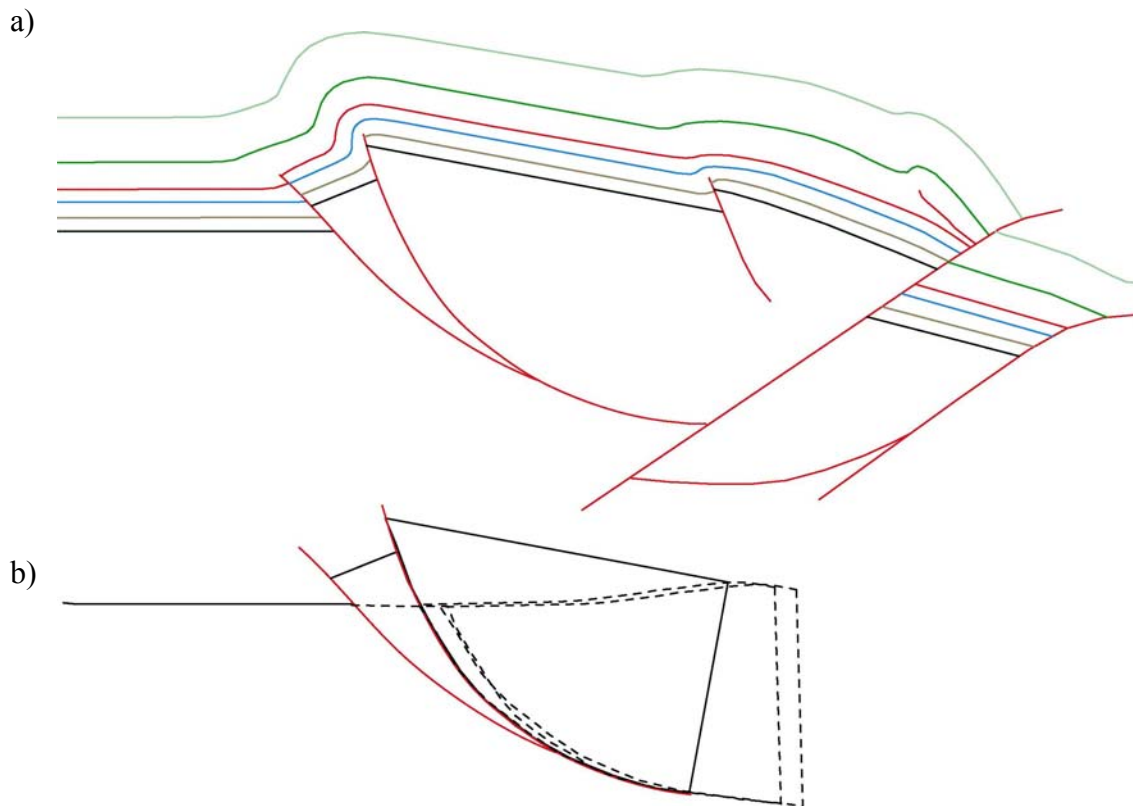


Fig. 15. Restorable 2D kinematic model of the Rattlesnake Mountain wedge (cross-section I-I'). (a) Shows the unrestored interpreted geometry and (b) shows the restored configurations of the wedge and rotated basement block (dashed lines) using a combination of fault-parallel flow (on faults shown in red) and inclined shear for both basement blocks (wedge displacement = 1,060 m, inclined shear = +30°; hanging wall block displacement = 2,700 m, inclined shear = -12°).

Rattlesnake Mountain master fault with a shallower geometry (e.g. Figs. 12m, n), then the wedge would restore to an unreasonably thick pre-deformation geometry.

The transition from a shallowly- to steeply-dipping upper wedge surface (e.g. Figs. 12l - n) is constrained by surface dip changes exposed within the crest and forelimb of the anticline. The two shallowly-dipping (approximately 46°-60°) forelimb segments (Figs. 12j, m/n) coincide directly to the two areas in which the top of the basement wedge dips most steeply. Where the interpreted wedge dip is shallowest (Fig. 12k), forelimb dips can exceed 90°. The dip of the top of the wedge and the anticlinal forelimb dip appear to be inversely related, suggesting that basement wedge geometry controls the geometry of forelimb folding. This spatial correlation between wedge and forelimb dip may indicate that internal strain experienced by the wedge, which effectively takes the place of faulting, translates into less fault-related folding of the overlying sedimentary cover rocks. Furthermore, the development of a steeply-dipping wedge top via internal strain may have affect the overlying forelimb like a rigidly rotating buttress that folded the overlying forelimb rocks in a NE-side-up rotational sense.

### *Line Length Balancing*

#### Rattlesnake Mountain

Line length unfolding in 2D Move of the interpreted lengths of the basement through Meeteetsee Formation surfaces in cross-sections A-A' through P-P' suggests that flexural slip and internal shortening within the sedimentary section, and block rotation and/or folding of the basement occurred during deformation (Fig. 15). Although thickness changes within the shale-rich Cambrian units occur adjacent to the Rattlesnake

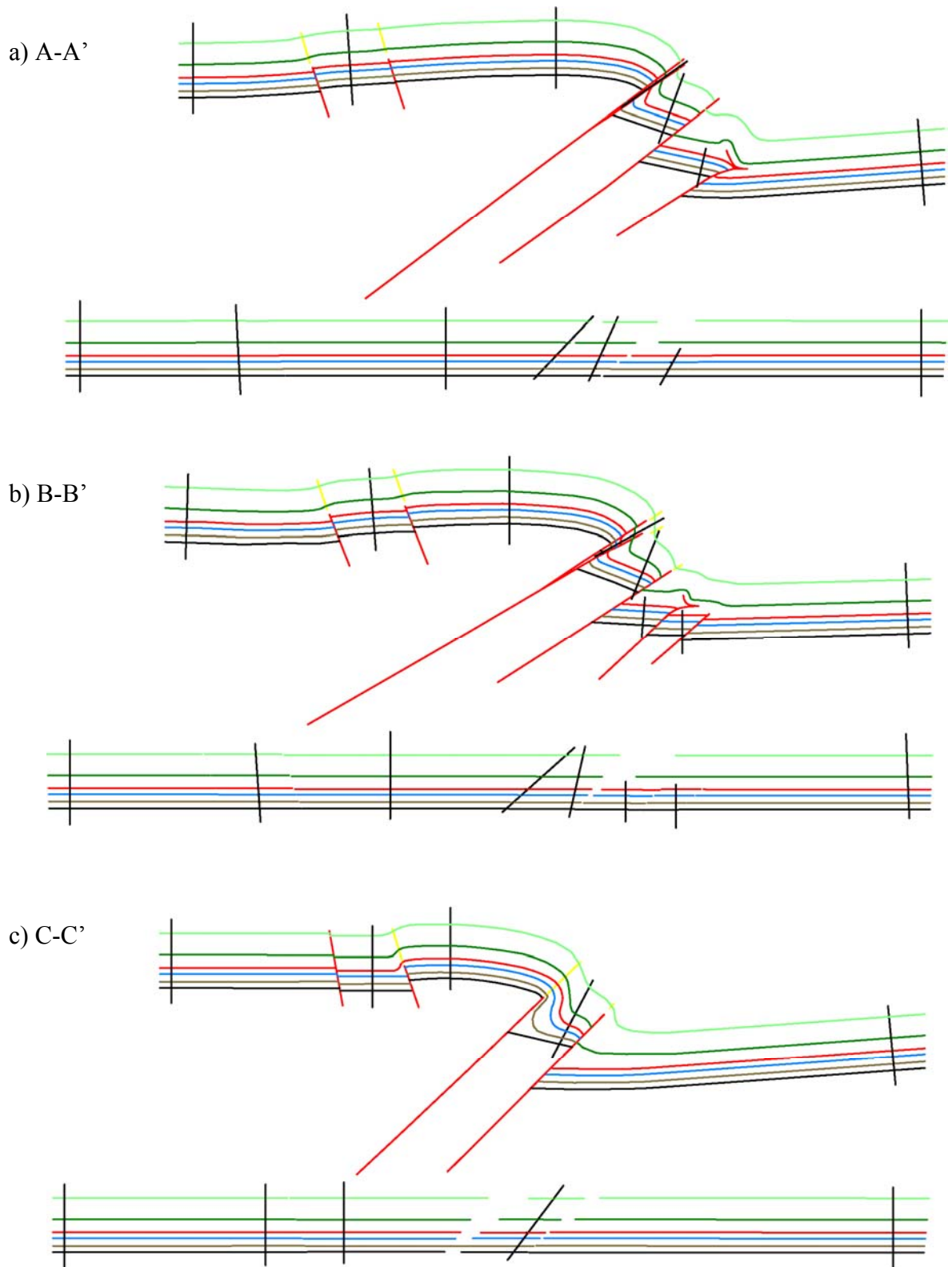
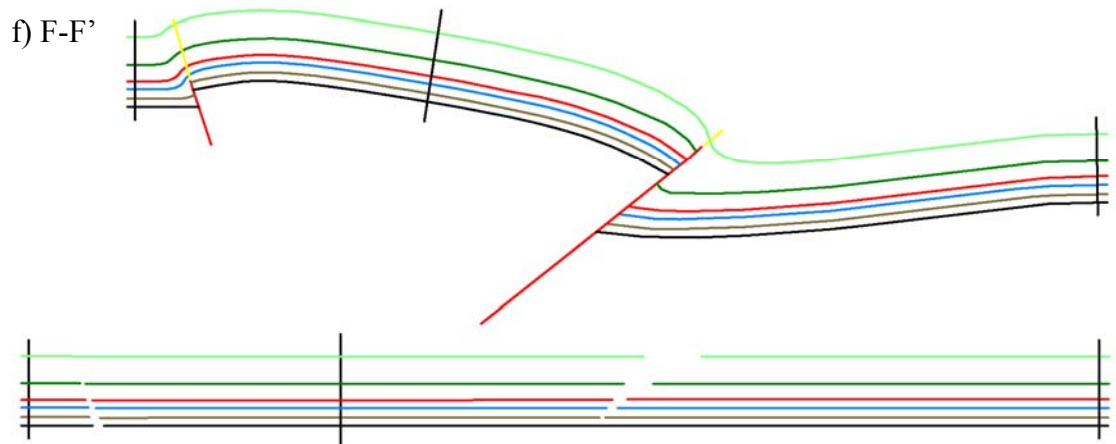
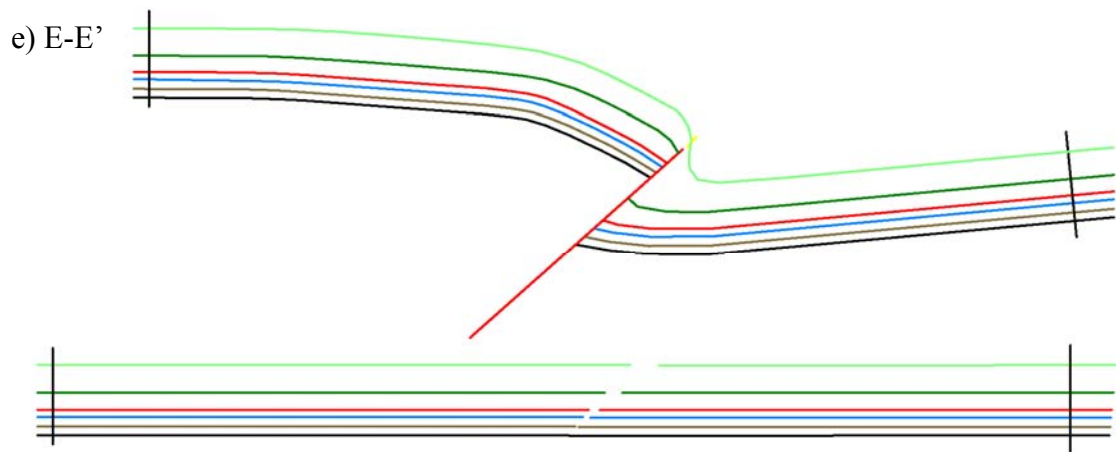
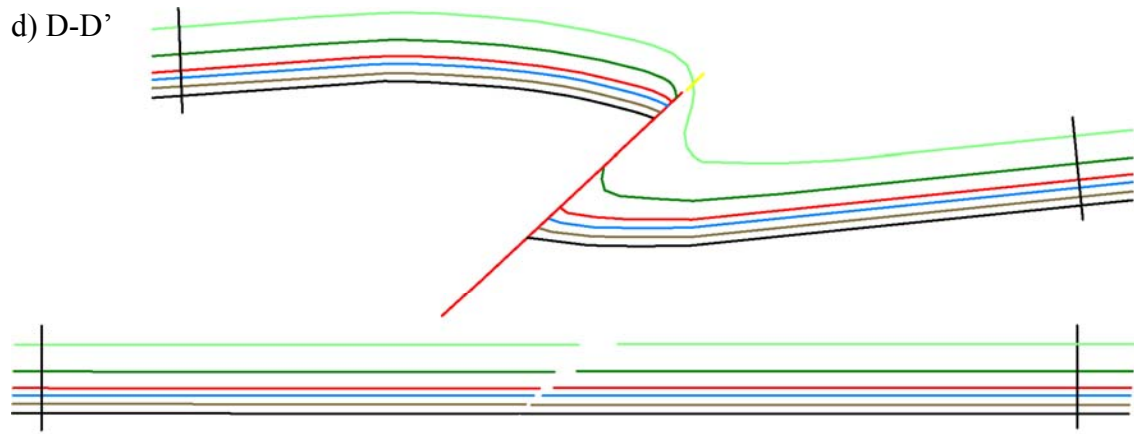
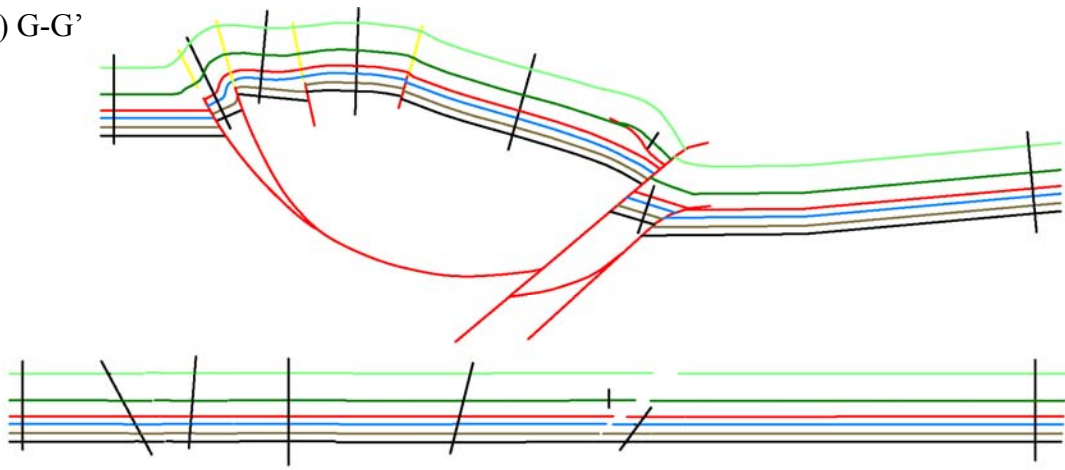


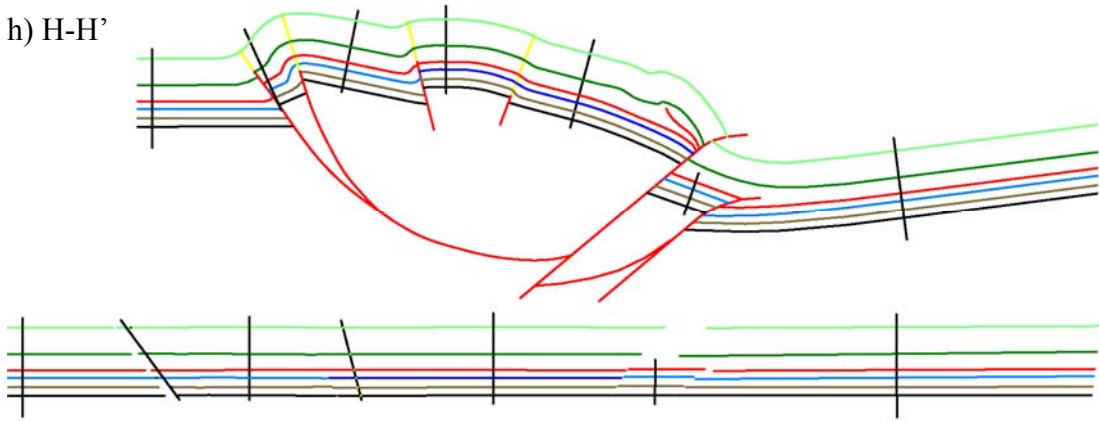
Fig. 15. Line length folding restoration of cross sections A-A' through P-P' (a-p, respectively) showing pin lines (upright black lines) and locations where blocks were split before unfolding (yellow lines).



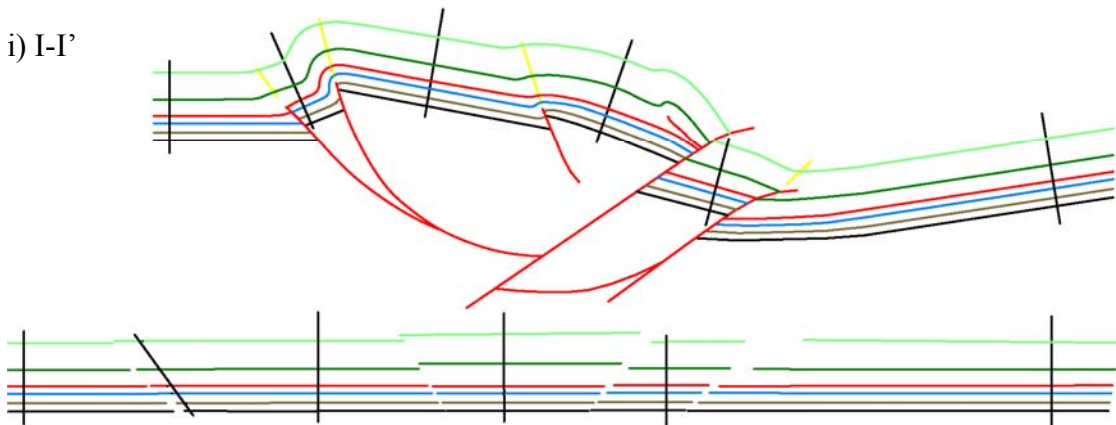
g) G-G'



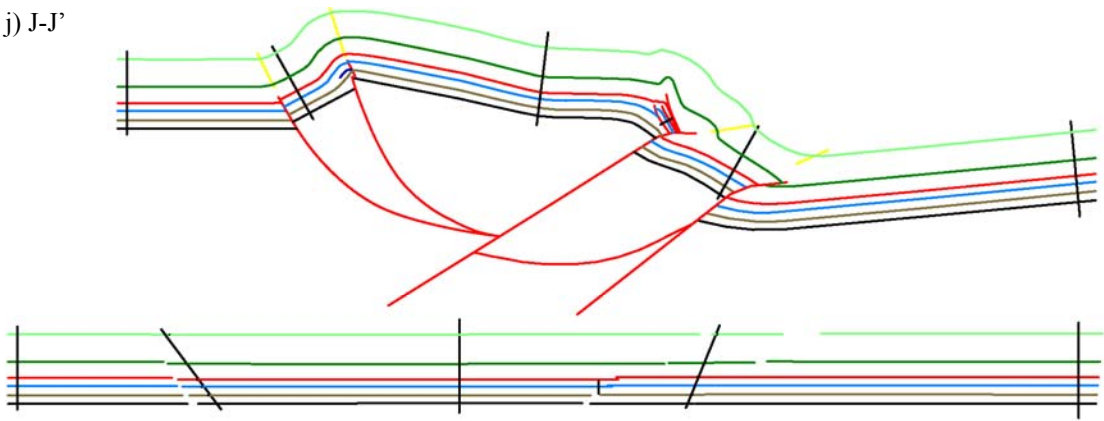
h) H-H'



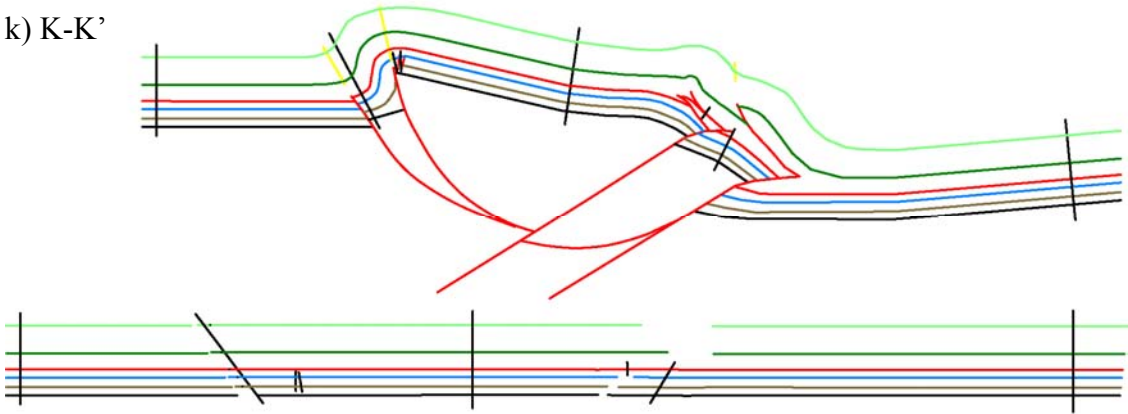
i) I-I'



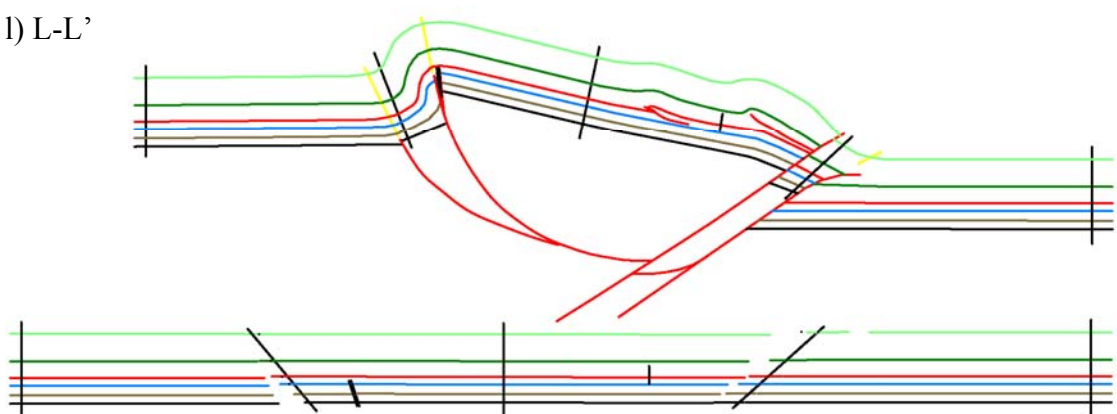
j) J-J'



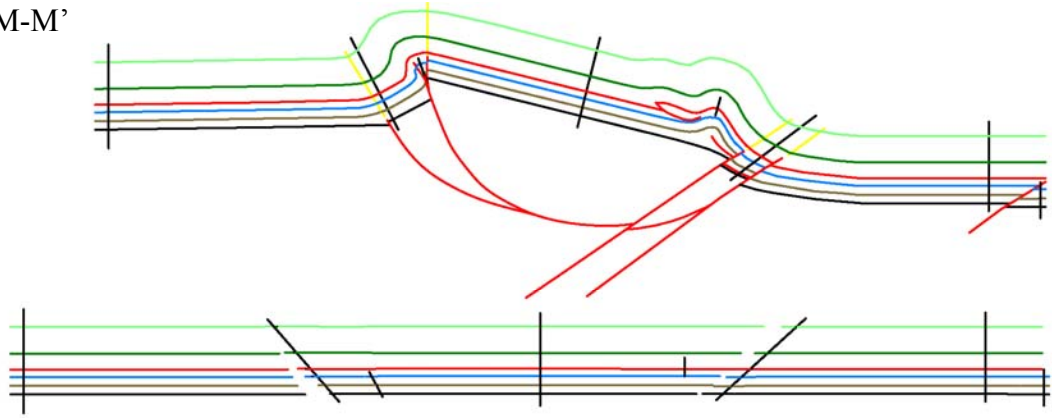
k) K-K'



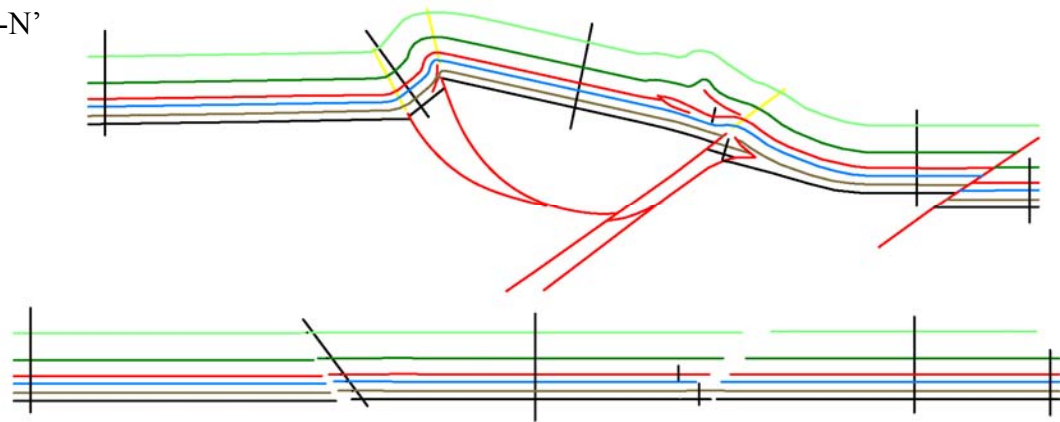
l) L-L'



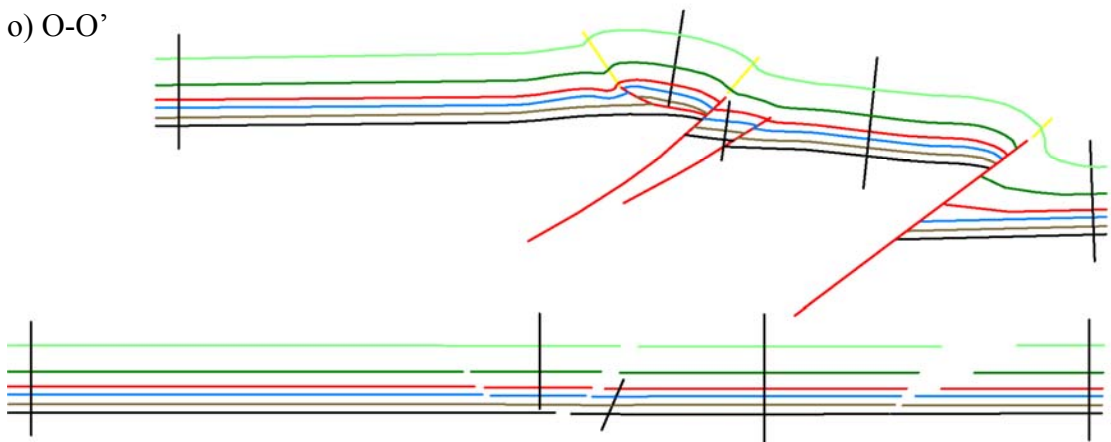
m) M-M'



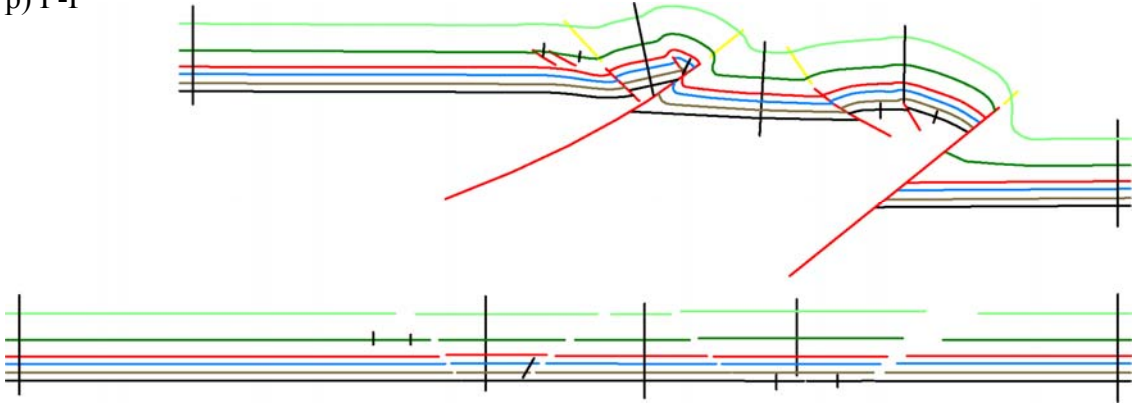
n) N-N'



o) O-O'



p) P-P'



Mountain basement fault in Shoshone Canyon, no obvious indications of significant thickness changes are present in the overlying Paleozoic strata, suggesting that line-length balancing is an appropriate cross-section validation technique here.

At Rattlesnake Mountain, the unfolded units above the basement wedge must be sheared in a top-to-the SW sense to restore line lengths, and the unfolded line lengths are usually slightly longer at higher stratigraphic levels (Fig. 15). The required top-to-the-SW shear during line length restoration suggests that top-to-the-NE shear occurred during deformation. This interpretation is consistent with the observation that on the SE side of the Shoshone Canyon exposure (Fig. 12n), top-to-the-NE faulting of the forelimb within the Paleozoic carbonates occurred. This structure produced thickening and flexural slip-like shear within the forelimb, and has been identified in the Rattlesnake Mountain anticline and other structures as a process commonly associated with flexural slip, or rabbit-ears folding (Stone, 1993).

Minor line length imbalance between higher and lower stratigraphic levels at Rattlesnake Mountain (Fig. 15) is likely the product of different fold mechanisms resulting from differences in mechanical stratigraphy with the Paleozoic through Mesozoic sedimentary sequence. The relative weakness of the shale-rich upper half of the sequence may have allowed greater interlayer flexural slip and/or internal shortening than the relatively stronger limestone and sandstone units of the middle and upper Paleozoic and lower Mesozoic formations. The occurrence of flexural slip at higher stratigraphic levels and other fold mechanisms, including trishear fault-propagation folding, at lower stratigraphic levels has been observed in other areas of the Rocky Mountain foreland with similar mechanical stratigraphy (Erslev and Hennings, 2004).

## Beartooth / Line Creek / Oregon Basin Fault Systems

Line length unfolding of the interpreted surface lengths above the Beartooth, Line Creek, and Oregon Basin Fault systems invariably shows shorter interpreted line lengths at higher stratigraphic levels. Either the cross-section interpretations are invalid or other processes must explain the apparent line length imbalance. Two principal uncertainties affect this discussion. First, much of the geometry and deformation style of the highest stratigraphic units, particularly Cretaceous units, are eroded away, and therefore remain speculative. More shortening within Cretaceous rocks may have occurred than can be observed in current surface exposures if higher amplitude folding and/or greater and higher-offset faulting occurred. Second, uncertainty as to the degree and influence of folding of the basement surface necessarily complicates any discussion of line length balance.

Along the length of the Beartooth, Line Creek, and Oregon Basin Fault systems, the cross-section interpretations and seismic data commonly show hanging wall and footwall cutoffs with non-parallel basement surfaces (e.g. Figs. 12a, h, o). The result is that the 2D line lengths of the stratigraphically lowest units are longer in cross-section than the length of stratigraphically higher units.

The uncertain influence of triangle zone geometries and basement-detached faulting on formation line lengths hinders precise identification of possible processes responsible for line length imbalance, however, some combination of the following hypotheses may explain the line length imbalance of the Beartooth, Line Creek, and Oregon Basin Fault systems:

- 1) Upward shallowing of the Line Creek Fault system. A shallowing of the Line Creek Fault as it enters the basin could have the effect of tilting the hanging wall to the NE via down-to-the NE rotation. Block rotation of the Rattlesnake Mountain hanging wall may play a role in this process, resulting in an apparent rotation of the hanging wall tip of the Line Creek Fault. This hypothesis is supported by the observation that in sections G-G' and L-L' through N'N', minimal folding of the Line Creek hanging wall tip occurs. Instead, the hanging wall forms an approximately flat, continuous surface from the Line Creek Fault zone to the crest of the Rattlesnake Mountain anticline. Upward shallowing of the Line Creek Fault system supports the triangle zone interpretation, and because much of the Cretaceous section above the associated basement-detached thrusts (i.e. Fish Hatchery anticline) has been eroded away; more detachment folds may have been present before erosion. This speculative geometry would result in greater line lengths within the uppermost units, and possibly line length balance.
- 2) Basement shear folding via either a) folding during faulting of both the hanging wall and footwall cutoffs; or b) fault-propagation folding of the basement surface before the fault tip propagated through the basement surface. These hypotheses requires a basement footwall cutoff interpretation in which folding is present proximal to the fault, which is supported by the geometries observed in sections J-J' to K-K'. The aforementioned clay model studies of the Line Creek/Rattlesnake Mountain fault system support these hypotheses. Similar to hypothesis (1) above, these two processes could produce line length balance because they favor out-of-the-basin shear and the associated SW vergent basement-detached structures.

- 3) Unresolved lengthening of line lengths within the uppermost sedimentary section proximal to the Line Creek Fault (e.g. Trishear-like, drag, or pure-shear folding). This process would result in longer line lengths higher in the section, and possibly in line length balance.
- 4) Shortening and structural thickening within Cretaceous shale units. In this hypothesis, 2D area balance may overshadow the need for line length balance. If area balance between upper and lower levels occurs, then bed lengths of the upper sedimentary section may have been shortened as the section was thickened. This hypothesis is difficult to test because few wells penetrate Cretaceous units within the basin's synclinal axis, where structural thickening would likely occur. However, the interpreted basement footwall cutoff location and the high relative formation top data of Cretaceous units from well 2921345 in cross-section F-F', as well as the general abundance of minor folds, indicates that thickening of Cretaceous units may have occurred in the synclinal axis at this location (Fig. 12).
- 5) Top-to-the NE directed shear of the upper sedimentary section within the Bighorn Basin. Basinward detachment and transport on subhorizontal bedding planes within basinal units has been documented in other Laramide arches (Stiteler et al., 2005) and implies that unresolved 2D area and line lengths move in or out of the cross-sections. This hypothesis is difficult to test without additional regional data.

#### *Summary of Sequential Kinematic Development*

Geometric restoration insights from cross-section construction and balancing, suggest the following kinematic sequence for the Line Creek and Rattlesnake Mountain fault systems:

- 1) Folding of the basement surface above the incipient Line Creek Fault system, perhaps due to propagation of a fault tip at depth.
- 2) Backthrusting of the Rattlesnake Mountain fault, possibly on a pre-existing structure, and synchronous slip on the eastern Line Creek Fault. The fault curvature and backlimb width modeled for the Rattlesnake Mountain rotational backthrust show that this fault was linked to the eastern Line Creek Fault.
- 3) Faulting of the western Line Creek Fault. 2D modeling suggests that this fault broke through the Rattlesnake Mountain block and that the western Line Creek Fault post-dated backthrusting on the Rattlesnake Mountain fault.

## 6. THREE-DIMENSIONAL ANALYSIS

### Constraints from 3D Modeling

The 2D Move/3D Move software suite facilitates 3D analysis and modeling by allowing surfaces to be easily created via extrapolation from cross-section lines. Due to the software's variety of surface creation algorithms and the complex variety of fold and fault cutoff shapes in the study area, the surfaces were created in a patchwork fashion, using individual algorithms to most reasonably model local surface shapes. The tools available for surface creation and editing in 3D Move allow fault terminations, splays, and slip transfers to be modeled in a variety of ways. A number of these structures are present between 2D cross-sections and their geometries are expressed as interpretations based on all available data.

### Observations

The southern plunge of the Beartooth arch along the NW margin of the Bighorn Basin is expressed at the surface as a decrease in the elevation of the basement nonconformity. Precambrian crystalline basement rocks below this nonconformity that crop out extensively throughout the Beartooth Mountains are covered by the overlying Phanerozoic sedimentary sequence beginning in the vicinity of Clark's Fork Canyon and continuing south. The southward loss of structural elevation of the basement nonconformity on the NW flank of the Bighorn Basin is complemented by an approximately equivalent southward decrease in elevation of the basement nonconformity at the base of the Bighorn Basin directly to the east. Data from wells drilled within the Bighorn Basin east of the east flank of the Beartooth arch document

this S/SE dip of the basin floor beginning near the Montana/Wyoming border, which defines the northern boundary of the Bighorn Basin (Figs. 12a - h).

Exposures of the basement and immediately overlying Cambrian rocks between the southernmost Beartooth arch and Pat O'Hara Mountain in Dead Indian Creek indicate that the basement nonconformity is subhorizontal until it is folded upward as a part of the N dipping backlimb of Pat O'Hara Mountain anticline (Pierce and Nelson, 1968). South of Pat O'Hara Mountain, an abrupt drop in the elevation of the basement surface of approximately 2 km occurs between the Rattlesnake Mountain footwall to the south and the Pat O'Hara Mountain hanging wall to the north. Seismic and well data from the Rattlesnake Mountain footwall block show no significant deformation within Mesozoic and Paleozoic units above basement and indicate that this basement block dips approximately 0.5° SSE (Figs. 12h - n).

Although the 2D geometry of the Beartooth, Line Creek, and Oregon Basin Fault systems is constrained by several strike-perpendicular 2D seismic lines, access to strike-parallel 2D seismic was limited in this study. Therefore, the 3D geometry of fault splay interactions in these systems is constrained principally by interpreting between 2D cross-sectional geometries. One strike-parallel, N-S-oriented 2D seismic line from the east flank of the Beartooth arch, however, shows that slip loss on the Beartooth Fault splays occurs via a gently S-plunging monoclinial fold of the basement surface. Similar to the dominantly two-splay nature of the Line Creek Fault system east of Rattlesnake and Pat O'Hara Mountains, faulting of the basement surface controlling the east-vergent Horse Center anticline is seen in seismic data to occur on two W-dipping basement faults. East and northeast of this structure, seismic and well data are limited and/or restricted to the

sedimentary cover rocks, leaving the 3D geometry of the intersection of the Line Creek and Horse Center footwalls and the Oregon Basin hanging wall open to interpretation.

The 3D geometry of the Rattlesnake and Pat O'Hara Mountain anticlines is constrained almost exclusively by surface exposures within Paleozoic rocks and constraints from 2D modeling. Surface data indicate that the eastern plunge of Pat O'Hara mountain anticline is notably less abrupt than the SE plunge of Rattlesnake Mountain anticline (approximately 30°-40° versus 50°-70°). The backlimb of Pat O'Hara Mountain anticline dips more steeply than Rattlesnake Mountain anticline's backlimb (15°-55° versus 12°-15°) and is cut by a steeply-dipping ENE striking fault with approximately 100 m of south-side-up offset (Pierce and Nelson, 1968).

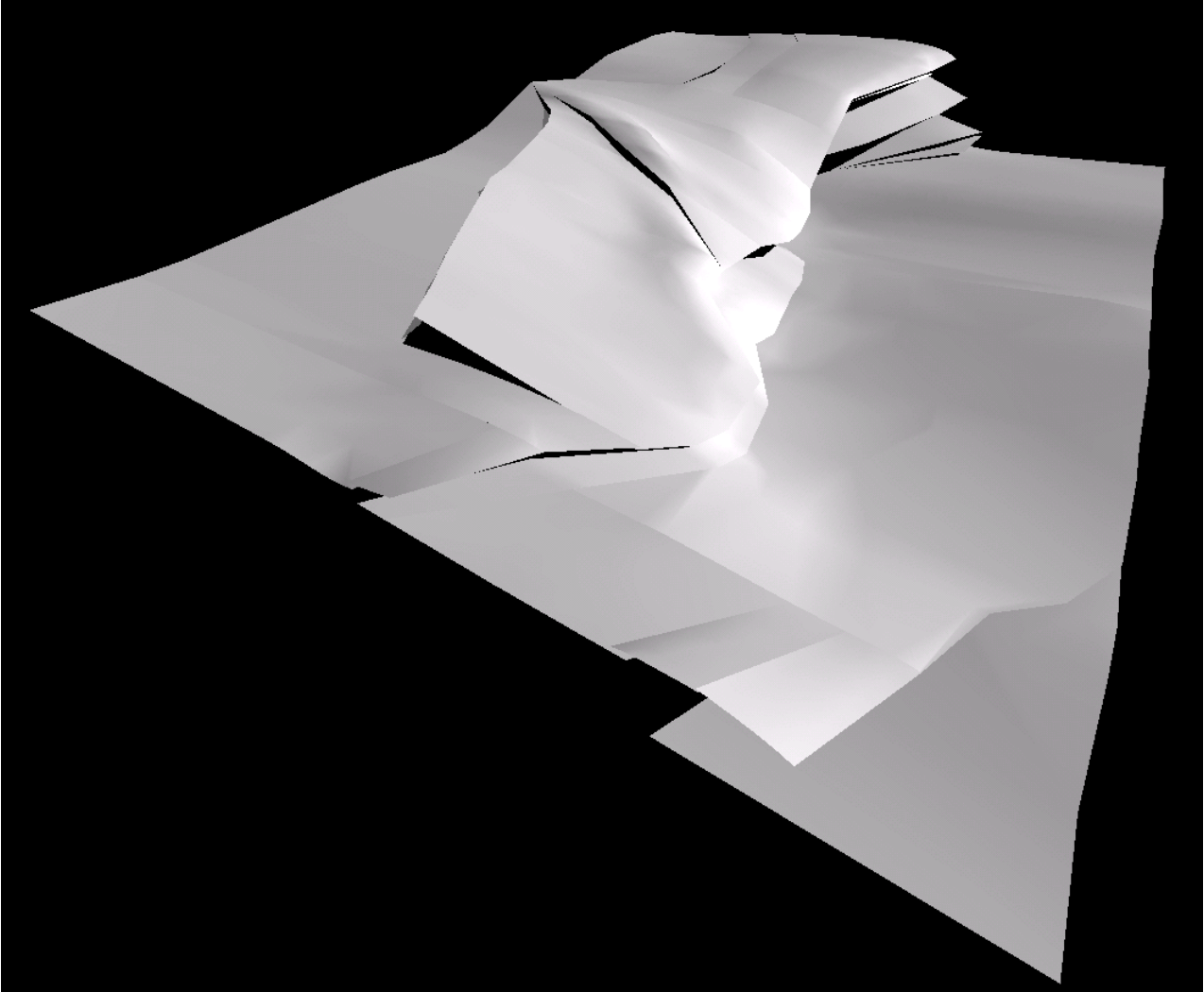
### Interpretations

#### *Beartooth/Line Creek Fault System*

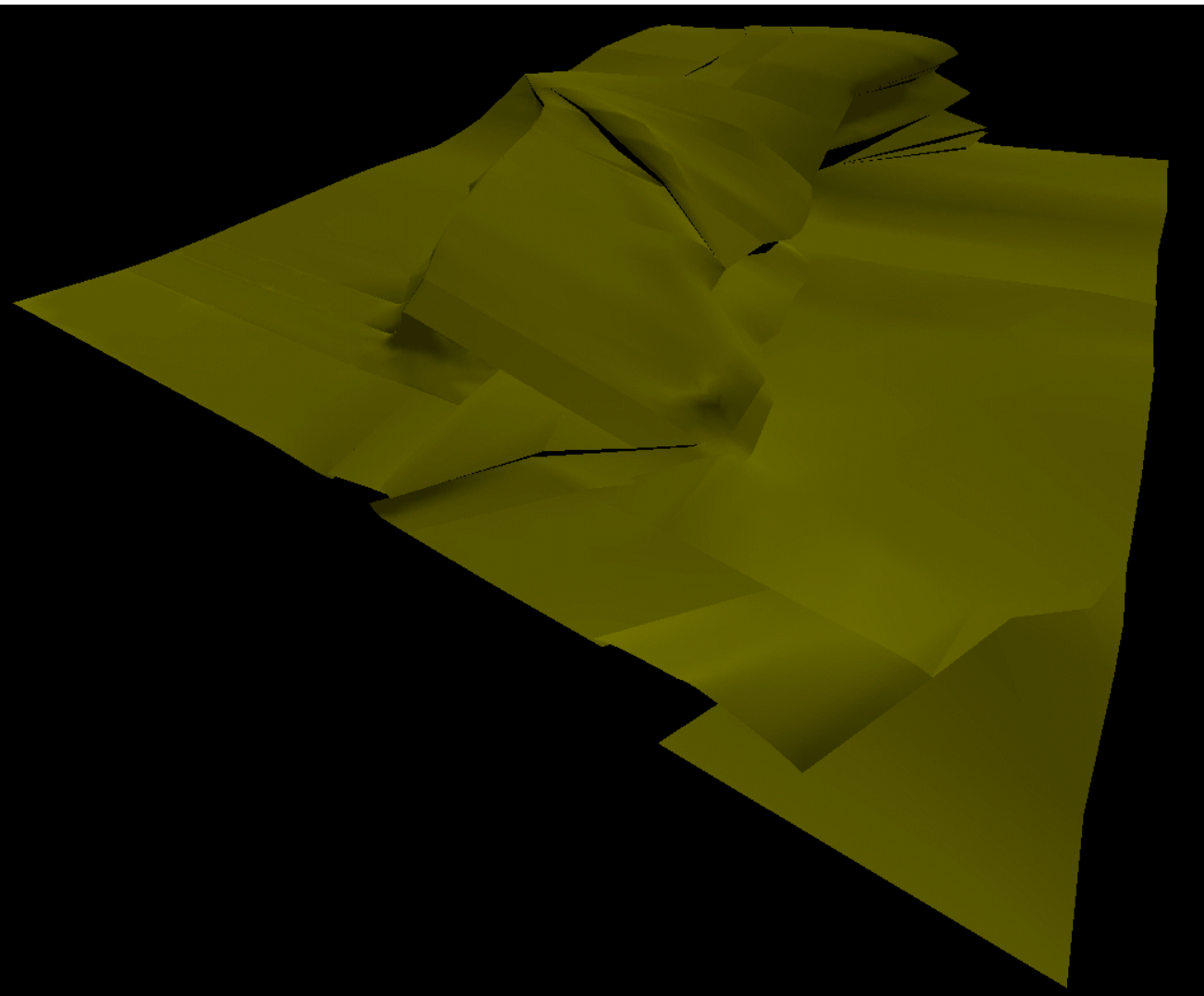
The Line Creek and Beartooth Faults are interpreted here as a single, connected fault system that extends the length of the study area from (at least) the east flank of the Beartooth arch near the Wyoming/Montana border to the Horse Center anticline (Fig. 16). The fault zone changes in both width and number of fault splays along this stretch. At the northwest boundary of the study area, seismic and well data clearly document the presence of at least four fault splays, defining the Line Creek/Beartooth Fault system's widest, most distributed zone (Fig. 12a, b). Southward, near cross-sections D-D' and E-E', seismic data indicates that slip on these four fault splays has been transferred to a single fault. This zone has been previously interpreted as a transition between two distinct faults, the southward termination of the Beartooth Fault system and the northwestward termination of the Line Creek Fault (Blackstone, 1986a). The

Fig. 16. Three-dimensional views looking NW from the SE corner of the model of the modeled (a) basement nonconformity, (b) top of Cambrian, (c) top of Madison Limestone, (d) top of Chugwater Formation, (e) top of Frontier Formation, and (f) top of Meeteetsee Formation surfaces using 3DMove.

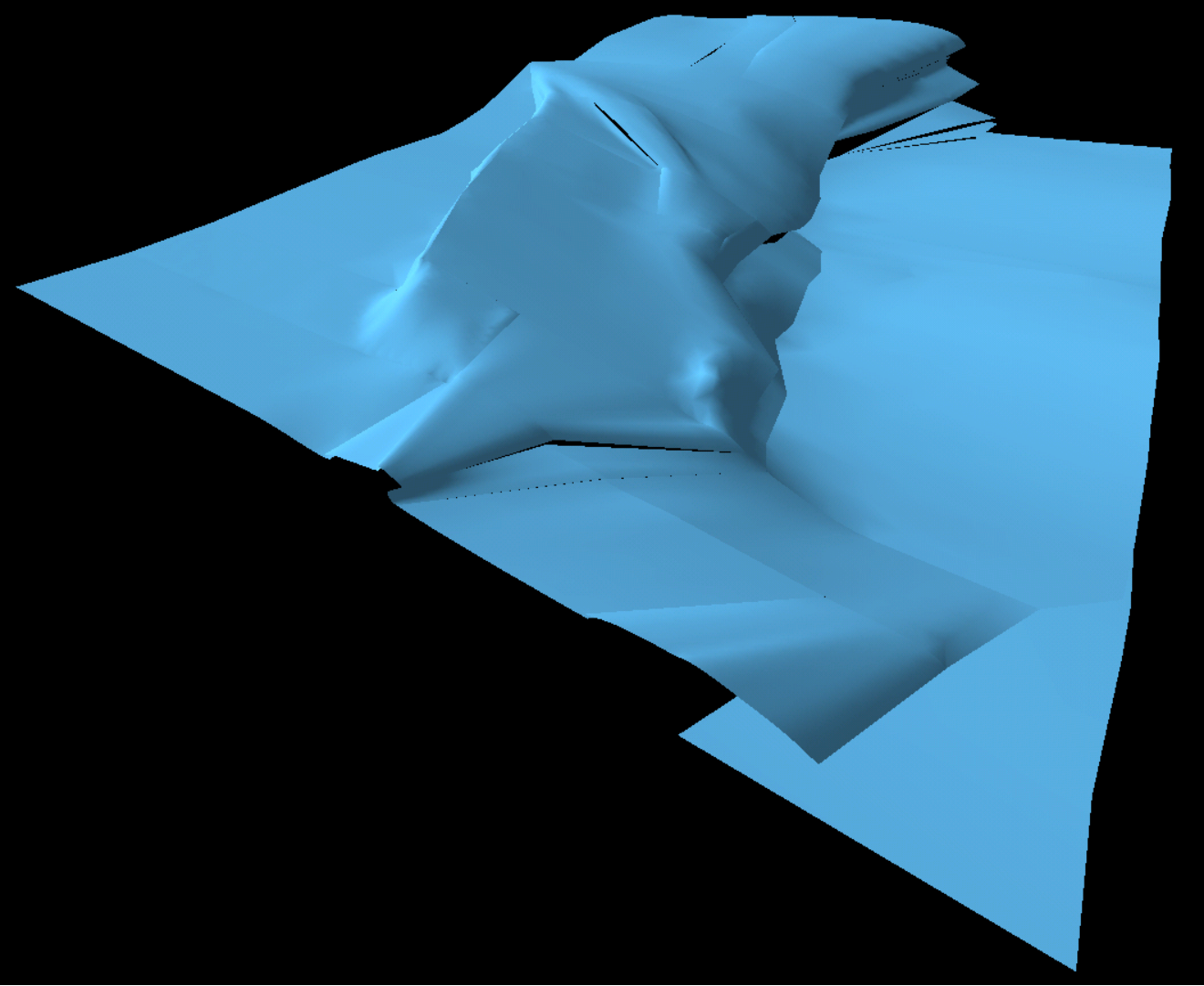
a)



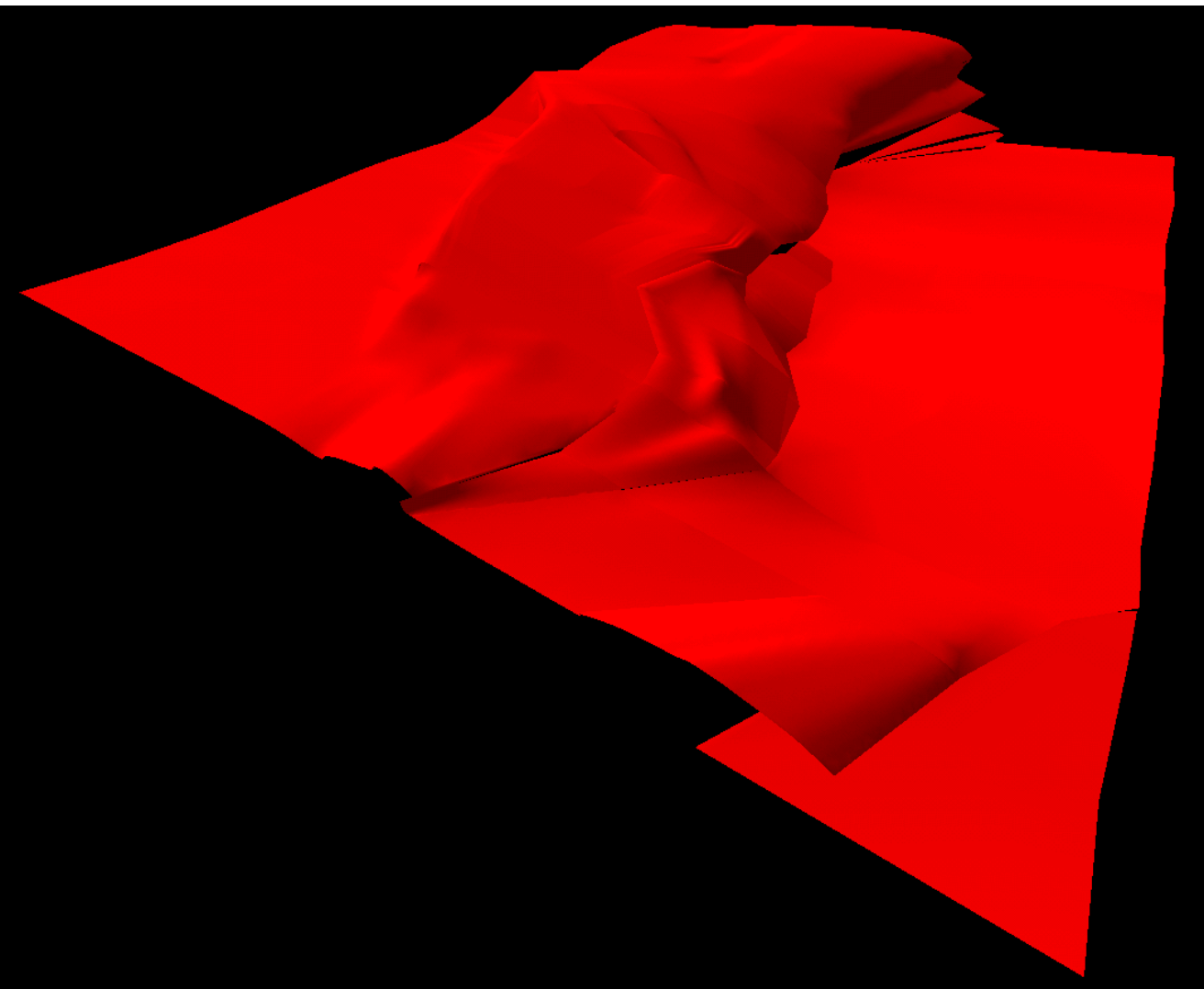
b)



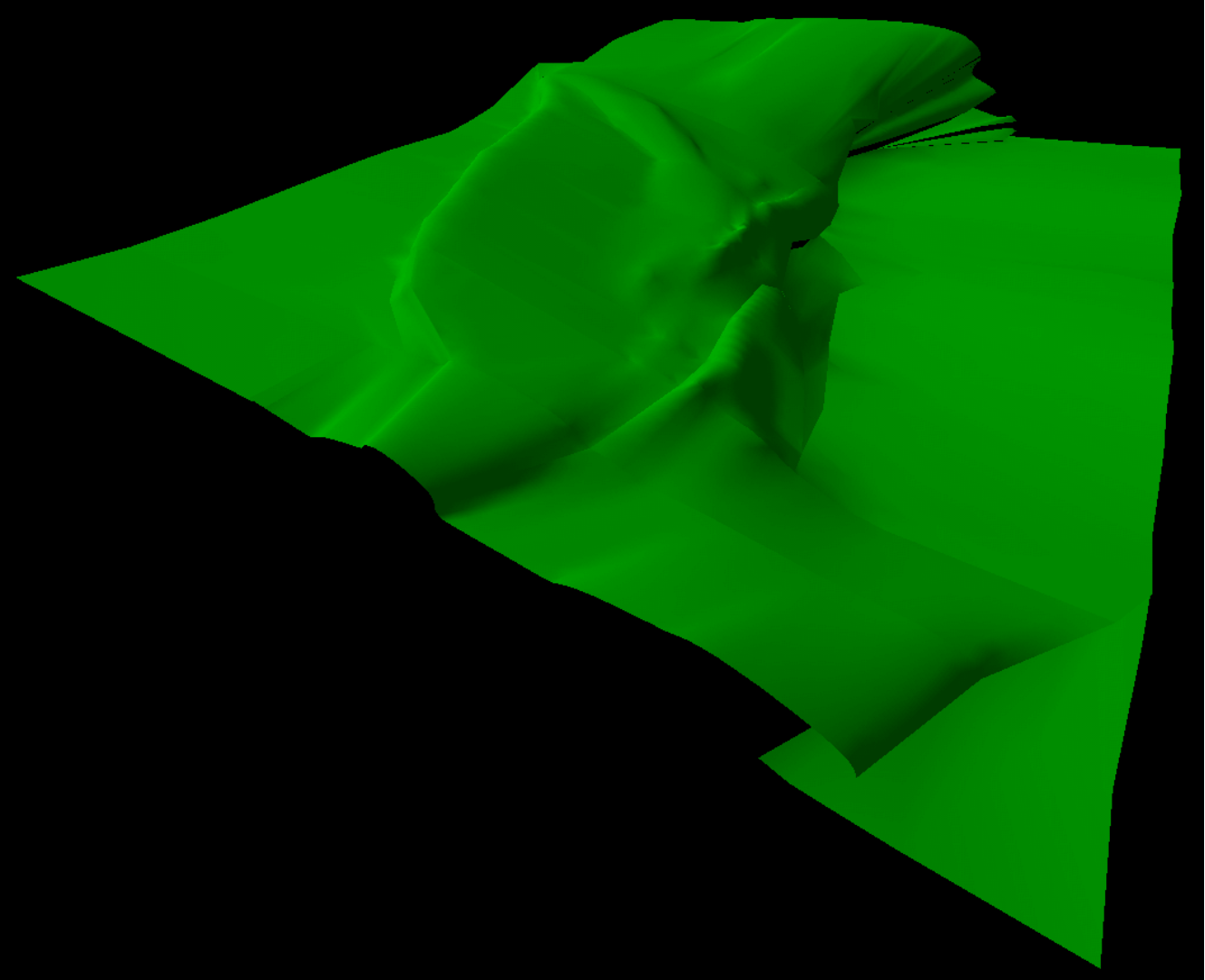
c)



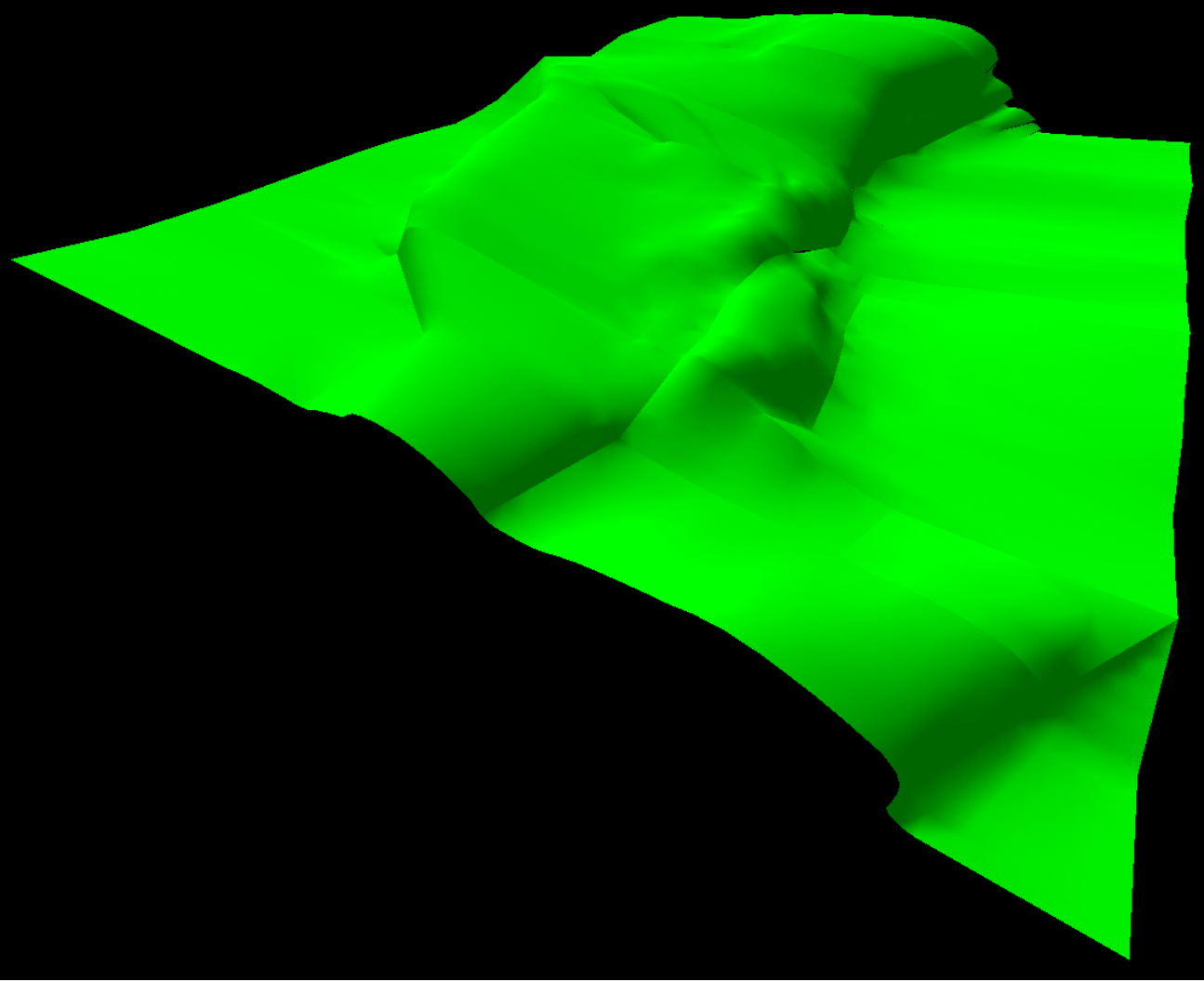
d)



e)



f)



interpretation that these two faults systems are part of a single system is based on the following observations:

- 1) The northwest projection of the Line Creek Fault from sections D-D'/E-E' to C-C' (Fig. 12), the location and strike of which are well defined by seismic data, projects directly into the Canyon Mouth anticline. The Canyon Mouth anticline is interpreted here as the northwest extension and surface expression of the Line Creek Fault.
- 2) The presence of a continuous, overturned, and unfaulted fold at the level of the Ordovician Bighorn Dolomite above the Line Creek Fault at this location (Canyon Mouth anticline, section C-C', Fig. 12) suggests that the Canyon Mouth anticline segment of the Line Creek Fault is not the only basin bounding fault at this location. Instead, the Line Creek Fault appears to distribute slip between at least two fault splays. The eastern of these two faults is interpreted here as the southern extension of one of the Beartooth Fault splays, the westernmost subsurface fault spay present in sections A-A' and B-B' (Figs. 16a, 17). The geometry of this fault's termination is interpreted as an intermediate level splay from the Line Creek Fault near section D-D' (Fig. 17).

Southeast of section F-F', seismic data again shows the presence of two faults associated with the Line Creek Fault zone, an observation that is also supported by data from well 2921417 (Fig. 12j). To the southeast, the eastern of these two faults shows an increase in offset that is complemented by a decrease in offset of the western splay, supporting the interpretation that slip is transferred to the eastern splay. The Geometry of this fault system resembles a basement-involved compressional relay ramp (Fig. 18).

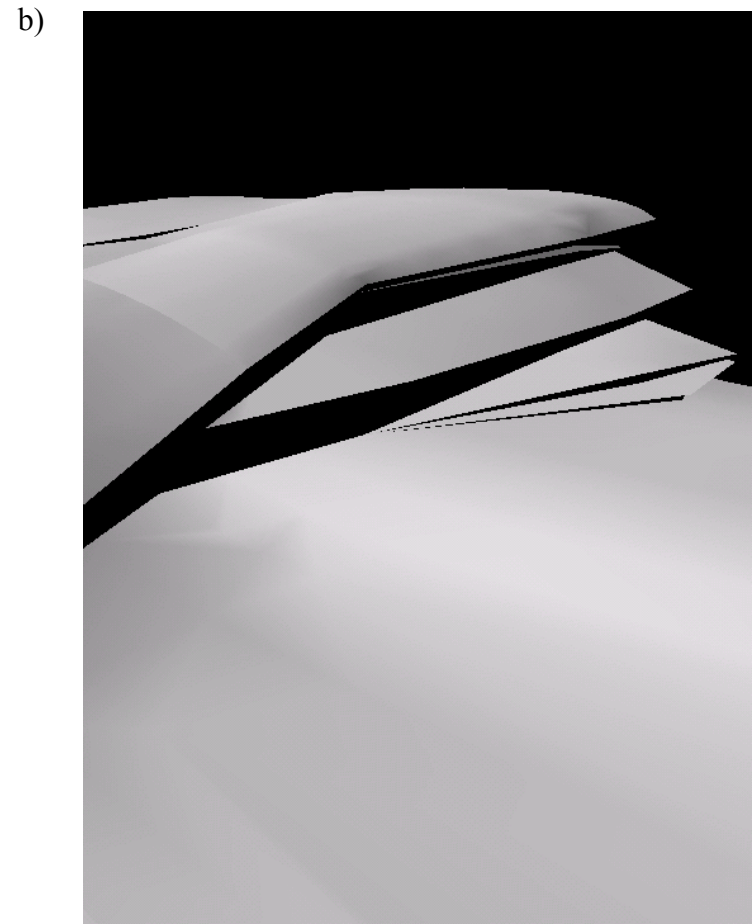
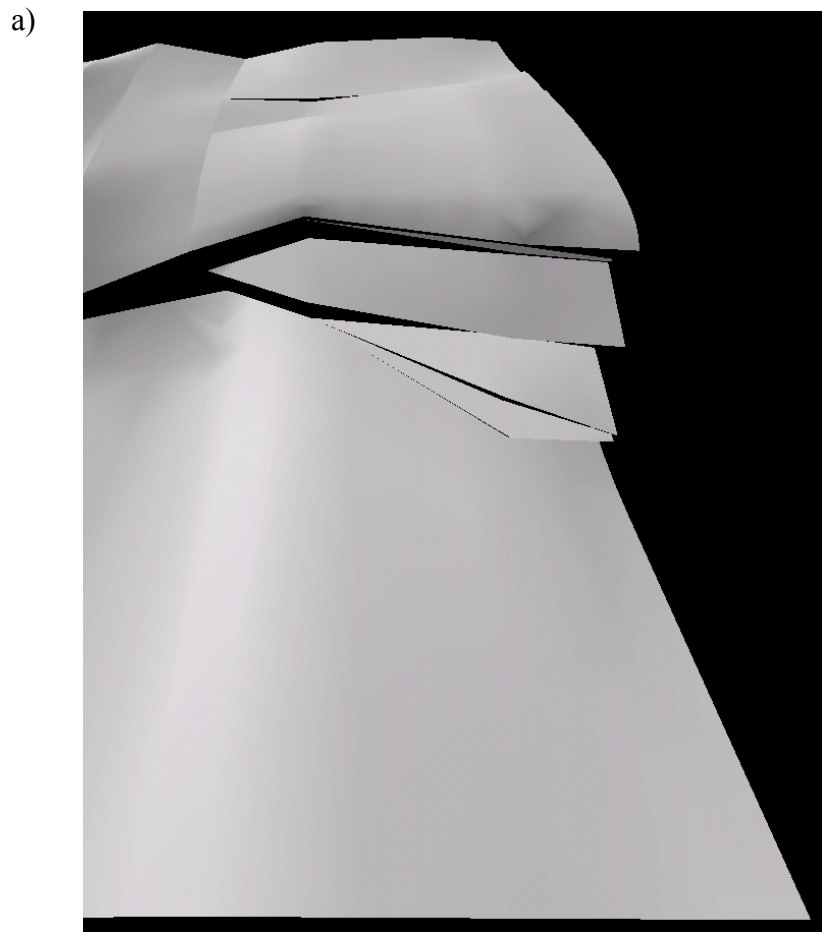


Fig. 17. Views of the top of the basement surface looking west (a) and northwest (b) from the NE corner of the model of fault terminations within the Beartooth Fault system.

a)



b)

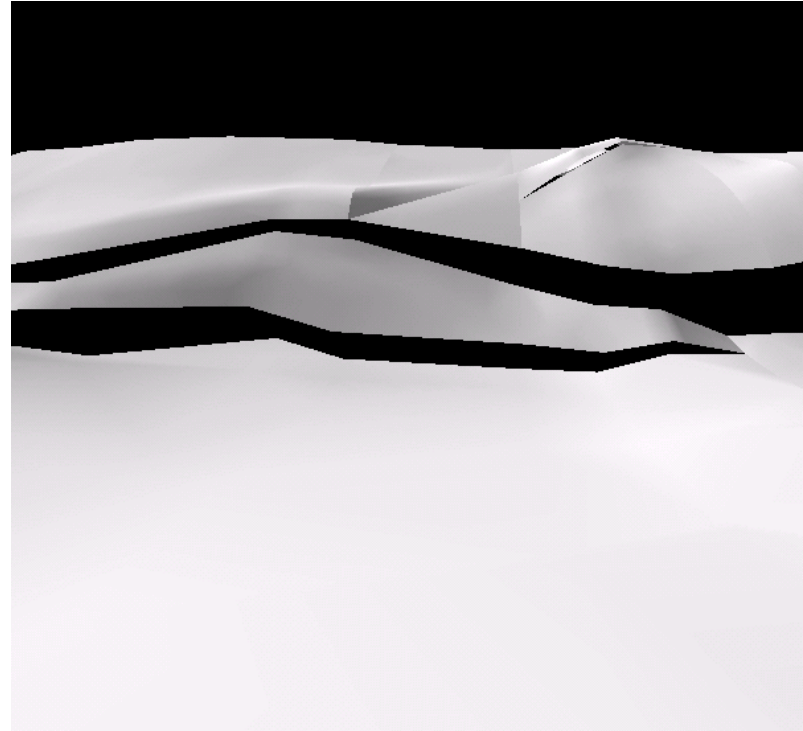


Fig. 18. Views of the top of the basement surface looking south and southwest (a and b, respectively) from the NE boundary of the model at the segment of the Line Creek Fault system with a geometry resembling a basement-involved compressional relay-ramp.

In the vicinity of the Horse Center anticline, seismic data shows a similarly spaced, two-fault system of basement faults controlling the east-vergent Horse Center anticline. The northward projection of these two faults into the approximate locations of the two Line Creek Faults provides one line of evidence that the Line Creek and Horse Center Fault systems are directly connected at depth.

#### *Rattlesnake Mountain/Pat O'Hara Mountain Anticline Intersection*

The anticlinal fold shapes observed in outcrop at Rattlesnake Mountain and Pat O'Hara Mountain anticlines were modeled in 3D Move and the 3D geometry of the intersection of these two structures provides an opportunity to understand their kinematic relationship. Although much of this intersection is covered by Tertiary volcanic rocks (Pierce and Nelson, 1968), including its westerly extension, an abrupt break in structural elevation along the southwest boundary of the 3D model suggests the Rattlesnake Mountain anticline terminates into Pat O'Hara Mountain anticline. This change in structural elevation occurs between the footwall of Rattlesnake Mountain anticline and the Pat O'Hara Mountain anticline backlimb. Pat O'Hara Mountain anticline's backlimb is gently folded into the N-S-trending Dead Indian Monocline at this location, illustrating that the loss of structural elevation of the Beartooth arch hanging wall occurs most abruptly at the Rattlesnake Mountain anticline footwall block. The hypothesis that Rattlesnake Mountain anticline terminates to the NW into Pat O'Hara Mountain anticline is further supported by the apparent westward continuation of the Pat O'Hara Mountain anticline fold shape, as exposed in cover rocks in several limited outcrops near the Rattlesnake Mountain/Pat O'Hara Mountain intersection (Pierce, 1966; Pierce and Nelson, 1968; see also discussion, chapter 5).

### *Cedar Mountain Tear Fault*

The surface expression of the abrupt southeast termination of the Rattlesnake Mountain anticline and this zone's abrupt transition from SW-directed thrusting (Rattlesnake Mountain anticline) to ENE/E directed thrusting (Horse Center anticline) suggests that strike-slip faulting, instead of complex basement folding, may be the mechanism by which this transition is accommodated (Fig. 19). However, because two more abrupt structural changes occur along the NE extension of the strike of this hypothesized tear fault, two working hypotheses can explain the structural geometry of the zone. In the first, the Line Creek Fault system and the Oregon Basin anticline terminate to the SE and N, respectively, against this regionally extensive tear fault (Fig. 20a). Such a fault would allow the Rattlesnake Mountain anticline, Line Creek Fault, Horse Center anticline, and Oregon Basin anticline structures, which all have suggestions of termination in surface map patterns along this linear zone, to move as independent basement blocks. The principal line of evidence from subsurface data that supports this hypothesis is an abrupt, approximately 1 km change in well top elevations NE of and along strike with the proposed Cedar Mountain tear fault (Fig. 21). Despite continuous, unfaulted surface outcrops above this location, these well data suggest a change in basement configuration and possibly the presence of a regionally extensive transfer fault.

Alternatively, the well data NE of the Rattlesnake Mountain termination can be interpreted as an abrupt change in the geometry of the thin-skinned Shoshone anticline, rather than an abrupt change in basement geometry. In this hypothesis, the Cedar Mountain tear fault extends only as far NE as the Line Creek Fault system, and

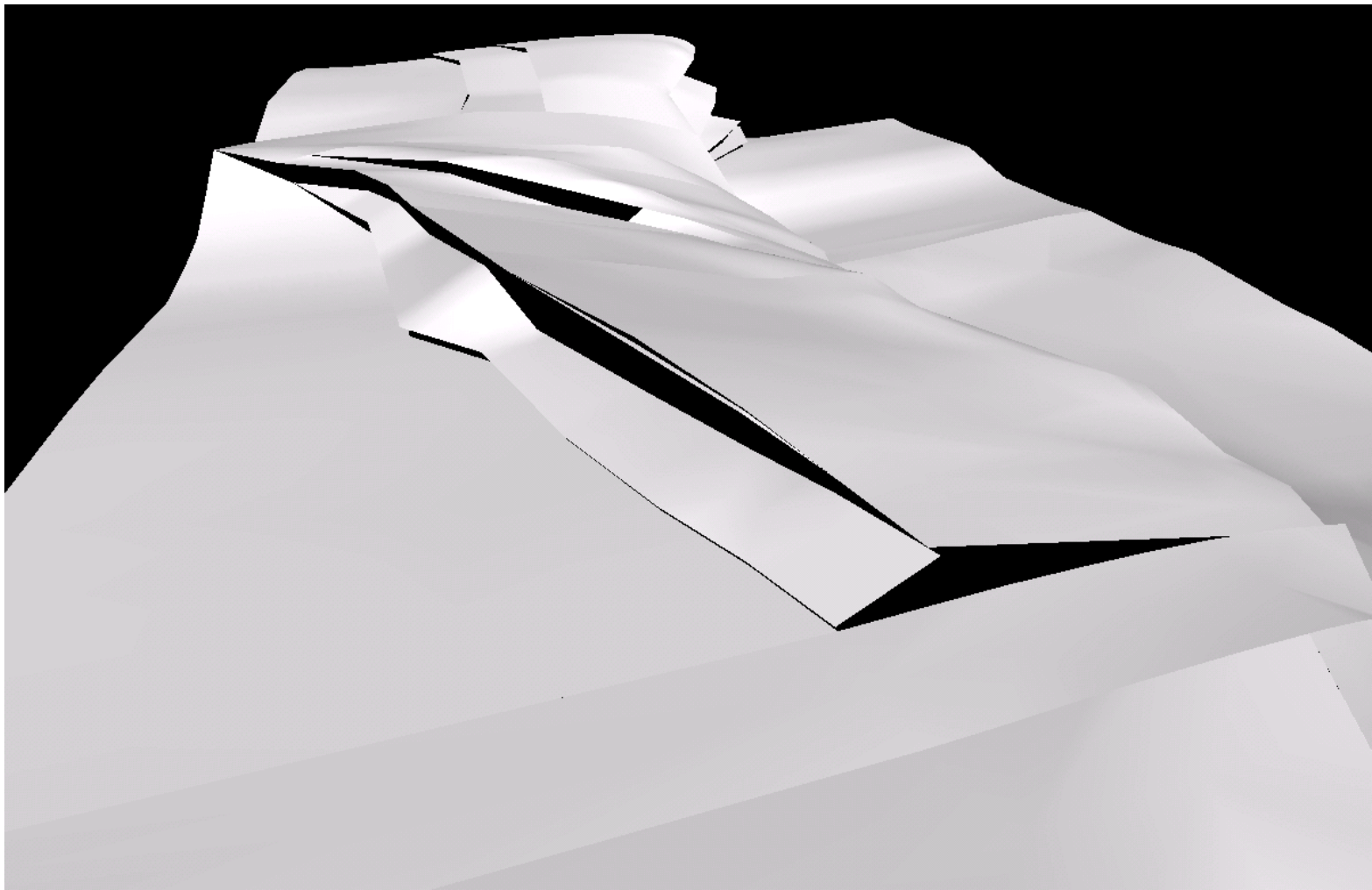
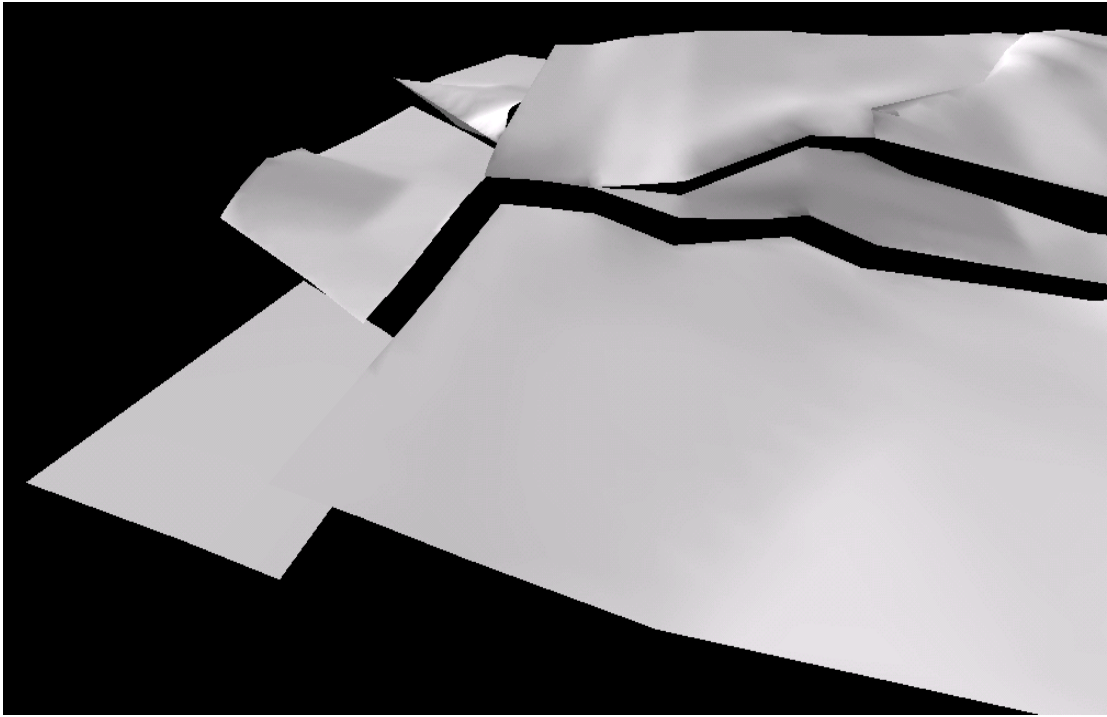


Fig. 19. View of the top of the basement surface looking north at the hypothesized basement tear fault at the SE plunge of Rattlesnake Mountain.

a)



b)

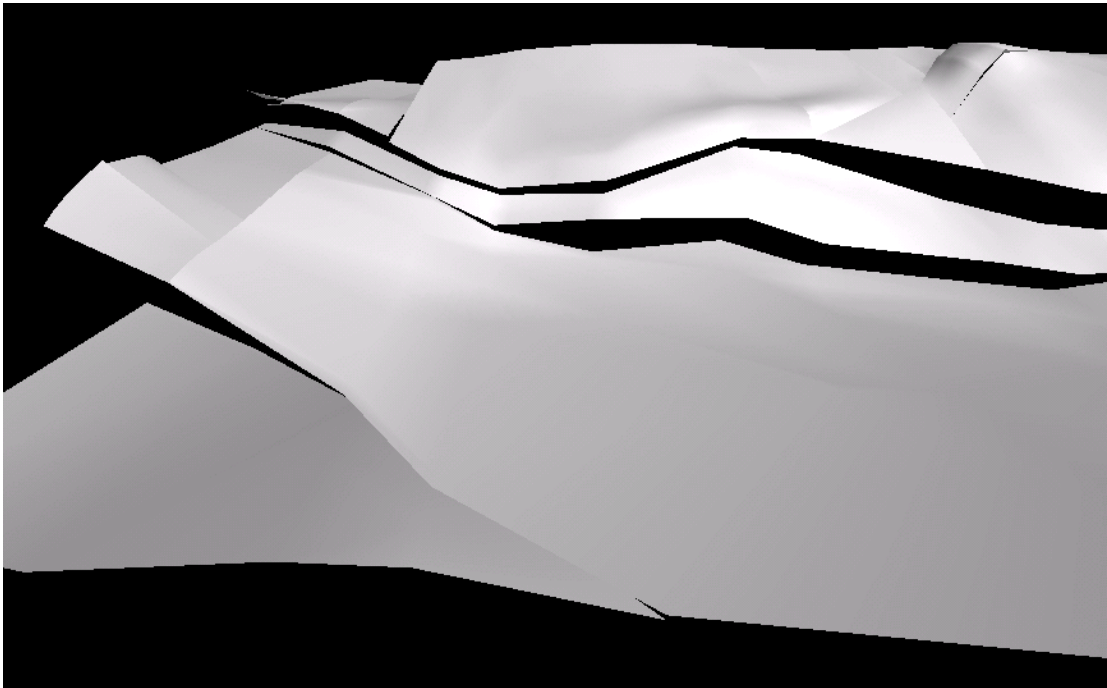


Fig. 20. Views looking southeast at two alternative basement surface models involving (a) a regional tear fault extending from SE Rattlesnake Mountain to northern Oregon Basin and (b) folding of the basement surface from the Oregon Basin hanging wall to the Line Creek footwall.

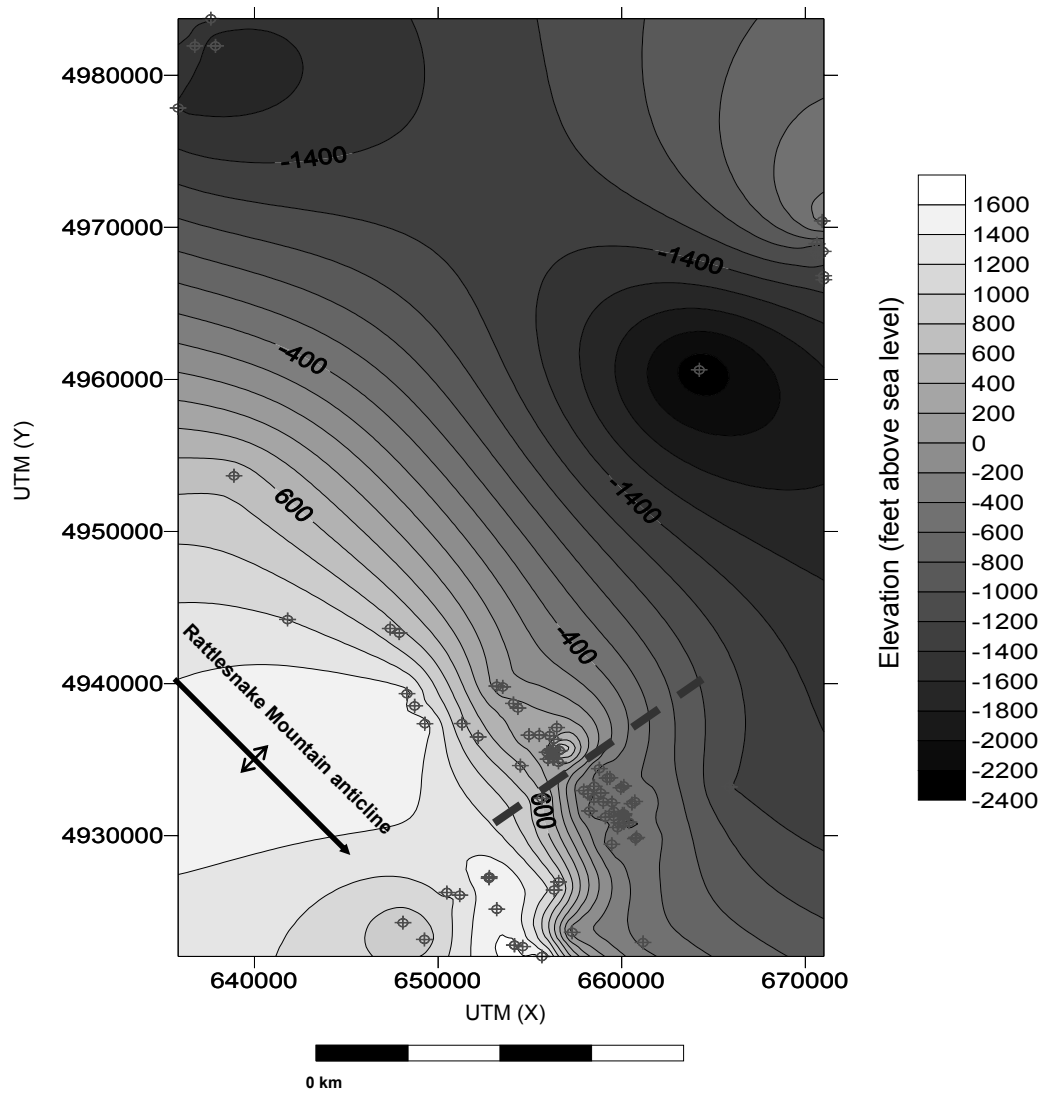


Fig. 21. Structure contour map of Chugwater top elevations from wells in the area immediately NE of the SE Termination of Rattlesnake Mountain anticline, between cross-sections N-N' and O-O'. Circles with crosses are well locations and dashed line is the location of hypothesized tear fault separating the wells that show an approximately 1 km elevation change in formation top elevations.

the Oregon Basin hanging wall and Line Creek footwall comprise a single, folded basement block (Fig. 20b). This hypothesis is supported by formation top and dip data from five wells on the northern plunge of Oregon Basin anticline, which indicate a continuous, approximately 20° north dipping monoclinally plunging fold at the level of the Mississippian Madison Limestone. In addition to the continuous, unfaulted surface exposures above this location, the hypothesis is further supported by the observations that the Oregon Basin Fault system may link northward with one of several east-vergent structures in the Bighorn Basin, as suggested in earlier studies (Blackstone, 1986a; Barlow & Haun, Inc., 1992) and in several 2D seismic lines along the fault's proposed NE extension (see discussion below).

#### *Northern Oregon Basin Anticline*

The second hypothesis outlined above favors an interpretation of the northern Oregon Basin anticline in which its monoclinally-plunging nose and the N-striking faults in the Bighorn Basin north of Oregon Basin anticline connect in the form of a single fault system. This proposed fault system requires a relatively abrupt change in vertical offset, from approximately 5 km to 200 m over a horizontal distance of 12 km (Fig. 16). Because this fault extends beyond the study area, regional shortening estimates in this area are uncertain. However, the limited amount of basement offset on the stretch of this fault system that is outside of the study area suggests that this uncertainty is minimal.

#### Three-dimensional Restoration

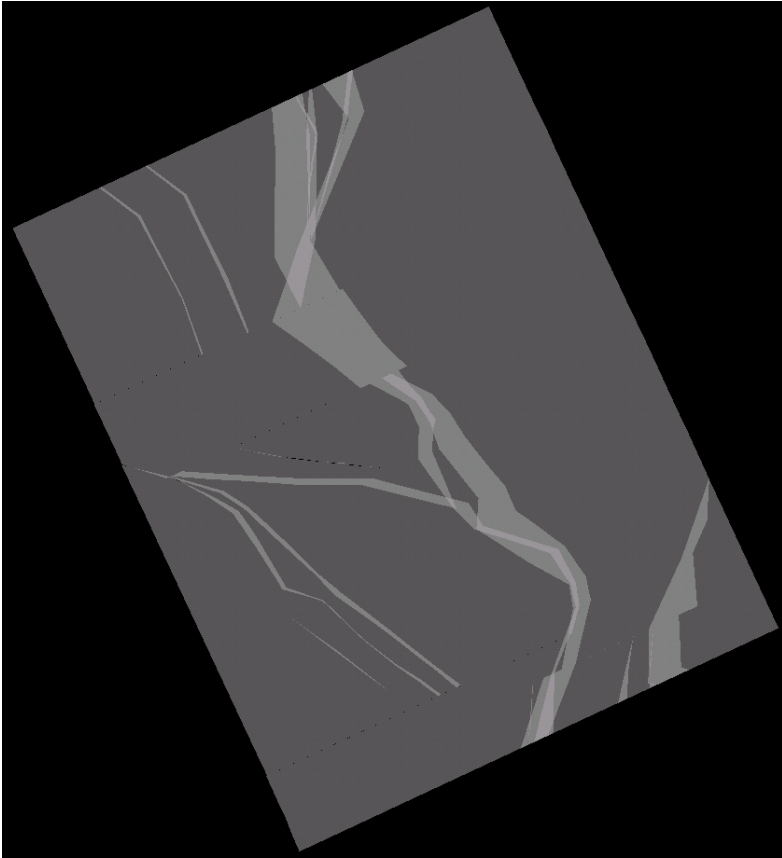
Three-dimensional restoration of the six modeled surfaces was accomplished using 3DMove's flexural slip flattening algorithm to flatten all patches of each surface to

a single elevation datum and then translate the patches and blocks along the 065° direction to simulate the restoration of fault heaves. This technique has the advantage of preserving line lengths and allowing gaps and overlaps in flattened fault blocks to be easily identified. Fig. 22 shows the basement surface restoration before and after fault heave restoration.

As can be verified by the 2D line length unfolding exercise, the two northernmost and two southernmost cross-sections (A-A', B-B', O-O', and P-P') show an approximately similar amount of shortening at the basement level, which is notably more than that observed in the twelve cross-sections between these two areas (sections C-C' to N-N'). This area of decreased shortening is approximately coincident with the zone containing hanging-wall backthrusts (Rattlesnake Mountain and Pat O'Hara Mountain anticlines) and folding of the basement surface proximal to the Line Creek Fault zone. These shortening estimates, however, are strongly dependent upon the interpreted fault angles of the Beartooth, Line Creek, and Oregon Basin Fault systems.

Increased shortening from NW to SE along the Line Creek Fault system (sections E-E' to N-N'), documented by increasingly large gaps between fault blocks from NW to SE (Fig. 22), requires a counter-clockwise rotation for restoration. This suggests regional clockwise rotation of basement blocks in this area during deformation. Shortening patterns revealed from 3D restoration of the sedimentary cover rock surfaces are similar to that seen at the basement level, however, they show less overall shortening and a less clearly-defined zone of decreased shortening between cross-sections C-C' and N-N'. This pattern is likely the result of different deformation mechanisms available to a

a)



b)

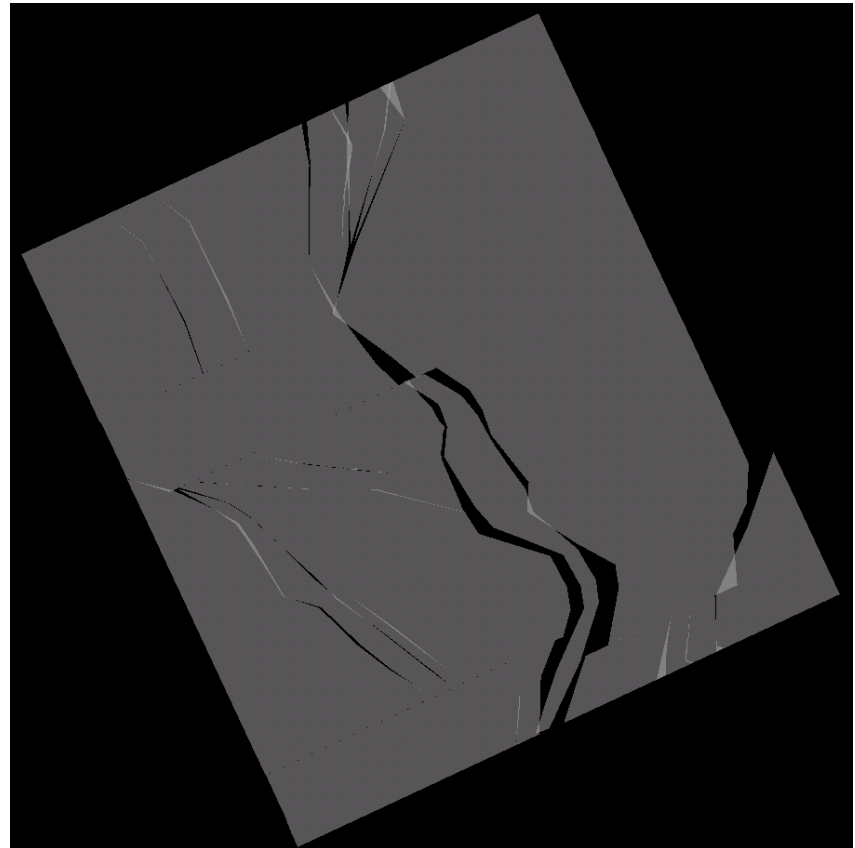


Fig. 22. Flattened basement surfaces with fault heaves unrepaired (a) and restored (b). Lighter areas indicate surface overlaps and black areas between surfaces are gaps.

heterogeneously layered sedimentary sequence, which may have included layer-parallel slip and internal shortening during folding (see discussion, chapter 5).

## 7. DISCUSSION AND CONCLUSIONS

Three-dimensional structural complexity at foreland arch transitions is commonly characterized by diversely-oriented faults and folds whose relationship to arch development can be enigmatic. Hypotheses concerning regional models of slip, changes in along-strike geometry, and the role of secondary structures in accommodating strain at foreland arch transitions were tested at the southern Beartooth arch transition using slip data from minor faults, balanced cross sections, and restorable 3D surface models. These analyses offered insights into the 3D kinematic development of foreland arch transitions by providing 2D and 3D kinematic and rheological constraints relating to fold mechanisms, basement block rotation, vertical-axis rotation, triangle zones, and fault propagation from different levels.

The hypothesis that shortening directions were multi-directional, either spatially or temporally, was tested by analyzing slip data from more than 1,500 slickensided minor faults in Paleozoic and Mesozoic sandstone units at 24 locations within the area. Data from minor faults in strata away from map-scale faults and folds suggest that the study area experienced regionally consistent, approximately uniform,  $065^{\circ}$  shortening during deformation. In strata near map-scale faults and folds, slip directions deviate from the interpreted  $065^{\circ}$  regional shortening direction and indicate that slip on structures oblique to the regional shortening direction was not perpendicular to fold trend.

At Pat O'Hara Mountain anticline, the inferred shortening direction is approximately  $025^{\circ}$ , which is intermediate between local dip directions (N-S) and the regional  $065^{\circ}$  shortening direction. These data may represent progressive counter-clockwise material rotation of the rocks during oblique-slip on the anticline's non-

optimally oriented basement fault, fold-related stress re-orientation, or partitioned slip. At Canyon Mouth anticline, the inferred shortening direction is similarly deviated in a counter-clockwise direction with respect to local dip direction, and may be explained by either 1) material rotation within a zone of oblique-slip, similar to the process inferred at Pat O'Hara Mountain, or by 2) local strain partitioning between N-S strike-slip faulting and E-W shortening, in which a northerly deviation in shortening direction resulted from N-S strike-slip faulting. At Rattlesnake Mountain anticline, minor fault data indicate that local shortening was perpendicular to structural trend and approximately 20° oblique to the regional shortening direction. These data may represent local, fold-related stress re-orientation within the anticline's steeply-dipping forelimb. Thus, the interpreted kinematic framework of the southern Beartooth arch transition suggests that the area experienced regionally-consistent, approximately 065° shortening with local deviations in shortening direction due to oblique-slip on non-optimally oriented basement structures, material rotation in zones of oblique-slip, strain partitioning, and/or local fold-related stress re-orientation.

The detailed geometry of the southern Beartooth arch transition zone was constrained using surface geologic mapping, more than 1,000 km of 2D seismic data, and 187 wells integrated with 16 balanced cross-sections and 3D surface models of six geologic units. The Beartooth Fault system is a distributed fault zone composed of four fault segments, with a total vertical separation of approximately 7 km. These fault segments are interpreted as splays from the westernmost Beartooth Fault, which terminate into this western segment at the transition with the Line Creek Fault zone near the Canyon Mouth anticline. This zone transitions to the SE into a narrower zone of

faulting, the Line Creek Fault system, which is characterized by 1-4 km of vertical separation and basement-involved, hanging wall backthrust structures with up to nearly 3 km of basement surface throw. These include the south-vergent Pat O'Hara Mountain anticline and the SW-vergent Rattlesnake Mountain anticline. Slip on the Line Creek Fault system is concentrated on one fault segment to the NW and is distributed between two segments to the SE. Southeast of the Line Creek Fault system, slip steps east to the Oregon Basin Fault, which shows a throw of the basement surface of nearly 4 km, all of which is concentrated on a single master fault. Within sedimentary rocks overlying basement, the dominant faulting and folding pattern is SW-directed, basement-detached backthrusting and associated folding above the Line Creek Fault system. These structures are tight to open secondary detachment folds with strike lengths ranging from approximately 2-5 km. They are interpreted as triangle-zone backthrusts that resulted from upward shallowing of the Line Creek Fault zone into the Phanerozoic sedimentary section.

Cross-sections A-A' through P-P' show that the basement surface experienced a variable amount of folding. At Rattlesnake Mountain, surface exposures and cross-sectional modeling show that the basement hanging wall block experienced little, if any folding. 2D restoration of the Rattlesnake Mountain anticline using a combination of the fault-parallel flow and antithetic, top-to-the-NE inclined shear algorithms in 2D Move software suggests that the anticline formed via rigid-block rotation on a curved master fault. An intermediate fault block between the Rattlesnake Mountain footwall and hanging wall is visible in seismic data as a uniformly SW-dipping block. The

deformation history of this block was best modeled using fault-parallel flow and synthetic, top-to-the-SW inclined shear restoration algorithms in 2DMove.

In contrast to the generally rigid basement behavior at Rattlesnake Mountain, the basement surface within the hanging wall of the Line Creek Fault system shows tilt domains with margins rotated up to approximately 25°. Within the Beartooth Fault system, uniformly-tilted (approximately 25° east) intermediate fault blocks may either reflect folding of the basement surface within the fault zone, or rotation of basement blocks associated with faulting. The basement folding observed near the Line Creek Fault system suggests the initial fault tip started well below the basement nonconformity and may have propagated upward independent of basement structures. In contrast, the interpreted lack of basement folding near the Beartooth Fault system suggests that the fault tips initiated at the basement nonconformity, and thus may have followed pre-existing structures. This interpretation is consistent with minor fault slip data at the surface near these two locations; near the Line Creek Fault system, inferred shortening directions are approximately perpendicular to the strike of the fault system, whereas near the Beartooth Fault system, inferred shortening directions are oblique to fault strike.

Three-dimensional modeling further constrained the detailed geometry of the southern Beartooth arch transition zone and allowed hypotheses concerning vertical-axis rotations and changes in regional shortening amount to be tested. The 3D geometry of structural transitions and terminations amongst primary and secondary basement-involved structures in the area was constrained by extrapolating 2D cross-sectional geometries into 3D surfaces using 3DMove software. The two-fault segment of the Line Creek Fault zone shows a transfer of slip from the western segment to the eastern

segment from NW to SE in a geometry similar to a compressional relay ramp but with sequential development. The spatial coincidence of this left-step in the Line Creek Fault system with the area's two basement-involved hanging wall backthrust suggests that the eastward transfer of slip may have occurred to accommodate rotational backthrusting on listric basement faults within the hanging wall. Alternatively, this two-fault segment may represent a broadly distributed zone of deformation along the Line Creek Fault system that included folding of the basement surface, possibly via fault tip initiation below the basement nonconformity. In contrast to the two-fault ramp geometry interpreted for the Line Creek Fault segments, 3D modeling suggests that fault segments associated with the Beartooth Fault system define an approximately 5 km wide zone in which slip is distributed on sub-parallel, merging fault segments.

Although the trend of the Beartooth arch and the western margin of the Bighorn Basin shows a map-scale southward jog at the east flank of the Beartooth arch, the fault systems connecting them merge in a continuous fashion. The westernmost Beartooth fault transitions into the Line Creek Fault, and the footwall of the Line Creek Fault system makes a gradual transition into the hanging wall of the Oregon Basin Fault via monoclinial folding of the basement surface. Secondary fault systems, however, show more abrupt structural transitions. Rattlesnake Mountain anticline's SE plunge is abrupt and is interpreted at the basement level as a NE striking tear fault, the Cedar Mountain tear fault. Pat O'Hara Mountain and Canyon Mouth anticlines plunge steeply to the east and southeast, respectively, and may terminate into the Line Creek Fault system.

Three-dimensional restoration of the rectangular basement surface patch covered in this study shows that shortening is highest in the area of the Beartooth Fault system to

the north and in the area of the Oregon Basin Fault to the south. Between these two areas, gaps in the restored basement surface suggests that either 1) shortening is several percent less in the area of the Line Creek Fault system and Rattlesnake Mountain anticline, 2) the fault angles interpreted in cross-sections are incorrect, or 3) slip is transferred outside of the cross-sections. Because shortening estimates are strongly influenced by interpreted fault angles, and thus the footwall and hanging wall lengths, these estimates are subject to the uncertainty associated with interpreting fault geometries from 2D seismic data. Three-dimensional restoration also suggests that shortening along the Line Creek Fault zone decreases from NW to SE, possibly indicating that clockwise vertical-axis rotation of several degrees occurred in this area during deformation. Several anticlinal structures located NE of this area within the Bighorn Basin could affect regional shortening balance calculations. For example, Elk Basin anticline, located approximately 40 km NE of the Line Creek Fault system, may account for the decrease in shortening along the Line Creek Fault system.

In summary, geometric changes at the southern Beartooth arch transition appear to have occurred due to a combination of lateral and vertical propagation of underlying basement faults which locally followed pre-existing structures during uniformly-oriented  $065^{\circ}$  shortening direction which was locally complicated by oblique-slip, vertical-axis rotations, and possibly fold-related stress re-orientation and strain partitioning. Both abrupt and gradual geometric transitions are present within the area, however, the primary fault systems bounding the Beartooth arch and northwestern margin of the Bighorn Basin are best characterized as gradual and continuous structural transitions. Secondary basement-involved structures in the area likely resulted from activation of pre-

existing basement structures, do not appear to have accommodated large-scale rotations or changes in shortening directions, and may have influenced the geometry of primary fault systems.

### Crustal-Scale Implications

If initial orogenic stresses activate optimally-oriented pre-existing weaknesses in the crust, progressive along-strike propagation of these activated weaknesses would necessitate complicated linkage zones. In this hypothesis, transition zones between foreland arches result from the strike-propagation and merging of arches, with individual geometries highly controlled by reactivated crustal weaknesses. At the southern Beartooth arch transition zone, the east flank of the Beartooth arch and the Oregon Basin Fault show minimal basement folding and backthrusting, suggesting that they occupied optimally-oriented weaknesses. In comparison, in the vicinity of the Line Creek Fault zone, folding and progressive abandonment of early fault splays may suggest the area is a linkage zone between two optimally-oriented crustal weaknesses. The basement folding, decrease in shortening, and hanging-wall backthrusts present within this proposed linkage zone may all reflect the merging of two independent basement weaknesses.

Alternatively, the Beartooth arch and southern Beartooth arch transition zone may instead have initiated as a single, continuous, fault-bounded basement arch whose along-strike variability resulted exclusively from reactivated basement structures. In this model, inherited basement structures within the southern Beartooth arch transition zone that were non-optimally oriented relative to the  $065^\circ$  shortening field may have caused a resistance to shortening, and thus basement folding and backthrusting. The approximately uniform kinematic signature within this zone would have resulted from the

presence of a single, continuous fault system at depth which broke through the surface along pre-existing basement weaknesses. Thus, along-strike changes in morphology (wide versus narrow fault zone, presence of basement folding) were produced by local basement weaknesses. In a variation of this hypothesis, the southern Beartooth arch transition zone may represent a series of left-stepping fault segments that were either reactivated or newly formed in response to a southward jog in the Beartooth arch's trend. An obliquely-reactivated N-S weakness at the east flank of the Beartooth arch may have caused a local perturbation in regional arch trend, and the left-stepping faults along the margin of the northwest Bighorn Basin may have accommodated a correction back to a regional, approximately NW-oriented arch trend.

#### Future Work

The foreland arch transition analyzed in this study will hopefully provide useful analogues for other areas in the Rocky Mountains and beyond; however, it remains only one among numerous structurally-complex transitional areas in this part of the earth's crust. Additional integrated studies that incorporate data from different crustal levels and foreland settings will improve our understanding of basement-involved foreland tectonics. By comparing the degree of influence that basement weaknesses and/or variations in shortening or vergence direction have throughout an orogen, the overall influence of these processes and their resulting geometric patterns may be better constrained and predicted.

Future geophysical studies that focus on imaging the structure of the middle and lower crust will improve the understanding of the at-depth relationship between foreland arches. For instance, if arch-bounding fault systems are geometrically linked at a

common detachment at mid- or lower-crustal levels, they may be better viewed as a system of related splays. However, if the geometry of these arch-bounding fault systems instead appears to closely follow older lithospheric fabrics, they may be better viewed as a systems of activated crustal weaknesses.

Orogen-scale balancing and kinematic studies will allow individual transition zones between arches to be analyzed within the context of how they facilitate crustal-scale strain. For example, if net shortening balance is observed between en echelon arches with similar interpreted shortening directions, their transition zones may be crustal-scale relay or transfer zones. Future studies of structural processes at foreland arch transition zones can benefit from comparative analyses both within individual orogens and between different orogens and may provide a pivotal link in our understanding of plate boundary processes and continental tectonics.

## REFERENCES

- Allison, M. L., 1983, Deformation styles along the Tensleep Fault, Bighorn Basin, Wyoming, Wyoming Geological Association 34<sup>th</sup> annual field conference guidebook, p. 63-76.
- Allmendinger, R. W. and Jordan, T. E., 1983, Andean tectonics related to geometry of subducted Nazca plate, Geological Society of America Bulletin, v. 94, p.341-361.
- Allmendinger, R. W., Figueroa, D., Snyder, D., Beer, J., Mpodozis, C., Isacks, B.L., 1990, Foreland shortening and crustal balancing in the Andes at 30 degrees S latitude, Tectonics, v. 9, p. 789-809.
- Allmendinger, R.W., 1998, Inverse and forward numerical modeling of trishear fault-propagation folds, Tectonics, v. 17, p. 640-656.
- Barlow & Haun, Inc., 1992, Structure contour map of NW/4 Bighorn Basin, Wyoming, Rocky Mountain Map Company, Casper, Wyoming.
- Bird, P., 1988, Formation of the Rocky Mountains, Western United States; a continuum computer model, Science, v. 239, p. 1501-1507.
- Bird, P., 1998, Kinematic history of the Laramide Orogeny in latitudes 35 degrees-49 degrees N, western United States, Tectonics, v. 17, p. 780-801.
- Blackstone, D. L. Jr., 1986a, Structural geology – northwest flank of Bighorn Basin: Park County, Wyoming and Carbon County, Montana, in Geology of the Beartooth Uplift and adjacent basins, Montana Geological Society and Yellowstone Bighorn Research Association joint field conference and symposium, p.125-135.
- Blackstone, D. L. Jr., 1986b, Foreland compressional tectonics; southern Bighorn Basin and adjacent areas, Wyoming, Report of Investigations - Geological Survey of Wyoming, Vol. 34, 27 p.
- Brown, W. G., 1983, Sequential development of the fold-thrust model of foreland deformation, in Lowell, J. D., ed., Rocky Mountain foreland basins and uplifts, Rocky Mountain Association of Geologists, Denver, Colorado, p. 57-64.
- Brown, W. G., 1984, Rattlesnake Mountain Anticline - a reverse fault interpretation, The Mountain Geologist, v. 21, p. 32-35.
- Brown, W. G., 1993, Structural style of Laramide basement-cored uplifts and associated folds, in Wyoming Geology, University of Wyoming, Wyoming Geological Survey, p. 313-371.

- Cahill, T. and Isacks, B. L., 1985, Shape of the subducted Nazca Plate, *Eos Transactions, American Geophysical Union*, v. 66, p. 299.
- Chapin, C. E., and Cather, S. M., 1981, Eocene tectonics and sedimentation in the Colorado Plateau-Rocky Mountain area, in Dickinson, W. R. and Payne, W. D., eds., *Relation of tectonics to ore deposits in the southern Cordillera: Arizona Geological Society Digest*, v. 14, p. 173-198.
- Compton, R. R., 1966, Analyses of Pliocene-Pleistocene deformation and stresses in northern Santa Lucia Range, California, *Geological Society of America Bulletin*, v. 77, p. 1361-1380.
- Coney, P. J., and Reynolds, S. J., 1977, Cordilleran Benioff zones, *Nature*, v. 270, p. 403-406.
- Cook, D. G., 1988, Balancing basement-cored folds of the Rocky Mountain foreland, *Geological Society of America Memoir* 171, p. 53-64.
- DeCelles, P. G., Gray, M. B., Ridgway, K. D., Cole, R. B., Srivastava, P., Pequera, N., and Pivnik, D. A., 1991, History and kinematics of foreland uplift from synorogenic conglomerate, Beartooth Range, Wyoming and Montana, *Geological Society of America Bulletin*, v. 103, p. 1458-1476.
- Dickinson, W. R., Snyder, W. S., 1978, Plate tectonics of the Laramide Orogeny, *Geological Society of America Memoir* 151, p. 355-366.
- Durdella, M. J., 2001, Mechanical modeling of fault-related folds; west flank of the Bighorn Basin, Wyoming, M.S. thesis, Purdue University, 129 p.
- Egan, S. S. and Urquhart, J. M., 1993, Numerical modeling of lithosphere shortening: applications to the Laramide orogenic province, western USA, *Tectonophysics*, v. 221, p. 385-411.
- Erslev, E. A., 1986, Basement balancing of Rocky Mountain foreland uplifts, *Geology*, v. 14, p. 259-262.
- Erslev, E. A., 1990, Heterogeneous Laramide deformation in the Rattlesnake Mountain Anticline, Cody, Wyoming, *Geologic field tours of western Wyoming and parts of adjacent Idaho, Montana, and Utah*, Geological Survey of Wyoming, v. 29, p. 141-149.
- Erslev, E. A., 1991, Trishear fault-propagation folding, *Geology*, v. 19, p. 617-620.
- Erslev, E. A., 1993, Thrusts, back-thrusts, and detachment of Laramide foreland arches, in Schmidt, C.J., Chase, R., and Erslev, E.A., eds., *Laramide basement*

deformation in the Rocky Mountain foreland of the western United States, Geological Society of America Special Paper 280, p. 339-358.

- Erslev, E. A., 1998, SELECT 1.2 worksheet and computer program, Department of Earth Resources, Colorado State University.
- Erslev, E. A., 2001, Multistage, multidirectional Tertiary shortening and compression in north-central New Mexico, Geological Society of America Bulletin, v. 113, p. 63-74.
- Erslev, E. A., 2005, 2D Laramide geometries and kinematics of the Rocky Mountains, Western U.S.A., in Karlstrom, K. E. and Keller, G. E., eds., The Rocky Mountain Region: An Evolving Lithosphere, Geophysical Monograph Series, v. 154, p. 7-20.
- Erslev, E. A. and Hennings, P. H., 2004, Variations in predicted reservoir heterogeneity due to multiple models of folding in basement-involved foreland anticlines, abstracts with programs, AAPG annual meeting.
- Erslev, E. A. and Larson, S. M., 2006, Testing Laramide hypotheses for the Colorado Front Range using minor faults, The Mountain Geologist, v. 43, p. 45-64.
- Erslev, E. A., and Rogers, J. L., 1993, Basement-cover geometry of Laramide fault-propagation folds, in Schmidt, C.J., Chase, R., and Erslev, E.A., eds., Laramide basement deformation in the Rocky Mountain foreland of the western United States, Geological Society of America Special Paper 280, p. 125-146.
- Foose, R. M., Wise, D. U., and Garbarini, S. G., 1961, Structural geology of the Beartooth Mountains, Montana and Wyoming, Geological Society of America Bulletin, v.72, p. 1143-1172.
- Gries, R., 1983, North-south compression of Rocky Mountain foreland structures, Field Conference - Rocky Mountain Association of Geologists, p. 9-32.
- Gries, R., 1990, Rocky Mountain foreland structures; changes in compression direction through time, in Letouzey, J., ed., Petroleum and tectonics in mobile belts; proceedings of the IFP exploration and production research conference, p.129-147.
- Hardy, S., and Ford, M., 1997, Numerical modeling of trishear fault propagation folding. Tectonics, v. 16, p. 841-854.
- Hennings, P. H., and Hager, 1996, Basement backthrusts and thin-skinned detachments in Goosebury Field, western Bighorn Basin, Wyoming, Wyoming Geological Association 47<sup>th</sup> annual field conference guidebook, p. 221-238.

- Humphreys, G., Hessler, E., Dueker, K., Farmer, L., Erslev, E. and T. Atwater, 2003, How Laramide-aged hydration of the North American Lithosphere by the Farallon Slab controls subsequent activity in the western U.S., *International Geology Review*, v. 45, 575-595.
- Johnson, G. D., 1934, Geology of the mountain uplift transected by the Shoshone Canyon, Wyoming, *Journal of Geology*, v. 42, p.809-838.
- Johnson, K. M. and Johnson, A. M., 2002, Mechanical analysis of the geometry of forced-folds, *Journal of Structural Geology*, v. 24, p. 401-410.
- Jordan, T. E., Isacks B. L., Allmendinger R. W., Brewer J. A., Ramos V. A, and Ando C. J., 1983, Andean tectonics related to geometry of subducted Nazca plate, *Bulletin of the Geological Society of America* v. 94, p. 341-61.
- Jordan, T. E., and R. W. Allmendinger, 1986, The Sierras Pampeanas of Argentina: A modern analogue of Rocky Mountain foreland deformation, *American Journal of Science*, v. 286, 737-764.
- Keefer, W. R. and Love, J. D., 1963, Laramide vertical movements in central Wyoming, *Contributions to Geology*, v. 2, p. 47-54.
- Love, J. D., and Christiansen, A. C., 1985, Geologic map of Wyoming: Reston, Virginia, U.S: Geological Survey, scale 1:500,000.
- Lowell, J. D., 1983, Foreland Deformation, in Lowell, J. D., ed., *Rocky Mountain foreland basins and uplifts: Rocky Mountain Association of Geologists*, p. 1-8.
- Maxson, J., and Tikoff B., 1996, Hit-and-run collision model for the Laramide orogeny, western United States, *Geology*, v. 24, p. 968-972.
- Molzer, P. and Erslev, E. A., 1995, Oblique convergence on east-west Laramide arches, Wind River Basin, Wyoming, *American Association of Petroleum Geologists Bulletin*, v. 19, p. 1377-1394.
- Mpodozis, C., and Ramos, V. A., 1989, The Andes of Chile and Argentina, in Ericksen George, E., Pinochet Maria Teresa, C., and Reinemund John, A., eds., *Geology of the Andes and its relation to hydrocarbon and mineral resources.: Circum-Pacific Council for Energy and Mineral Resources, Earth Science Series: Houston, TX, United States, Circum-Pacific Council for Energy and Mineral Resources*, p. 59-90.
- McQuarrie, N. and Chase, C. G., 2000, Raising the Colorado Plateau, *Geology*, v. 28, p. 91-94.

- O'Connell, P. J., 1996, Kinematics of the eastern flank of the Beartooth Mountains, Montana and Wyoming, Wyoming Geological Association guidebook 47, p. 189-220.
- Oldow, J. S., Bally, A. W., Ave Lallemand, H. G., and Leeman, W. P., 1989, Phanerozoic evolution of the North American Cordillera: United States and Canada, in Bally, A. W. and Palmer, A. R., eds., *The Geology of North America, an overview*: Boulder, Colorado, The Geological Society of America, v. 1A, p. 139-232.
- Petit, J. P., 1987, Criteria for the sense of movement on fault surfaces in brittle rocks. *Journal of Structural Geology*, v. 9, p. 597-608.
- Pierce, W. G., 1965a, Geologic map of the Clark Quadrangle, Park County, Wyoming U.S. Geological Survey Geologic Quadrangle Map GQ-0477, scale 1:62,500.
- Pierce, W. G., 1965b, Geologic map of the Deep Lake Quadrangle, Park County, Wyoming, U.S. Geological Survey Geologic Quadrangle Map GQ-0478, scale 1:62,500.
- Pierce, W. G., 1966, Geologic map of the Cody quadrangle, Park County, Wyoming, U.S. Geological Survey Geologic Quadrangle Map GQ-542, scale 1:62,500.
- Pierce, W. G., 1970, Geologic map of the devils tooth quadrangle, park county, wyoming, U.S. Geological Survey Geologic Quadrangle Map GQ-817, scale 1:62,500.
- Pierce, W. G. and Nelson, W. H., 1968, Geologic map of the Pat O'Hara Mountain Quadrangle, Park County, Wyoming, U.S. Geological Survey Geologic Quadrangle Map GQ-0755, scale 1:62,500.
- Pierce, W. G. and Nelson, W. H., 1969, Geologic map of the Wapiti Quadrangle, Park County, Wyoming, U.S. Geological Survey Geologic Quadrangle Map GQ-0778, scale 1:62,500.
- Pierce, W. G., 1987, Heart Mountain detachment fault and clastic dikes of fault breccia, and Heart Mountain break-away fault, Wyoming and Montana, Centennial field guide, Rocky Mountain section of the Geological Society of America, v. 2, p. 147-154.
- Saleeby, J., 2003, Segmentation of the Laramide slab-evidence from the southern Sierra Nevada region, *Geological Society of America Bulletin*, v.115, p. 655-668.
- Smalley, R.F., Jr. and Isacks, B. L., 1987, A high resolution local network study of the Nazca Plate Wadati-Benioff zone under western Argentina, *Journal of Geophysical Research*, v. 92, p. 13,903-13,912.

- Stanton, H. I., 2002, Rotational fault-bend folding and backlimb tightening in Rocky Mountain basement-involved structures: Sheep Mountain, Bighorn Basin, Wyoming, M.S. thesis, Colorado State University, 140 p.
- Stanton, H. I., and Erslev, E. A., 2004, Sheep Mountain: backlimb tightening and sequential deformation in the Bighorn Basin, Wyoming, Wyoming Geological Association Guidebook 54, p. 75-87.
- Stearns, D. W., 1971, Mechanisms of drape folding in the Wyoming Province, in Renfro, A. R., ed., Symposium on Wyoming Tectonics and their Economic Significance. Wyoming Geological Association, Annual Field Conference, 23<sup>rd</sup> Guidebook, p. 125-143.
- Stearns, D. W., 1975, Laramide basement deformation in the Bighorn Basin – the controlling factor for structure in the layered rocks, Wyoming Geological Association 27<sup>th</sup> annual field conference guidebook, p. 149-158.
- Stearns, D. W., 1978, Faulting and forced folding in the Rocky Mountain foreland, in Mathews, V., III, ed., Laramide folding associated with block faulting in the western United States, Geological Society of America Memoir 151, p. 1-37.
- Stiteler, T. C., Young T. J., Meisling K. E., Hanson W. B., 2005, A structural model of Jonah and South Pinedale fields, Wyoming, AAPG Rocky Mountain Section meeting abstract.
- Stone, D. S., 1984, The Rattlesnake Mountain, Wyoming, debate: a review and critique of models, *The Mountain Geologist*, v. 22, p. 37-46.
- Stone, D. S., 1993. Basement-involved thrust-generated folds as seismically imaged in the subsurface of the central Rocky Mountain foreland, in: Schmidt, C.J., Chase, R. B., and Erslev, E. A., eds., Laramide Basement Deformation in the Rocky Mountain Foreland of the Western United States, Geological Society of America, Special Paper 280, 271-318.
- Suppe, J. and D. A. Medwedeff, 1984, Fault-propagation folding, Geological Society of America Abstract Program, p. 670.
- Suppe, J., and Medwedeff, D., 1990, Geometry and kinematics of fault-propagation folding: *Eclogae Geologicae Helvetiae*, v. 83, p. 409-454.
- Tikoff, B., and Maxson, J., 2001, Lithospheric buckling of the Laramide foreland during Late Cretaceous to Paleogene, western United States, *Rocky Mountain Geology*, v. 36, p. 13-35.
- Varga, R. J., 1993, Rocky Mountain foreland uplifts: Products of a rotating stress field or strain partitioning?, *Geology*, v.21, p. 1115–1118.